Dipl.-Ing. Katrin Unger, BSc

Smart Hydrogels via Initiated Chemical Vapor Deposition

Humidity, Light and pH Responsive Polymer Films for Biosensors, Drug Delivery Systems and Cell Cultivation Platforms

DOCTORAL THESIS

to achieve the university degree of

Doktorin der technischen Wissenschaften

submitted to

Graz University of Technology

Supervisor

Assoc.Prof. Dr. Anna Maria Coclite

Institute of Solid State Physics

Graz, January 2021

Katrin Unger:

Smart Hydrogels via Initiated Chemical Vapor Deposition, Humidity, Light and pH Responsive Polymer Films for Biosensors, Drug Delivery Systems and Cell Cultivation Platforms © Graz, January 2021

AFFIDAVIT

I declare that I have authored this thesis independently, that I have not used other than the declared sources/resources, and that I have explicitly indicated all material which has been quoted either literally or by content from the sources used. The text document uploaded to TUGRAZonline is identical to the present doctoral thesis.

Date, Signature

Abstract

In this thesis, stimuli-responsive hydrogels, or also called smart hydrogels, and their application in device setups are investigated. Smart hydrogels are polymer networks which comprise active groups that react towards certain external stimuli, such as temperature, light, pH, electric field or different analytes, with a response in a change of shape, wettability, optical parameters, elastic or dielectric properties. Often a thin film of such material over a delicate and structured surface is required. For this purpose, the method of initiated chemical vapor deposition (iCVD) is utilized as polymerization technique, which is a powerful tool to dryly synthesize smart conformal coatings. Within a study of this thesis, an adaption of iCVD with vibrating substrates is proposed to expand the possible application to smart encapsulation of pharmaceutical powders. Furthermore, an investigation of hydrogels of 2-hydroxyethyl methacrylate (HEMA) cross linked with ethylene glycole dimethacrylte (EGDMA), p(HEMA-co-EGDMA), is presented. An interpretation of the swelling in humid environment by Flory-Huggings theory reveals a solvent-polymer interaction parameter that decreases with increasing relative humidity. This suggests a glassy skin formation at low humidity level caused by molecular arrangements, where the unpolar polymer backbone faces outwards to minimize the surface energy. The surface of the studied p(HEMA-co-EGDMA), is further functionalized with azobenzene groups to obtain a smart hydrogel that reacts upon exposure of light. Through photoisomerization, azobenzene reversible changes configuration from trans-to-cis, which results in a dipole moment increase and therefore a more water affine surface. With illuminating the functionalized hydrogel with UV light, the swelling can be enhanced from 13 % to 25 %. The cytocompatibility is confirmed by fibroblast cell cultivation experiments, which makes this material also suitable in the field of light induced drug delivery, light manipulated microfluidic systems or light controlled cell cultivation platforms. Additionally, a developed pH skin sensor based on delicate temporary tattoo paper with a pH responsive hydrogel as sensors active material is presented. The response of the fabricated sensors dielectric properties is measured with impedance spectroscopy when exposed to artificial sweat with different pH values between pH 4 and pH 6, verifying the phase shift at 1000 Hz as an excellent pH related parameter. It is also proved, that the sensor can be operated by a non-sophisticated Arduino setup. In this study, for the first time, a vapor-based deposition method is demonstrated to coat a tattoo paper with a responsive polymer, which extends the possible techniques to coat tattoo-based biological applications, such as sweat sensors or wound monitoring systems.

Kurzfassung

Diese Arbeit beschäftigt sich mit Funktionshydrogelen, oder auch smarte Hydrogele genannt, und deren technischen Anwendungen. Smarte Hydrogele sind Polymernetzwerk bestehend aus funktionellen Gruppen welche auf Umwelteigenschaften wie, Temperatur, Licht, pH-Wert, elektrische Felder oder chemische Analyten mit einer Änderung in Hinsicht der Form, der Benetzbarkeit, der optischen -, elektrischen - oder elastischen - Eigenschaften, reagieren. In vielen Fällen sind dünne Schichten auf empfindlichen und strukturierten Oberflächen gefordert. Aus diesem Grund wurde die initiierte chemischen Gasphasenabscheidung (iCVD) als Synthesemethode herangezogen. In einem Teil dieser Arbeit wird eine Adaption von iCVD mittels vibrierender Substrate vorgestellt, um diese Methode zur Beschichtung von pharmazeutischen Pulvern zu erweitern. Des Weiteren werden Hydrogele aus 2-Hydroxyethylmethacrylat (HEMA), vernetzt mit Ethylenglykoldimethacrylat (EGDMA), p(HEMA-co-EGDMA) untersucht. Die Auswertung der Anschwellung der Hydrogele bei steigender Luftfeuchte mittels Flory-Huggings-Theorie zeigt einen abnehmenden Lösungsmittel-Polymer-Wechselwirkungsparameter. Dies deutet auf eine glasartige Hautbildung bei niedriger Luftfeuchte hin, welche durch eine Umordnung der Molekülorientierung bewirkt wird, bei der das unpolare Polymerrückgrat nach außen zeigt um die Oberflächenenergie zu minimieren. Darüber hinaus wird die Oberfläche der p(HEMA-co-EGDMA) Hydrogele mit Azobenzengruppen modifiziert, um ein smartes Hydrogel welches auf Licht reagiert zu erzeugen. Photoanregung induziert in Azobenzene eine Isomerisierung von trans-zu-cis, was einen Anstieg des Dipolmoments bewirkt und in einer wasseraffinen Oberfläche resultiert. Durch Belichtung der funktionalisierten Hydrogele mit UV Licht kann die Wasseraufnahme von 13 % auf 25 % gesteigert werden. Die Zellenverträglichkeit wird durch Fibroblasten-Zellkultivierungsexperimente bestätigt, wodurch sich diese Hydrogele auch für den Bereich der lichtinduzierten Arzneimittelfreisetzung, der lichtmanipulierten mikrofluidischen Systeme oder der lichtgesteuerten Zellkultivierung empfehlen. Ebenso wird ein entwickelter pH Sensor für die Haut auf Basis eines temporären Tattoo Papiers mit einem pH aktiven Hydrogel als Sensormaterial vorgestellt. Die dielektrischen Eigenschaften des Sensors in künstlichem Schweiß mit pH-Werten zwischen pH 4 und pH 6 werden mittels Impedanzspektroskopie ermittelt. Wobei die Phasenverschiebung bei 1000 Hz als hervorragender pH-bezogener Parameter ermittelt wird. Auch wird gezeigt, dass der Sensor mittels einfachem Arduino-Setup betrieben werden kann. In dieser Entwicklung wurde zum ersten Mal eine dampfbasierte Abscheidungsmethode angewendet, um ein Tattoo-Papier mit einem reaktionsfähigen Polymer zu beschichten, was die möglichen Techniken zur Beschichtung von tattoo-basierten biologischen Anwendungen, wie Schweißsensoren oder Wundüberwachungssystemen, erweitert.

Acknowledgements

First, I would like express my sincere gratitude to my supervisor Anna Maria Coclite. Her excellent guidance was and is always based on providing distinguished individual support and encouraging own ideas. Combined with her smart approaches regarding research questions she generated an exceptional working environment in which I could fully develop myself and my scientific skills. She inspired me and shaped my way of thinking. I want to especially thank her for supporting me during my pregnancies and helping me to realize my own research project.

I also want to express my great appreciation for my former supervisor of my Master's thesis, Roland Resel, who provided new insights and invaluable advice also during my PhD time. Moreover, l am most grateful to Francesco Greco for our scientific discussions and collaborations. Furthermore, I would like to thank Harald Kerschbaumer, Birgit Kunert and Elisabeth Stern for their kind help with equipment, chemicals and bureaucracy.

I am grateful to former and current group members and visiting students, Georg Urstöger, Paul Christian, Martin Tazreiter, Paul Salzman, Alberto Perrotta, Julian Pilz, Fabian Muralter, Paul Kindlhofer, Taher Abu Ali, Stefan Pachmajer, Lisanne Demelius and Gianfranco Decandia. Special thanks to Marianne Kräuter and Richard Berger who I am honored to be close friends with. Thank you for sharing our office, time and thoughts, for throwing cheese when it was needed and for educated me with Simpson videos when words were not enough.

Certainly, I am deeply grateful for my family, especially my parents, Ruth and Erwin, for their unconditional love and support throughout my entire live. You have taught me kindness, always have had an open ear for me and sparked my affection to the great mystery of life, the universe and everything. Thank you, also to my siblings, Lisa und Martin for sharing fun and creative times and encouraging me when it was needed.

Last but not least, I am utterly thankful for sharing my life, thoughts and time with my amazing partner Peter and for our two wonderful children, Ria and Finn, who have turned our life completely upside down but also have made it colorful and marvelous. Thank you!

Contents

Chapter I

Introduction of Smart Hydrogels

Understanding and mimicking of matter, structures and their reactions present in nature have become of huge interest in the last decades as an inspiration to design materials with additional functionalities.[1,2] Indeed, such materials which are able to respond to an external condition, such as temperature,[3,4] pressure,[5] electric or magnetic fields,[6,7] light[8] or chemical compounds,[9] are already the decisive basis of many applications, including sensors, actuators or active coatings, among others.[10] The branch of soft matter, including liquids, colloids, polymers, foams, gels and liquid crystals, has gained attention within this research field because of similar properties that can be found in biological systems.[11,12] In the year of 1991, Pierre-Gilles de Gennes, also called the "founding father of soft matter", received the Nobel Prize in physics for studying order phenomena within liquid crystals and polymers.[13] Among others, Pierre-Gilles de Gennes also dedicate himself to the topic of polymer gels.[14,15] These gels comprise of a physically or chemically cross-linked polymer-network and an entrapped solvent, resulting in a macroscopic viscoelastic solid-like appearance while on the molecular length scale a liquid-like behavior is present. Such gels are called hydrogels, if the dispersion solvent is water (see figure 1) and have pervaded our daily live in various applications such as an example contact lenses,[3] disposable diapers,[16] cosmetic or wound gels.[17]

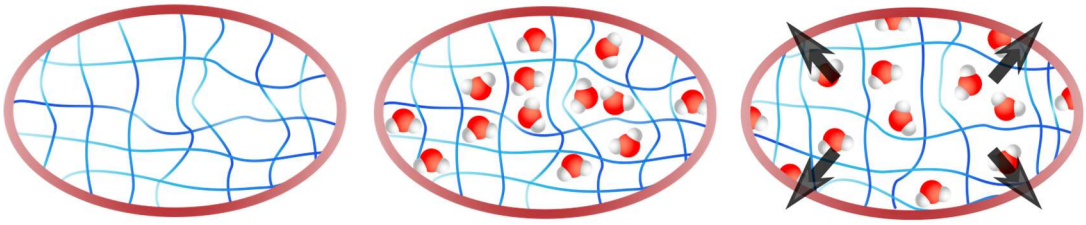

Figure 1: A cross-linked hydrogel swells when water molecules penetrate into the voids of the network matrix.

If additionally, such polymer-network comprise elements that actively change upon exposure to an external stimulus, these materials are named stimuli-responsive or smart hydrogels.[18,19] Nature herself has already evolved stunning smart hydrogel within living tissue.

Around almost every cell within the body exists an extracellular matrix comprised of collagen protein fibers embedding water and also can have responsive behavior such as an example the elastic response towards strain in cartilage or influencing wound healing processes.[20,21] Generally, stimuli, like temperature, pressure,[22] light, humidity, pH, electric fields[23] or chemical analytes, induce a phase change within the hydrogel causing a response in different forms such as swelling or shrinking, change of optical parameters, wettability, dielectric or elastic properties.[18,24] Smart hydrogels gained high potential in versatile biomedical purposes such as drug delivery systems,[25,26] scaffolds for tissue engineering,[27] biosensors and actuators among others.[28] The interest in this topic still increase exponentially, as the publication number about smart hydrogels within the last decades evidences (see figure 2).

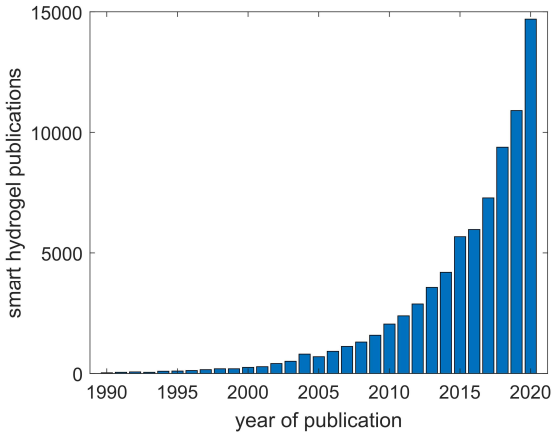

Figure 2. Amount of published papers with the term "smart hydrogel" in time.[*]

The response properties to a certain stimulus of a smart hydrogel is conditioned by its chemical compounds and its microscopic shape. To design a smart hydrogel for a specific function within the research field of material science certain tools are applicable. In first place, the polymerization technique, which are typically divided in solution- and vacuum- based deposition methods. Already divers smart hydrogels as well as self-healing hydrogels were developed with solution-based methods.[29] Drawbacks of these techniques are sometimes the un-conformal coatings caused by surface tension, the inapplicability to certain substrates that might degrade with the used solvents and the entrapment of toxic solvents within the hydrogel. Especially for biological purposes the hydrogel needs to be entirely free of noxious inclusions that might get released during usage. On the other hand, vacuum-based techniques, namely chemical vapor deposition (CVD) methods, are able to synthesize conformal and functional smart hydrogels

[*] Evaluated data referring to the number of results by google-scholar.

within a complet dry direct deposition step. Because of the reduced pressure within a typical CVD process, chemicals adsorb out of the gas-phase on the substrate and react there with radical species or precursors, activated by temperature,[30] plasma,[31] UV-radiation or lasers.[32] The disadvantages of CVD methods are often the costly vacuum setup, the limits towards certain chemicals that cannot be vaporized and the slow growth of films. Nevertheless, these techniques provide an excellent expansion of possible combination of different substrates and homogeneous thin coatings of smart polymer-hydrogels of distinct chemical compositions. Possible CVD methods, including plasma enhanced chemical vapor deposition (PECVD),[33] were reactants are generated by a plasma or initiated chemical vapor deposition (iCVD), were a moderately hot filament (< 280 °C) decomposes the precursor, have been already utilized to synthesize smart responsive hydrogels. While special caution towards the plasma within a PECVD process needs to be considered caused by the destructive nature of the highly energetic ions towards the substrates and the chemicals, the iCVD process, on the other hand, provides conditions with mild pressure (> 100 mTorr) and low substrate temperature (20 - 60 °C) and suits therefor also delicate substrate such as pharmaceutics,[34] tissue paper or even ionic liquids[35]. The iCVD method was invented by the group of Karen Gleason at the Massachusetts Institute of Technology in the year 2005.[36–38] Precursor molecules and the monomer species, which are the building blocks of the synthesized polymer, enter the vacuum chamber as vapors. At a filament, heated to about 250 °C, the precursors labile bond (typically O-O bonds) decompose. The resulting radicals adsorb together with the monomer species at the surface and act as an initiator for the free radical chain polymerization. Because the degradation temperature of the monomers is typically above 350 °C, the functional groups within the monomers can be fully retained during an iCVD deposition.[39–41] Smart hydrogels, responding to temperature, humidity or pH were already successfully polymerized via iCVD[42] in aspects of applications as sensors,[43,44] actuators[45,46] or responsive encapsulation of pharmaceutics,[47] where the drug is entrapped and gets released in the body only at certain conditions.

In the first part of this thesis, fundamental properties of hydrogels in aspects of thermodynamics and kinetics will be discussed. Extending the topic to smart hydrogel with special caution towards stimuli of temperature, humidity, light and pH will be followed by a throughout description of the iCVD process and its use in the domain of smart hydrogel applications. Within this section a study of vibrating substrates within iCVD depositions of powder will be presented that should emphasize the possibility of this methods to also conformal coat pharmaceutical particles with smart encapsulation for drug delivery systems.[48]

The second part focuses on the key analyzation methods used within this work, namely X-ray reflectivity, infrared spectroscopy, spectroscopic ellipsometry and electrochemical

impedance spectroscopy, which were used to characterize the morphology parameters, such as film thickness or surface roughness, chemical composition of hydrogels with different functional groups, optical properties and dielectric and ion-conducting properties. Explicitly focusing on how in-situ measurements can be performed during exposure of the thin smart hydrogel film towards an external stimulus.

In the third part, results of three studies on smart hydrogels deposited via iCVD will be presented. The first being a throughout investigation of a hydrogel responding towards humidity.[49] Although it might seems predictable, that hydrogels respond to humidity, the outcome of this work reveals an interesting behavior at low relative humidity levels. Within the second study, a light responsive biocompatible hydrogel was developed. With a surface functionalization of the hydrogel with azobenzene groups a reversible swelling change when exposed to UV irradiation was achieved.[50] The third study presents a pH skin sensor based on temporary tattoo that utilize a pH responsive hydrogel as active sensing media. This is the first proposed all-polymer tattoo sensor and hydrogel-based pH skin sensor and the first study on vapor deposited smart material on temporary tattoo paper as substrate by now.

I.1 References

1. Cai, G., Ciou, J. H., Liu, Y., Jiang, Y. & Lee, P. S. Leaf-inspired multiresponsive MXene-based actuator for programmable smart devices. *Sci. Adv.* **5**, 1–12 (2019).

2. Zhang, M. *et al.* 3D printing of Haversian bone-mimicking scaffolds formulticellular delivery in bone regeneration. *Sci. Adv.* **6**, (2020).

3. Liu, B. W. *et al.* Synthesis and self-assembly of CO2-temperature dual stimuli-responsive triblock copolymers. *Macromolecules* **47**, 2938–2946 (2014).

4. Qin, Z. *et al.* Atomically precise nanoclusters with reversible isomeric transformation for rotary nanomotors. *Nat. Commun.* **11**, 1–6 (2020).

5. Yu, X. *et al.* Graphene-based smart materials. *Nat. Rev. Mater.* **2**, 1–14 (2017).

6. Cho, H. *et al.* Mechano-thermo-chromic device with supersaturated salt hydrate crystal phase change. *Sci. Adv.* **5**, 1–9 (2019).

7. Ghamkhari, A., Ghorbani, M. & Aghbolaghi, S. A perfect stimuli-responsive magnetic nanocomposite for intracellular delivery of doxorubicin. *Artif. Cells, Nanomedicine Biotechnol.* **46**, S911–S921 (2018).

8. Garg, S. *et al.* Conductance Photoswitching of Metal–Organic Frameworks with Embedded Spiropyran. *Angew. Chemie - Int. Ed.* **58**, 1193–1197 (2019).

9. Li, Y. *et al.* Smart polymer-based calcium-ion self-regulated nanochannels by mimicking the biological Ca2+-induced Ca2+ release process. *NPG Asia Mater.* **11**, (2019).

10. Liu, Y., Mu, L., Liu, B. & Kong, J. Controlled switchable surface. *Chemistry - A European Journal* vol. 11 2622–2631 (2005).

11. Nawrotek, K. Current Approaches to Peripheral Nervous Tissue Regeneration – Mimicking Nature. A review. *J. Res. Innov. Nat. Med. Heal. Sci.* **1**, 16–33 (2015).

12. Vatankhah-Varnosfaderani, M. *et al.* Mimicking biological stress–strain behaviour with synthetic elastomers. *Nature* **549**, 497–501 (2017).

13. De Gennes, P. G. Soft matter. *Science (80-.).* **256**, 495–497 (1992).

14. De Gennes, P. G., Hébert, M. & Kant, R. Artificial muscles based on nematic gels. *Macromol. Symp.* **113**, 39–49 (1997).

15. De Gennes, P. G. Liquid-liquid demixing inside a rigid network. Qualitative features. *J. Phys. Chem.* **88**, 6469–6472 (1984).

16. Chawla, P., Ranjan Srivastava, A., Pandey, P. & Chawla, V. Hydrogels: A Journey from Diapers to Gene Delivery.

17. Wasiak, J., Cleland, H., Campbell, F. & Spinks, A. Dressings for superficial and partial thickness burns. *Cochrane Database of Systematic Reviews* vol. 2013 (2013).

18. Nath, N. & Chilkoti, A. Creating 'smart' surfaces using stimuli responsive polymers. *Adv. Mater.* **14**, 1243–1247 (2002).

19. Echeverria, C., Fernandes, S., Godinho, M., Borges, J. & Soares, P. Functional Stimuli-Responsive Gels: Hydrogels and Microgels. *Gels* **4**, 54 (2018).

20. Sutherland, A. J., Converse, G. L., Hopkins, R. A. & Detamore, M. S. The bioactivity of cartilage extracellular matrix in articular cartilage regeneration. *Adv. Healthc. Mater.* **4**, 29–39 (2015).

21. Fick, J. M., Thambyah, A. & Broom, N. D. Articular cartilage compression: How microstructural response influences pore pressure in relation to matrix health. *Connect. Tissue Res.* **51**, 132–149 (2010).

22. Hiratani, T., Kose, O., Hamad, W. Y. & Maclachlan, M. J. Stable and sensitive stimuli-responsive anisotropic hydrogels for sensing ionic strength and pressure. *Mater. Horizons* **5**, 1076–1081 (2018).

23. Longo, G. S., Olvera De La Cruz, M. & Szleifer, I. Controlling swelling/deswelling of stimuli-responsive hydrogel nanofilms in electric fields. *Soft Matter* **12**, 8359–8366 (2016).

24. Maji, S., Jerca, V. V., Jerca, F. A. & Hoogenboom, R. Smart polymeric gels. in *Polymeric Gels* 179–230 (Elsevier, 2018). doi:10.1016/b978-0-08-102179-8.00007-7.

25. Perrotta, A., Werzer, O. & Coclite, A. M. Strategies for Drug Encapsulation and Controlled Delivery Based on Vapor-Phase Deposited Thin Films. *Adv. Eng. Mater.* **20**, 1–21 (2018).

26. Sun, Z., Song, C., Wang, C., Hu, Y. & Wu, J. Hydrogel-Based Controlled Drug Delivery for Cancer Treatment: A Review. *Mol. Pharm.* **17**, 373–391 (2020).

27. Park, H. J. *et al.* Paper-based bioactive scaffolds for stem cell-mediated bone tissue engineering. *Biomaterials* **35**, 9811–9823 (2014).

28. Wang, T. *et al.* Bioinspired Smart Actuator Based on Graphene Oxide-Polymer Hybrid Hydrogels. *ACS Appl. Mater. Interfaces* **7**, 23423–23430 (2015).

29. Tanan, W., Panichpakdee, J. & Saengsuwan, S. Novel biodegradable hydrogel based on natural polymers: Synthesis, characterization, swelling/reswelling and biodegradability. *Eur. Polym. J.* **112**, 678–687 (2019).

30. Zhao, X., Wei, C., Gai, Z., Yu, S. & Ren, X. Chemical vapor deposition and its application in surface modification of nanoparticles. *Chem. Pap.* **74**, 767–778 (2020).

31. Coclite, A. M. & Gleason, K. K. Initiated PECVD of organosilicon coatings: A new strategy to enhance monomer structure retention. *Plasma Process. Polym.* **9**, 425–434 (2012).

32. Goto, T. Thermal barrier coatings deposited by laser CVD. *Surf. Coatings Technol.* **198**, 367–371 (2005).

33. Kim, H. J. *et al.* Highly sensitive three-dimensional interdigitated microelectrode biosensors embedded with porosity tunable hydrogel for detecting proteins. *Sensors Actuators, B Chem.* **302**, 127190 (2020).

34. Werzer, O., Tumphart, S., Keimel, R., Christian, P. & Coclite, A. M. Drug release from thin films encapsulated by a temperature-responsive hydrogel. *Soft Matter* **15**, 1853–1859 (2019).

35. Krauter, M., Tazreiter, M., Perrotta, A. & Coclite, A. M. Deposition of Ion-Conductive Membranes from Ionic Liquids via Initiated Chemical Vapor Deposition. *Macromolecules* **53**, 7962–7969 (2020).

36. Chan, K. & Gleason, K. K. Initiated chemical vapor deposition of linear and cross-linked poly(2-hydroxyethyl methacrylate) for use as thin-film hydrogels. *Langmuir* **21**, 8930–8939 (2005).

37. Lau, K. K. S. & Gleason, K. K. Initiated Chemical Vapor Deposition (iCVD) of poly(alkyl acrylates): A kinetic model. *Macromolecules* **39**, 3695–3703 (2006).

38. Lau, K. K. S. & Gleason, K. K. Initiated Chemical Vapor Deposition (iCVD) of poly(alkyl acrylates): An experimental study. *Macromolecules* **39**, 3688–3694 (2006).

39. Tenhaeff, W. E. & Gleason, K. K. Initiated and oxidative chemical vapor deposition of polymeric thin films: ICVD and oCVD. *Adv. Funct. Mater.* **18**, 979–992 (2008).

40. Coclite, A. M. *et al.* 25th Anniversary Article: CVD polymers: A new paradigm for surface modification and device fabrication. *Adv. Mater.* **25**, 5392–5423 (2013).

41. Alf, M. E. *et al.* Chemical vapor deposition of conformal, functional, and responsive polymer films. *Adv. Mater.* **22**, 1993–2027 (2010).

42. Coclite, A. M. Smart surfaces by initiated chemical vapor deposition. *Surf. Innov.* **1**, 6–14 (2013).

43. Buchberger, A., Peterka, S., Coclite, A. M. & Bergmann, A. Fast optical humidity sensor based on hydrogel thin film expansion for harsh environment. *Sensors (Switzerland)* **19**, 1–11 (2019).

44. Muralter, F., Greco, F. & Coclite, A. M. Applicability of Vapor-Deposited Thermoresponsive Hydrogel Thin Films in Ultrafast Humidity Sensors/Actuators. *ACS Appl. Polym. Mater.* **2**, 1160–1168 (2020).

45. Tufani, A. & Ozaydin Ince, G. Protein gating by vapor deposited Janus membranes. *J. Memb. Sci.* **575**, 126–134 (2019).

46. Oh, M. S. *et al.* Control of Reversible Self-Bending Behavior in Responsive Janus Microstrips. *ACS Appl. Mater. Interfaces* **8**, 8782–8788 (2016).

47. Werzer, O., Tumphart, S., Keimel, R., Christian, P. & Coclite, A. M. Drug release from thin films encapsulated by a temperature-responsive hydrogel. *Soft Matter* **15**, 1853–1859 (2019).

48. Unger, K. & Coclite, A. M. Conformal coating of powder by initiated chemical vapor deposition on vibrating substrate. *Pharmaceutics* **12**, 1–11 (2020).

49. Unger, K., Resel, R. & Coclite, A. M. Dynamic Studies on the Response to Humidity of Poly (2-hydroxyethyl methacrylate) Hydrogels Produced by Initiated Chemical Vapor Deposition. *Macromol. Chem. Phys.* **217**, 2372–2379 (2016).

50. Unger, K. *et al.* Novel Light-Responsive Biocompatible Hydrogels Produced by Initiated Chemical Vapor Deposition. *ACS Appl. Mater. Interfaces* **9**, 17408–17416 (2017).

Chapter II

Fundamentals of Smart Hydrogels

This chapter provides insight about thermodynamic descriptions and kinetics of swelling of hydrogels and smart hydrogels responding to pH, light and temperature. Further a description of initiated chemical vapor deposition will be followed by state-of-the-art applications of smart hydrogels deposited via initiated chemical vapor deposition.

II.1 Thermodynamic Description of Hydrogels

The first thermodynamic description of gel-solvent swelling interaction was done by M.L. Huggins, P.J. Flory and J. Rehner in the year 1943. In thermodynamic equilibrium the Helmholtz free energy F of a system is minimized. Within the Flory-Rehner theory,[1] the change of the free energy when a slightly cross-linked gel and a solvent intermix can be seen as a sum of a term corresponding due to mixing ΔF_{mix} and another one due to elastic deformation due to entanglement of the polymer chains ΔF_{el}.

$$\Delta F = \Delta F_{mix} + \Delta F_{el} \qquad II - 1$$

Although the assumptions within this theory (such as incompressible molecules, no contribution of ionic groups in the change of the free energy or that the overall thickness increase is proportional to the elongation of single chains) simplify the system drastically, the proposed description can help understand and interpret the experimental results.

The contribution of ΔF_{mix} can be described by the Flory-Huggins solution theory.[2,3] Starting with

$$\Delta F_{mix} = \Delta U_{mix} + T\Delta S_{mix} \qquad II - 2$$

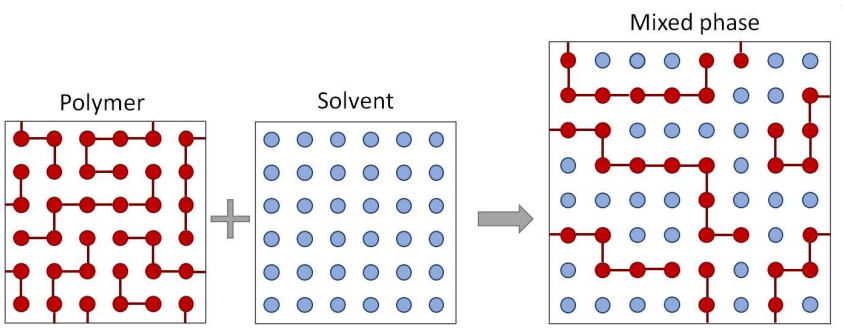

Figure 3: Schematic of intermixing of a polymer with a solvent according to Flory-Huggins theory.

With ΔU_{mix} the change of the inner energy, T the temperature and ΔS_{mix} the change in the entropy. The change in the inner energy can be derived with the assumption, that the n_m monomer units within the polymer and n_s solvent molecules occupy lattice sites with Z neighbors (see figure 3). If the polymer and the solvent intermix three interaction needs to be considered namely, the solvent-solvent interaction ε_{SS}, the solvent-monomer interaction ε_{SM} and the monomer-monomer interaction ε_{MM}. The change of ΔU_{mix} is then derived with:

$$\Delta U_{mix} = U_{S+M} - U_S - U_M$$
$$= Z(\phi_S^2 \varepsilon_{SS} + 2\phi_S \phi_M \varepsilon_{SM} + \phi_M^2 \varepsilon_{MM}) - \frac{Z}{2}\phi_S \varepsilon_{SS} - \frac{Z}{2}\phi_M \varepsilon_{MM} \qquad II - 3$$

$$\Delta U_{mix} = \frac{Z}{2}\phi_S \phi_M (2\varepsilon_{SM} - \varepsilon_{SS} - \varepsilon_{MM}) \qquad II - 4$$

$$\frac{1}{k_B T}\Delta U_{mix} = \chi \phi_S \phi_M \qquad II - 5$$

$$\chi := \frac{Z}{k_B T}(2\varepsilon_{SM} - \varepsilon_{SS} - \varepsilon_{MM}) \qquad II - 6$$

With $\varphi_{S/M}$ being the density $n_{S/M}/(n_S + n_M)$ and $\varphi_S + \varphi_M = 1$ of species in the lattice.

The entropic term of the starting configuration of total separated phases is 0. When the polymer and the solvent intermix the entropic term in respect to one lattice site is the Boltzmann constant k_B times the natural logarithm of the number of microstates n.

$$S_{mix} = \frac{k_B}{n}\left(ln(n!) - ln(n_S!) - ln(n_M!)\right) \qquad II - 7$$

$$ln\,(a!) = a\,ln(a)\; -\; a \qquad \textit{II - 8}$$

$$S_{mix} = -k_B\left(\phi_S\,ln\,(\phi_S) + \phi_M ln\,(\phi_M)\right) \qquad \textit{II - 9}$$

Finally leading to the free energy of mixing:

$$\frac{1}{k_B T}\Delta F_{mix} = \overbrace{\chi\phi_S\phi_M}^{\Delta U_{mix}} + \overbrace{\phi_S\,ln\,(\phi_S) + \phi_M ln\,(\phi_M)}^{\Delta S_{mix}} \qquad \textit{II - 10}$$

The elastic contribution ΔF_{el} is an entropic energy loss caused by the entanglement of the N_c polymer chain. With V being the volume per atom:[4]

$$\Delta S_{el} = \frac{3N_c k_B}{2}(ln(\alpha)\; -\; \alpha^2 + 1) \qquad \textit{II - 11}$$

$$\alpha := \left(\frac{V}{V_0}\right)^{\frac{1}{3}} \qquad \textit{II - 12}$$

With ΔF_{el}= -TΔS_{el}, and inserting ΔF_{el} and ΔF_{mix} of equation II - 10 into equation II - 1, the following term for the overall free energy can be derived.

$$\frac{1}{k_B T}\Delta F = \overbrace{\chi\phi_S\phi_M + \phi_S\,ln\,(\phi_S) + \phi_M ln\,(\phi_M)}^{\Delta F_{mix}} + \overbrace{\frac{3N_c k_B}{2}(\,\alpha^2 - ln(\alpha)\; - 1)}^{\Delta F_{el}} \qquad \textit{II - 13}$$

The derived equation has only one material related parameter, which is the polymer solvent interaction, or also called Flory-Huggins parameter χ. Typically, this parameter for a certain polymer solvent system is derived empirically. If $\chi < 0.5$, the solvent molecules can easily penetrate into the polymer network while if $\chi > 0.5$, the solvent is considered with poor solvability towards the polymer.[5]

For smart hydrogels χ exhibits a drastic change in a certain environmental domain depending on temperature, pressure, light, pH, electric or magnetic fields or chemical compounds. Within the Flory-Rehner theory, χ is dependent on the temperature, the polymer-polymer, polymer-solvent and solvent-solvent interaction. Within a certain stimuli domain χ can exhibit a

drastic change caused by new interactions such as an example, new dipol-dipol interactions caused by temperature or photoisomerization or ionic interactions caused by a change in the pH. While below a critical point during a stimulus domain, $\chi < 0.5$ resulting in a dominating entropic term $-T\Delta S$ compared to the inner energy ΔU and mixing is preferred.[6] At a critical point the inner energy and the entropic term are of similar scale, resulting in two mixed phases while above the critical point the system completely de-mix, as can be seen in figure 4.

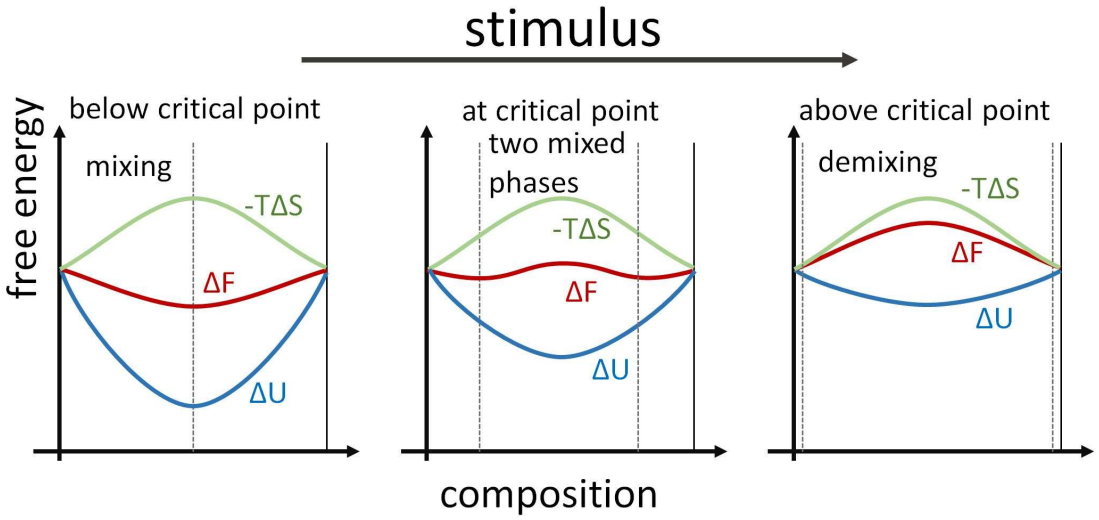

Figure 4: Free energy of a smart hydrogel exposed to its stimulus.

II.2 Kinetics of Swelling

While so far just equilibrium hydrogel swelling referring to a steady-state was described, in this section the transient behavior of the hydrogel from one equilibrium state to another will be in focus. The swelling in time of a hydrogel immersed in water is driven by the gradient of concentration of water species from the surface to the inner volume of the hydrogel which induces a difference in chemical potential. Most models for dynamic hydrogel swellings are based on Fick's laws, which describes the diffusion flux J caused by a concentration gradient. Fick's second law, relating the diffusion, or change of concentration in time $\partial c/\partial t$, with the diffusion coefficient D, and the change in concentration c:

$$\frac{\partial c}{\partial t} = \Delta\,(D\,\Delta c) \qquad \textit{II - 14}$$

Convection effects, typically present in hydrogels at the glassy front between solvent and hydrogel molecules, need to be considered.[7] Therefore, a term with the convective velocity v needs to be added:[8]

$$\frac{\partial c}{\partial t} = \Delta\,(D\,\Delta c) - v\,\nabla \mathrm{c} \qquad \textit{II - 15}$$

This partial differential equation is typically not analytically solvable. Approaching this problem, different categories of methods have been derived including the most common one: the approximation and the numerical calculation. The numerical approach is typically done for complex 3D structures via finite element method.[9] The space within the structure is divided by a small mesh resulting in subparts called finite elements. Within one of these elements the solution can be obtained by an approximation of the function.

But often an approximation calculation provides a good enough description, without having to apply the finite element analysis. Plenty of approximation solutions have been derived for different hydrogels and purposes.[10,11] Of these, the two most common will be presented. The first one is the "power law", proposed by Peppas et. al, that express the change in volume ΔV by a function k multiplied by the time t to the power of an adjustable parameter:[12]

$$\Delta V = k t^{n} \qquad \textit{II - 16}$$

If $n = 1/2$, the diffusion would be purely Fickian, while if $n = 1$, the diffusion would be convectional driven. Values of n between ½ and 1 result in anomalous diffusion (see figure 5).

The second approximation method was proposed by Berens-Hopfenberg and describes the swollen thickness M_t/M_∞ with a converging exponential curve, with A and b being adjustable parameters:[13]

$$\frac{M_t}{M_\infty} = \left(1 - A\, e^{-bt}\right) \qquad \textit{II - 17}$$

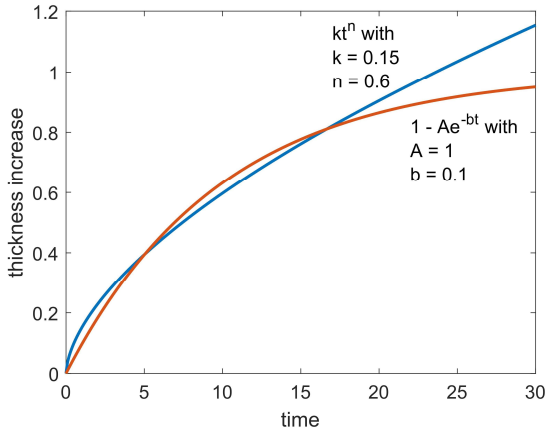

Figure 5: Comparison of the Power law and the Berens-Hopfenberg law models for the variation of swelling in time.

II.3 Smart Hydrogels

A smart hydrogel exhibits a change in the swelling when exposed to a certain stimulus, as presented in figure 6.[14] Possible stimuli are humidity, pressure, light, pH, electromagnetic fields or temperature. In the followed section, temperature, pH and light responsive hydrogels will be briefly discussed.

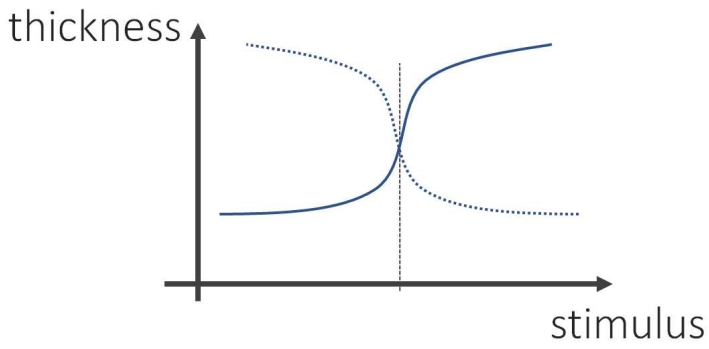

Figure 6: Smart hydrogel swelling when exposed to an external stimulus. The thickness increase can either be a positive sigmoidal shaped curve related to a water uptake, or a negative one related to a water release.

II.3.1 pH Responsive Hydrogels

The polymer-chain of a pH responsive hydrogel has weak acid (or base) functional groups incorporated.[15,16] With increasing pH such polymers exhibit a phase transition at the materials dissociation constant pKα. If the functional groups are acids, below pKα the acidic groups are fully protonated and orient towards each other, which results in a collapsed and shrunken hydrogel. Above pKα, the acid group releases a proton resulting in ionized side chains within the polymer which repel each other, creating open voids in the hydrogel where water molecules are incorporated. On the opposite, if the functional groups are bases, below pKα, the groups will be positively ionized and swollen, while above pKα the groups will be protonated and collapsed.

II.3.2 Temperature Responsive Hydrogels

Among the possible stimuli of responsive hydrogels, temperature is the most studied one.[17–19] The swelling of temperature responsive hydrogel in the temperature domain exhibits a phase transition at the critical temperature. If the system changes with heat to a phase separated state, i.e. a shrunken or collapsed hydrogel, the critical temperature is called lower critical solution temperature (LCST), while if the hydrogel changes from a shrunken to a swollen state with the temperature, the critical temperature is called upper critical solution temperature (UCST). The most explored temperature responsive hydrogels are polymers containing of N-isopropylacrylamide (NIPAAm). In water, upon heating the polymer contracts while upon cooling swells, fully reversibly. With a typical LCST in water of ~32 °C, these polymers gained attraction in the field of biomedicine.[20–23] An example of a thin film NIPAAm swelling curve upon heating from 27 °C to 48 °C is depicted in figure 7. The thickness during the temperature ramp decreases from 122 nm to 103 nm. The color change of a thin film hydrogel sample upon exposure to the stimulus is caused by interference phenomena related to the film thickness. In figure 8 a NIPAAm thin film was deposited on a wafer substrate. To blue color indicating a film thickness of around 100 nm. When cooled, the color changes to orange, which is related to a thickness increase to about 200 nm.

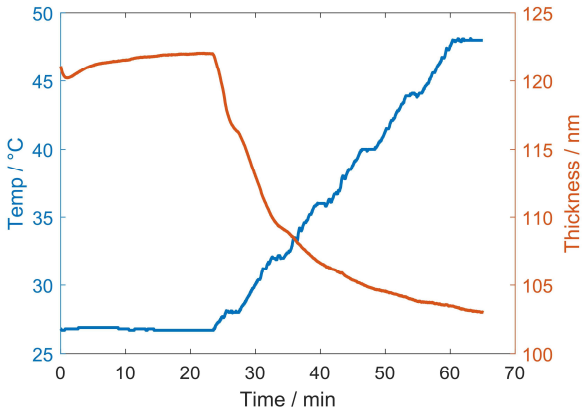

Figure 7: NIPAAm thickness during ramping of the temperature.

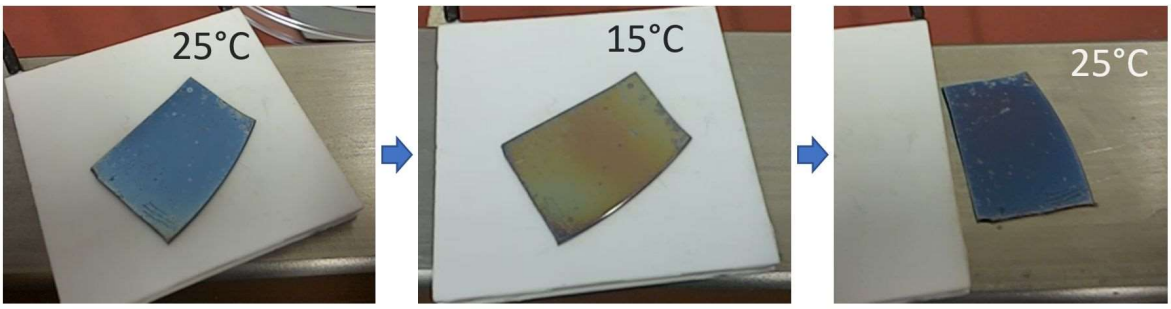

Figure 8: NIPAAm thin film on silicon wafer substrate. The color of the thin film is due to interference dependent on the thin film thickness and the reflective index. When cooled, the humidity in air cause the hydrogel to swell and the color changes from blue (~100 nm) to orange (~ 200 nm).

II.3.3 Light Responsive Hydrogel

The advantages of light as an external stimulus are extensive. Not only the stimulus can be provided non-invasively, moreover it can be performed spatially discrete with only little thermal impact. Photochromic moieties are attached as functional groups to the polymer backbone.[24,25] With irradiation these molecules convert light into a photoreaction, such as isomerization, cleavage or dimerization (see figure 9). The most common photoactive compound in this section is azobenzene.[26] With irradiation of UV light, it isomerizes from trans to cis configuration which results in a dipole moment change from 0 to 3 Debye.

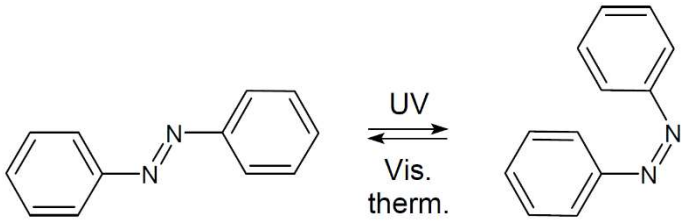

Figure 9: Azobenzene within a hydrogel polymer chain. With photo-isomerization azobenzene change from trans-to-cis, which is reversible with temperature or irradiation with green light.

II.4 Initiated Chemical Vapor Deposition

Initiated chemical vapor deposition (iCVD) is a vacuum based deposition method where the monomer and precursor species are delivered out of their gas-phase. At a hot filament, the precursor molecules decompose and form radicals which react further with monomer species as can be seen in figure 10. The great advantage of iCVD compared to traditional CVD, where the substrate temperature is elevated to the decomposition temperature of the monomers, is that the filament temperature is low enough to selectively trigger only the initiator decomposition. In addition, the substrate temperature can be kept low, allowing moderate process conditions for the substrate.[27–30] A schematized iCVD process is illustrated in figure 10.

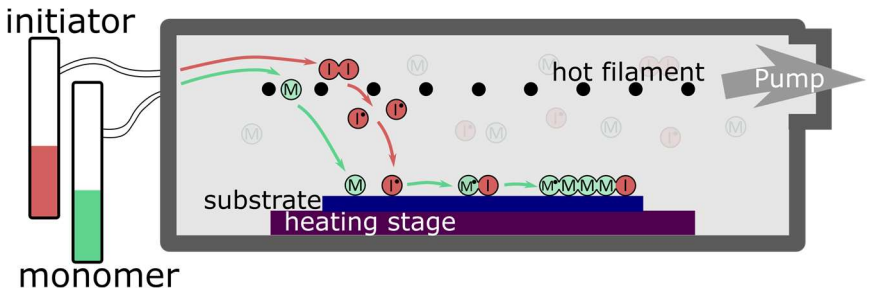

Figure 10: Schematic of an iCVD reactor with the polymerization steps. The initiator is fed into the reactor and decompose at the hot filament. The monomer species retain structure because the decomposition temperature is above the temperature of the hot filament. At the substrate the free radical chain polymerization processes.

Within the iCVD process the polymers are formed via free radical chain polymerization.[31] A precursor species decomposes at the filament into two initiator radicals. Commonly used compounds are peroxides, as the labile O-O bonds homolytic dissociate at temperatures of about < 200 °C which is typically smaller as the dissociation temperature of the monomer species (> 350 °C). In the following chemical equations R_x denotes attached chemical groups.

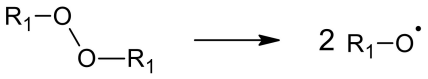

II - 18

The monomer species typically need to comprise a vinyl bond which reacts with the radical and together forms a chain radical. While the vinyl bond is needed for the polymer backbone, the attached chemical groups R_x enables the possibility to functionalize the gained polymer. By carefully choosing proper monomer species, the synthesized polymer gets its final mechanical and responsive properties.

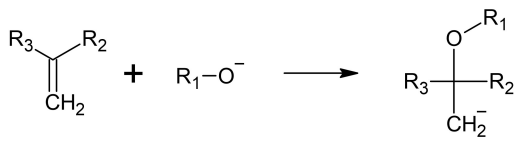

II - 19

By repeatedly adding monomer species to the chain, a polymers propagation can contain thousands to hundred-thousands of monomer units. The growth stops with a final termination step. A radical chain reacts with another radical, which can be either an initiator radical or more likely a chain radical. The terminated chain is neutral and the chain growth stops.

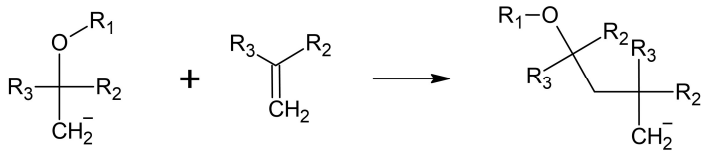

II - 20

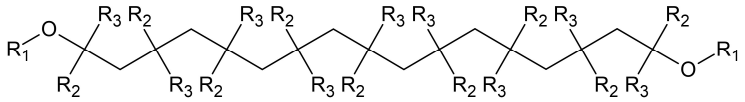

II - 21

Considering ideal gases, within the process the partial pressure p_M of each species in relation to its saturation pressure p_{Sat} gives a relative information about the amount of monomer species on the surface. As a rule of thumb, the relation of p_M over p_S should be below 0.7 during iCVD depositions as otherwise condensation of the gases on the surface have to be expected.

$$\frac{p_M}{p_{Sat}} < 0.7 \qquad \textit{II - 22}$$

Typically, during an iCVD deposition the thin film growth can be monitored in-situ with laser interferometry as depicted in figure 11, therefore, highly controllable thicknesses can be achieved.

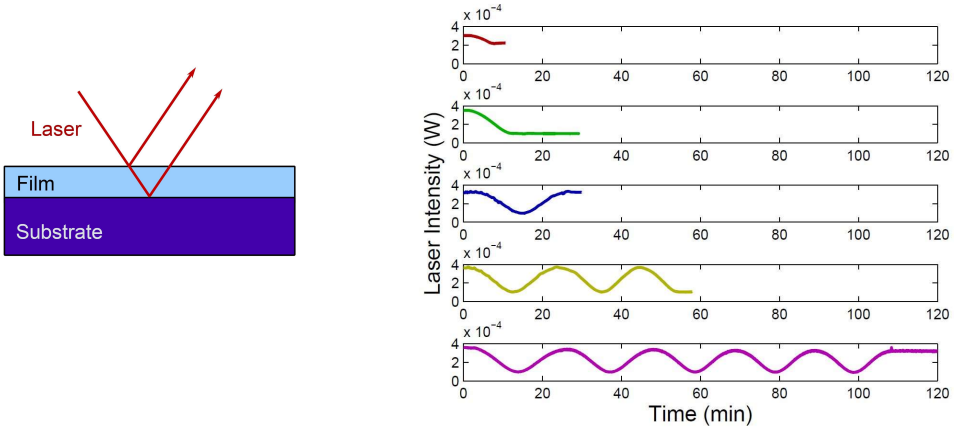

Figure 11: Schematic of laser interferometry and results of laser intensity of 5 depositions of different achieved thicknesses of 50 nm, 100 nm, 200 nm, 500 nm and 1000 nm.

II.5 Conformal Coating of Powder by Initiated Chemical Vapor Deposition on Vibrating Substrate

pharmaceutics

Conformal Coating of Powder by Initiated Chemical Vapor Deposition on Vibrating Substrate

by Katrin Unger and Anna Maria Coclite *

Institute of Solid State Physics, Graz University of Technology, 8010 Graz, Austria

* Author to whom correspondence should be addressed.

Pharmaceutics **2020**, *12*(9), 904; https://doi.org/10.3390/pharmaceutics12090904

Received: 16 July 2020 / Revised: 2 September 2020 / Accepted: 18 September 2020 / Published: 22 September 2020

(This article belongs to the Special Issue Coating Design: From Nanoparticle to Solid Dosage)

Reference: Katrin Unger, Anna Maria Coclite; Conformal coating of powder by initiated chemical vapor deposition on vibrating substrate. *Pharmaceutics* **12**, 1–11 (2020).

II.5.1 Preface

This report was conducted at the Graz University of Technology. The thesis' author designed the modification of the iCVD reactor, provided the sample preparation, performed the experimental characterizations, data evaluation and wrote the manuscript. Anna Maria Coclite supervised the project and helped in the manuscript preparation. The presented contribution is reproduced identical in text and illustration with permission from the publisher.

II.5.2 Abstract

Encapsulation of pharmaceutical powders within thin functional polymer films is a powerful and versatile method to modify drug release properties. Conformal coating over the complete surface of the particle via chemical vapor deposition techniques is a challenging task due to the compromised gas–solid contact. In this study, an initiated chemical vapor deposition reactor was adapted with speakers and vibration of particles was achieved by playing AC/DC's song "Thunderstruck" to overcome the above-mentioned problem. To show the possibilities of this method, two types of powder of very different particle sizes were chosen, magnesium citrate (3–10 μm, cohesive powder) and aspirin (100–500 μm, good flowability), and coated with poly-ethylene-glycol-di-methacrylate. The release curve of coated magnesium citrate powder was retarded compared to uncoated powder. However, neither changing the thickness coating nor vibrating the powder during the deposition had influence on the release parameters, indicating, that cohesive powders cannot be coated conformally. The release of coated aspirin was as well retarded as compared to uncoated aspirin, especially in the case of the powder that vibrated during deposition. We attribute the enhancement of the retarded release to the formation of a conformal coating on the aspirin powder.

Keywords: iCVD; initiated chemical vapor deposition; powder coating; conformal coating; vibrating substrate; vibrating powder; thunderstruck; encapsulation of particles

II.5.3 Introduction

Current coating techniques for encapsulating pharmaceutical powders within polymer films are typically wet spray-based methods. A polymer-solution, -suspension or -emulsion gets atomized into small droplets and floats within a hot carrier gas on a fluidized powder bed. After drying, a thin polymer film with well-defined properties is covering the particles [1]. Even though this technique provides a large variety of coated forms, it is not applicable to all polymers and pharmaceutical powders as toxic solvents may remain in the structure or the pharmaceutics may degenerate under the harsh process conditions. A dry synthesis, such as chemical vapor deposition (CVD) technique, of the polymer directly on the pharmaceutical particles surface are preferential as contaminations with solvents can be neglected [2,3].

Among the possible chemical vapor deposition methods, initiated chemical vapor deposition (iCVD) suits the requirements to coat pharmaceutics as it operates without plasma, works under mild pressure (>100 mTorr) and low substrate temperature (20–60 °C) and is, therefore, also suitable for delicate substrates such as tissue paper, pharmaceutics or even ionic

liquids [4–6]. iCVD was invented in 2005 by the group of Karen Gleason at the Massachusetts Institute of Technologies and is a vacuum-based free radical polymerization technique [7–9]. The initiator species are decomposed by a relatively hot filament (<280 °C) and start the polymerization. At this temperature the monomer species do not degrade, thus their functionality can be retained during the deposition [10–12]. Although iCVD seems to be a promising technique to coat pharmaceutical powders or particles, there are only few works on this topic [13–16]. The standard iCVD reactors fit perfectly the requirements to ensure efficient gas–solid contact on substrates where all surfaces can be reached by the vapors. Indeed, already tubes, overhanging structures or fibers in the sub-micrometer region have been successful conformally coated [16–19]. Obtaining a conformal coating on powders is more difficult because of the several contact areas among the particles, which prevent the vapors to absorb or diffuse on the whole particle surface. This is especially the case for pharmaceutical powders, compared to other powders such as catalytical powders, which need to be conformally coated over the complete surface area. Since drug release times typically increase with the coating thickness [3]. If a defect—in terms of a non-coated or only little coated area—is present, this point acts as a door that opens easily and lets the drug dissolve through it more quickly than desired. Typical coating techniques for pharmaceutical powders impose movements of the particles to cope with this problem. The previous studies on iCVD particle coatings ensured a good gas–solid contact either by using a 360°-degree rotary cylinder reactor [14] or by manually shaking the powder [15]. The first solution is elegant but needs an elaborate setup. In the second, the deposition process needs to be interrupted several times to open the reactor to manually shake the powder. The drawbacks of this technique are that it does not provide a continuous polymerization throughout the thickness, has statistical non-conformal coating thicknesses and takes a lot of time.

In this study, speakers were introduced in the reactor to shake pharmaceutical powder during the iCVD process. Utilizing sonic vibration during chemical vapor depositions has already proven to enhance the coatings' conformality on particles [20,21]. Explicitly, a vibration by a non-monotonic frequency is recommended, as played in AC/DC's song "Thunderstruck", because it leads to chaotic motion which is beneficial compared to movements caused by monotonic frequencies [22]. The modification of the reactor is easy and can be applied to all common vacuum reactors. For comparison, the powders were also coated on a non-vibrating stage. This configuration, where the gases flow over the particles which do not move, is called flat hearth [3]. For the coating, a polymer of ethylene-glycol-di-methacrylate (p-EGDMA) was chosen. Typically, this monomer is used as a crosslinker in functional polymers to ensure water stability [23,24]. As a homo polymer it forms a strong network that is water-resistant. This monomer

was chosen because of its bio-compatibility [25], it is easy to deposit and is a non-functional homo polymer.

Proper model powders for this preliminary study were chosen following the theory of Geldart. In this theory powders can be classified in terms of particle size and density which can be linked to how easy they can be fluidized via gases [26]. Although the theory is about fluidized powder beds and not about in vacuum vibrating powders, the principles, like particle interaction, are also valid in vacuum. The theory classifies powders in four groups. The easiest powders to fluidize fall into groups A and B. Group A gathers powders with small particle size (20–150 μm) and density smaller than 2 g/cm3, while group B contains powders composed of particles with a size of 40 μm to 500 μm and a density range between 1–4 g/cm3. Group C contains powders which are cohesive mainly due to their small particle size (<20 μm), strong electrostatic forces and Van der Waals attraction. These powders are difficult to fluidize as the attraction forces among the particles dominate over external applied forces. Finally, group D includes the large particles (>500 μm). Powder beds of this group exhibits only little expansion due to fluidization resulting in a poor gas–solid contact.

In this study, two powders were chosen, magnesium citrate and aspirin, which belong to the group C and the group B, respectively. Magnesium citrate is a common dietary supplement and used as food additive to regulate acidity. Further, it is hygroscopic, highly water soluble and has an excellent bioavailability [27,28]. Typically, the powder is white, has a small particle size (<20 μm) and is cohesive with the tendency to agglomerate into clusters. The second powder is aspirin which is a known pain killer and, further, used to treat fever and inflammation [29]. Although it is poorly water soluble it has a good bioavailability due to the good solvability in acid environment, as present in human stomach. The chosen aspirin has a particle size of around 200 μm and falls into group B. The powder can be easily fluidized and gases then have access to the complete particle surface.

II.5.4 Materials and Methods

Film Preparation

The magnesium citrate powder (by Gatt-Koller—Pharmazeutika, Graz, Austria) and the aspirin powder (Herba Chemosan Apotheker-AG, Graz, Austria) were coated with a polymer of ethylene glycol-dimethacrylate (EGDMA, Aldrich 98%, Vienna, Austria) via iCVD in a custom-built reactor, described elsewhere [30]. The *te*rt-Butyl peroxide (TBPO, Aldrich 98%, Vienna, Austria), which acts as initiator, as well as the EGDMA, were used without further purification and were fed into the reactor with a flowrate of (1.00 ± 0.03) sccm and (0.15 ± 0.02) sccm, respectively. While the TBPO jar was kept at room temperature, the EGDMA monomer was heated to 80 °C. The working pressure during the deposition was 500 mTorr. The temperature of the sample holder was kept at 30 ± 2 °C by a chiller/heater system (Thermo Scientific Accel 500 LC, Thermo Fisher Scientific, Karlsruhe, Germany). The initiator molecules were thermally decomposed by a filament array of nickel-chromium wires (Goodfellow, UK), heated to 270 ± 5 °C. The film thickness was monitored in situ via laser interferometry (He–Ne Laser with λ = 633 nm, Thorlabs GmbH, Dachau, Germany) with a reference silicon wafer sample. The magnesium citrate powder and the aspirin powder were placed in petri dishes.

The magnesium citrate and the aspirin powders were coated simultaneously in the same deposition run. The thickness of the deposition was tracked on a reference silicon wafer which was in an additional petri dish. Afterwards the thickness of the p-EGDMA coating on the silicon wafers was measured via spectroscopic ellipsometry (J. A. Woollam ESM-300) with a spectral region from 370 to 1000 nm under four different incident angles (60°, 65°, 70°, 75°). The data were fitted with a three-layer model containing a silicon and a native silicon (2 nm) layer as substrate and a Cauchy layer, representing the p-EGDMA coating. As previous studies of iCVD depositions on pharmaceutics on flat substrates had shown, a coating thickness of 200 nm is sufficient to provide a retarded release, which is an indication of a closed layer [31–33]. Therefore, in this study depositions with coating thicknesses of 100, 200, 300 and 400 nm were performed.

In the deposition runs with vibration, the petri dishes with the powders were placed on speakers (Visaton Speaker 2952, 1 W nom, 2 W max, 8 Ω), of which one of them was connected by feed-through from the inside of the reactor to an external amplifier (see figure 1). These speakers were chosen because of two reasons: First, a petri dish could easily be placed on top of the speaker membrane, fixed by rubber band and, therefore, stayed in good contact with the vibrating area. Secondly, it was flat enough to fit under the filament in the iCVD reactor. During the deposition one speaker was playing "Thunderstruck" by AC/DC (vibration frequency 50–10,000 Hz), while the second one was not vibrating. The second sample should act for direct comparison of powders which were deposited with vibration to that without vibration. The power

of the amplifier was increased until the particles of the powder were visibly bouncing. The depositions thickness was 200 nm.

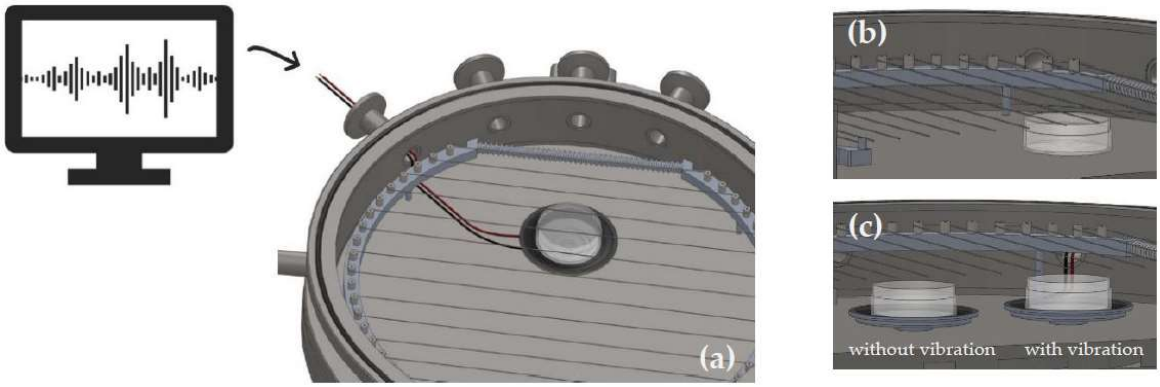

Figure 1. (a) overview of an initiated chemical vapor deposition (iCVD) reactor with inserted speaker and petri dish. (b) cross section of the setup when performing a flat hearth deposition. (c) cross section of the setup when performing depositions with speakers. Both petri dishes are placed on speakers but only one vibrated during the deposition.

Characterization

Scanning electron microscopy (Jeol JSM-6490LV, Labco GmbH, Pressbaum, Austria) was used to observe the magnesium powder. To diminish electrostatic distortion, a small amount of magnesium powder was smeared on a conductive carbon tape and measured with 20 kV electron beam voltage. Light microscopy (Olympus BX51, Olympus Austria GmbH, Vienna, Austria) was performed to visualize the grain size of the aspirin powder. The particle size distribution was analyzed with the software ImageJ (1.53a). To measure the angle of repose, a photo from the side of a powder pile was taken (KSV Instruments LTD camera 200, KSV Instruments, Helsinki, Finland).

The release tests of the encapsulated magnesium citrate (8 ± 0.2 mg) were performed in demineralized water and the pH of the solution was repeatedly measured with a pH glass electrode (Haoshi H101 pH electrode) connected via a sensor interface to an Arduino. The Arduino powered the glass electrode and was used as a read out terminal. Each 300 ms a pH data point was passed via USB com port to a commercial computer, visualized and stored by a standard application which emulates serial interfaces (Tera Term). The pH values were related to the weight-percentage of the released magnesium citrate through a calibration curve with a 2 mg/mL solution of magnesium citrate in demineralized water. Increments of 0.25 mL were inserted in 150 mL demineralized water and the pH was measured. The pH was related to the inserted weight with a linear fit and, therefore, to the release.

The release test of the encapsulated aspirin was performed with measuring optical absorption spectra (UVVIS Shimadzu 1800, Shimadzu, Korneuburg, Austria) of 3 mg of encapsulated aspirin in 3 mL of demineralized water in time. The aspirin powder was inserted in a quartz cuvette of 1 cm in optical path length and 4 mL in volume and the water was filled into the cuvette with a plastic syringe. In the first hour, a spectrum was taken each 4 min and afterwards each hour in the wavelength region between 190 nm and 350 nm. All spectra were baseline corrected and divided by a reference spectrum of a quartz cuvette with demineralized water. To calibrate the data to link the absorption to the release, in weight percentage of the already dissolved aspirin powder, absorption spectra were taken with solutions of aspirin of known concentrations (1 mg/mL, 0.66 mg/mL, 0.33 mg/mL, 0.166 mg/mL, 0.08 mg/mL, 0.05 mg/mL and 0.027 mg/mL). The peak height of the absorption band of aspirin at 272 nm was linked to the concentration which was used further to calculate the release.

To quantify and compare the time constants of the release from coated and uncoated powders, the release curves were fitted with an exponential model of the form: $c\,(1-e^{-bt})$. The time τ_c and τ_{uc}, where the fit of the release of coated powder and the dissolution of uncoated powder exceeded 1/e (36.8%) was determined. The delay factor was calculated with the ratio τ_c/τ_{uc}. A higher delay factor implies a more effective coating that acts as a barrier that slows down the release.

II.5.5 Results and Discussion

The grain size and shape of the two powders, magnesium citrate and aspirin, were observed using a microscope. In figure 2.a, the magnesium citrate powder is shown. The particle shape is irregular and the grain size is small with a diameter of (8 ± 9) µm. The particles agglomerate into bigger clusters, which is typical for hygroscopic cohesive powders, such as magnesium citrate. The angle of repose of the magnesium citrate (figure 3.a) was measured to be (46 ± 2)°, suggesting poor flowability [34]. In comparison, aspirin (figure 3.b) has a mean grain size of (200 ± 100) µm. The measured angular of repose of the aspirin figure 3.b) is (28 ± 2)° suggesting the aspirin particles would have excellent flow properties. The particles are well defined, easily flowing and crystalline. The magnesium citrate and aspirin proved to be of the group C and the group B of the theory of Geldart, respectively [26].

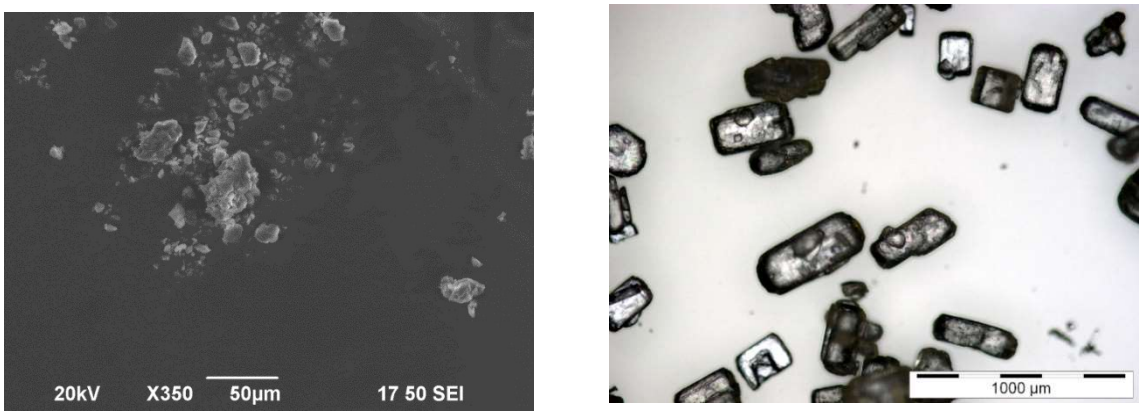

(**a**) (**b**)

Figure 2. *(**a**) Scanning electron microscope image of the magnesium citrate powder. (**b**) Light microscope image of the aspirin powder.*

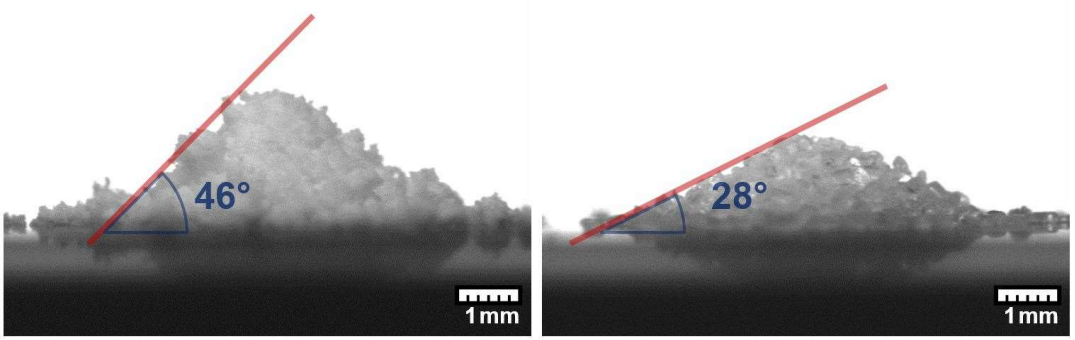

(**a**) (**b**)

Figure 3. *Photo of a powder pile of magnesium citrate (**a**) and aspirin (**b**). Red line marks the angle of repose of the pile.*

To measure if the deposition of the magnesium citrate was successful, release tests were performed. The change of pH value in time of a dissolving coated powder in demineralized water was measured. In figure 4.a, the pH value in time of dissolving magnesium citrate without coating is pictured. In the first 2 min there was no powder added to the demineralized water and the pH value was constant at 7.2. After 2 min the powder was added and immediately the pH value dropped from 7.2 to 5.5 within 1 min. This indicates that the magnesium citrate dissolves in water and induces a change in pH, as expected. The calibration curve, which links the pH value with the concentration of dissolved magnesium citrate, is plotted in figure 4.b. The pH value decays with

the amount of magnesium citrate. The best fit to the data was found with a linear regression with a coefficient of determination R^2 of 0.94, while other functions (e.g., exponential decay) lead to larger errors.

The release curves of the uncoated magnesium citrate powder, of the one coated with a nominal thickness of 420 nm and with a nominal thickness of 120 nm of p-EGDMA, both in the flat hearth deposition, are compared in figure 5.a. While the uncoated powder dissolved within a minute, the release of the coated powder was retarded. After 10 min about 63% of the magnesium citrate was released. The time, where the dissolution curve of the uncoated powder exceeded 1/e was calculated to be $\tau_{uc} = (0.22 \pm 0.05)$ min. While the time for magnesium citrate coated with a nominal thickness of 120 nm was $\tau_c = (2.4 \pm 0.7)$ min. The delay factor was estimated to be $\tau_c/\tau_{uc} = 11.0 \pm 0.9$ for the powder coated with 100 nm nominal thickness and 9.2 ± 0.4 for the powder coated with 420 nm of nominal thickness. The difference in the release of the powder with nominal 120 nm coating and nominal 420 nm coating is negligibly small which seems unintuitive as thicker coatings should lead to slower release [2].

In figure 5.b, the release curve of magnesium citrate coated with help of a vibrating powder bed with a nominal coating thickness of 210 nm is plotted. Again, the release of a coated powder is retarded compared to a non-coated powder. After 10 min both, the powder which vibrated and which not vibrated during coating, exceeded 67% of release. The delay factor was calculated to be 6.5 ± 0.7 for the powder which was not vibrating and 7.4 ± 0.7 for the vibrating one. Both release curves are within their measurement errors in agreement with each other.

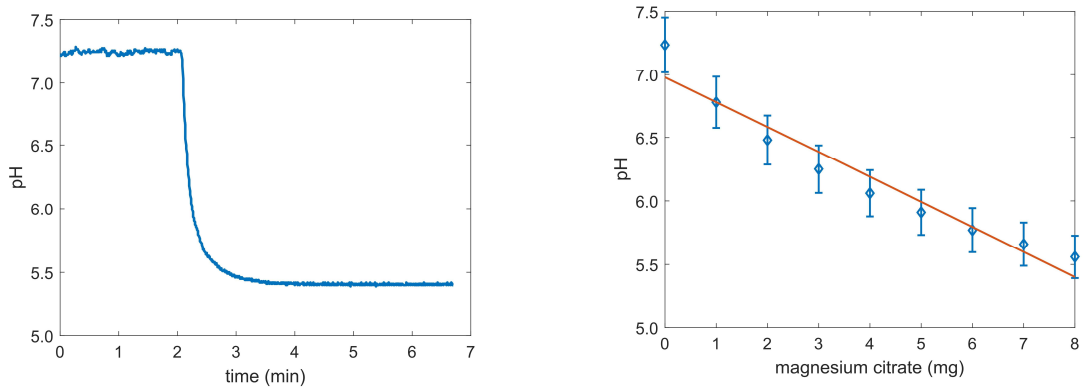

Figure 4. (a) Variation of pH in time of dissolving magnesium citrate. (b) Calibration curve to link the dissolved magnesium citrate with a pH value.

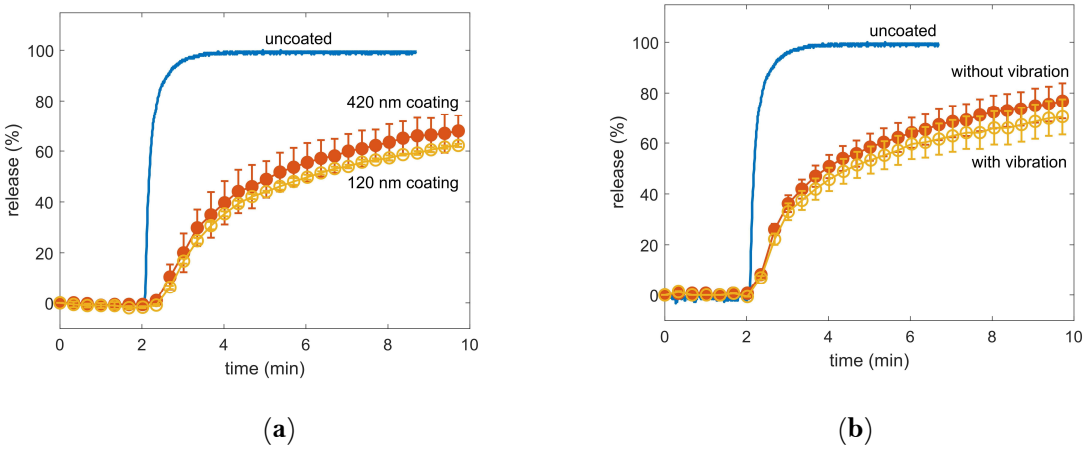

Figure 5. (a) Release curve of magnesium citrate coated with a nominal coating thickness of 420 nm and a nominal coating thickness of 120 nm polymer of p-EGDMA. Samples were placed on the reactor bottom as in figure 1.b. (b) release curve of magnesium powder coated with and without vibration both with a nominal thickness of 210 nm. Samples were placed on speakers as in figure 1.c.

Neither coating thickness nor providing a good gas–powder contact by vibration leads to a change in the release delay. A hypothetical explanation could lie in the cohesion of the magnesium powder. The small particles agglomerate to clusters with a large inner surface area. Due to diffusion limitations or clogging phenomena the coating of the inner area is limited and converge with deposition time. Although the coating of the outer part of the cluster increases, the inner part may be already converged. A schematic of a coated cluster is depicted in figure 6.a.

While the surface of the cluster is homogeneously coated, the inner volume has only little coating. With increasing volume, the surface to volume fraction decreases. Therefore, the surface area of larger clusters plays a subordinate role compared to the inner volume of the cluster. Coming back to the measured results this leads to the hypothesis, that the highly cohesive magnesium citrate agglomerates to large clusters, that cannot be disconnect via vibration and, therefore, do not get uniformly coated as such. In this case, when immersing the powder, water penetrates via small voids into the cluster and burst them open. Then the release is mainly driven by the particles, that are in the inner volume of the cluster and neither the coating thickness nor the movement of the powder during deposition has an influence.

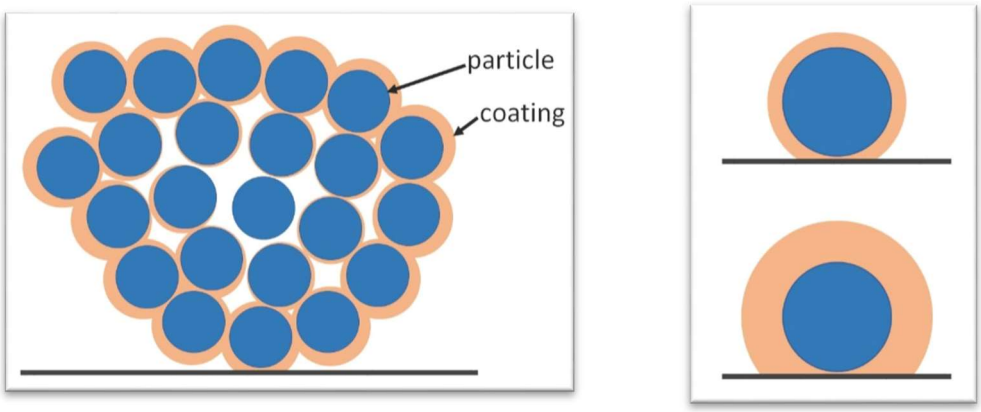

(**a**) (**b**)

Figure 6. (a) Schematic of coating problems in cohesive powder. Due to diffusion limitations and clogging phenomena the inner region of agglomerated clusters is less coated. (b) Contact of particles with surfaces are weak points in a flat hearth deposition.

The release of the aspirin was measured with optical absorption measurements. In figure 7.a, a representative of the absorption spectra of coated aspirin in time steps are plotted. With time the typical absorption bands of aspirin at 193 nm, 225 nm and 277 nm rise [35]. Comparing the spectra of uncoated aspirin dissolved within 10 min with coated aspirin released in 5 h, the absorption bands positions and heights are alike (figure 7.b). This indicates, that the release of coated powder is retarded but the chemical structure of aspirin retained during the vibration and the deposition. After approximately 10 h a shoulder at 303 nm appears and starts to increase. This peak is attributed to the formation of salicylic acid. In water, aspirin gradually hydrolyses to acetic and salicylic acids [36]. The height of the absorption band at 277 nm was used in the calibration and is plotted versus the aspirin concentration in figure 7.c. The calibration has approximately a linear trend (linear regression with a R^2 of 0.94) and was used further to calculate the release,

which is the percentage of powder weight that already dissolved. The release of uncoated aspirin is within 30 min at 80% and converges to 85%. The p-EGDMA coating itself has no absorption at 273 nm. The aspirin powder coated with a nominal thickness of 135 nm, 290 nm, 325 nm and 400 nm in the flat hearth deposition is retarded compared to the uncoated aspirin, as it can be seen in figure 8a. The time where the dissolution of the uncoated powder reached 1/e was calculated with $\tau_{uc} = (0.13 \pm 0.09)$ h. The time where the release of the powder coated with 135 nm of nominal coating thickness exceeded 1/e was $\tau_c = (7.5 \pm 0.9)$ h. The resulting delay factor was calculated with $\tau_u/\tau_{uc} = 54 \pm 5$. For the aspirin powders coated with 290 nm, 325 nm and 400 nm the delay factor were 58 ± 10, 58 ± 4 and 45 ± 10, respectively. The release time of the coated aspirin differs only marginally between different coating thicknesses. The release properties in a flat hearth iCVD deposition cannot be tuned with the deposition thickness. The aspirin does not agglomerate to bigger clusters and the hypothesis of a diffusion limitation to inner particles within the clusters cannot be applied. The typical problem of a flat hearth deposition is the inhomogeneous gas–solid contact. If particles are in contact with the reactor wall or with other particles, the gas cannot reach this surface area. As schematized in figure 6.b, the weak point of the coating is the contact-area from a particle to a surface. Although the upper part of the particle can be coated thicker and thicker, the weak point does not change which would explain why the thickness of the coating has no influence on the release.

The release curves of the aspirin powder which was deposited under vibration is compared to the non-vibrating powder in figure 8.b. For such comparison, the non-vibrating sample was placed at the same height as the vibrating sample, in order to have them at equal distance to the filament and, therefore, at the same temperature. The release of the aspirin which vibrated is much slower than that of non-vibrating aspirin. The delay factors of the release from powder coated without vibration and with vibration was 14 ± 5 and 69 ± 11, respectively. Compared to the delay factor of magnesium citrate coated in the same way, which were 6.5 ± 0.7 and 7.4 ± 0.7 without and with vibration, respectively, the delay of coated aspirin is higher suggesting, that the depositions led to a more effective coating as a release barrier on aspirin then on magnesium citrate. However, while the delay factors of magnesium citrate, coated with and without vibration, differ only within the statistical error, the delay factor of aspirin coated with vibration is significantly higher to that of aspirin coated without vibration.

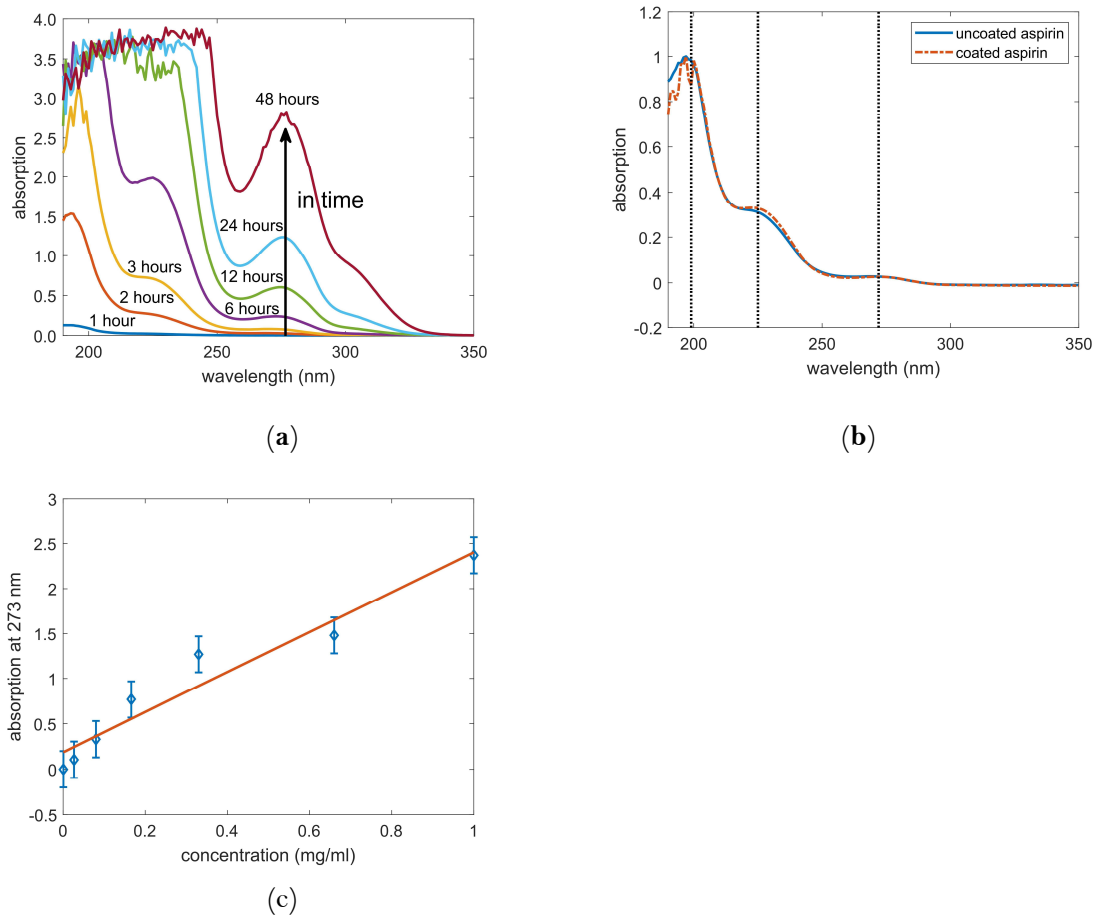

*Figure 7. (a) Representative absorption spectra of coated aspirin powder. In time the absorption bands of aspirin increase due to the present of dissolved aspirin. (b) Scaled absorption spectra of uncoated aspirin dissolved within 10 min and coated aspirin released within 5 h. The absorption bands are alike, indicating a retention of chemical structure during the coating process. (**c**) Calibration curve, which links the peak height of the absorption band at 272 nm to the concentration of aspirin in the water.*

A vibrating deposition has better gas–solid contact and hypothetically produces a more homogenous coating throughout the complete particle without weak points as it can be suspected under flat hearth conditions, resulting in an enhancement of the retarded release.

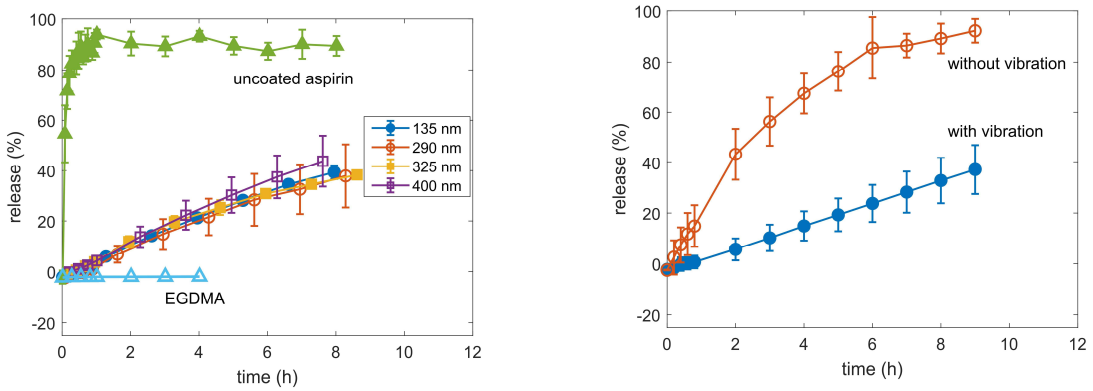

(**a**) (**b**)

Figure 8. (a) Release curve of uncoated aspirin and coated with different thicknesses. Samples were placed on the reactor bottom as in figure 1.b. (b) release curve of powder which was vibrating and which was not vibrating during deposition both with a nominal thickness of 200 nm. Samples were placed on speakers as in figure 1.c.

II.5.6 Conclusions

The aim of this study was to show the possibilities and limitations of utilizing speakers to provide vibration of powders during an iCVD deposition. Two different powders, magnesium citrate and aspirin, were coated with a polymer of EGDMA. While in one deposition the thickness of the coating was varied, in another deposition the powders were forced to vibrate with aid of speakers, playing "Thunderstruck" of AC/DC. The release of the coated magnesium citrate is retarded compared to an uncoated magnesium citrate, but neither the coating thickness nor vibration during the deposition changes the release time. This could be due to the fact that magnesium citrate is hygroscopic powder with a small particle size that agglomerates to large clusters. During the coating process the inner particles of a cluster are coated less due to clogging or diffusion phenomena. When the powder is immersed in water the cluster breaks and the inner particles are mainly contributing to the release. Therefore, the release of magnesium citrate coated with different thicknesses and the release of the magnesium citrate which were vibrated and which were not vibrated are the same. The release of the coated aspirin powder retarded as well as compared to the uncoated aspirin. While the coating thickness does not change the release time, the vibration during deposition causes a slower release. During the deposition for the variation of coating thickness, the powder is not moving and each particle touches others or walls. These surfaces are not or only have little accessibility during coating and are weak points when immersing the coated powder in water. Although the other surfaces on each particle are coated

with different thicknesses, the amount and size of these weak points is statistically the same within each sample, hence the coating thickness has no influence on the release time. The vibration during coating causes a more retarded release. It seems that the vibration provides a better gas–solid contact which caused a uniform coating. This study demonstrates, that with a small adaption of an iCVD reactor with speakers, certain powders (particles >100 μm, good flowability) can be coated uniformly.

Author Contributions: Conceptualization, K.U.; Formal analysis, K.U.; Funding acquisition, A.M.C.; Investigation, K.U.; Supervision, A.M;C. Validation, K.U.; Writing—original draft, K. U.; Writing—review & editing, K.U. and A.M.C. All authors have read and agreed to the published version of the manuscript.

Funding: The European ResearchCouncil (ERC) is gratefully acknowledged for funding this project under the European Union's Horizon 2020 research and innovation program (Grant Agreement 715403). Open Access Funding by the Graz University of Technology is also kindly acknowledged.

Acknowledgments: Furthermore, we want to thank Oliver Werzer, for suggesting and providing the aspirin powder and Martin Kornschober for rendering the iCVD reactor.

Conflicts of Interest: The authors declare no conflict of interest.

II.5.7 References

1. Saleh, K.; Guigon, P. Chapter 7 Coating and encapsulation processes in powder technology. Handb. Powder Technol. 2007, 11, 323–375, doi:10.1016/S0167-3785(07)80042-X.
2. Perrotta, A.; Werzer, O.; Coclite, A.M. Strategies for Drug Encapsulation and Controlled Delivery Based on Vapor-Phase Deposited Thin Films. Adv. Eng. Mater. 2018, 20, 1–21, doi:10.1002/adem.201700639.
3. Vahlas, C.; Caussat, B.; Serp, P.; Angelopoulos, G.N. Principles and applications of CVD powder technology. Mater. Sci. Eng. R Rep. 2006, 53, 1–72, doi:10.1016/j.mser.2006.05.001.
4. Tenhaeff, W.E.; Gleason, K.K. Initiated and oxidative chemical vapor deposition of polymeric thin films: ICVD and oCVD. Adv. Funct. Mater. 2008, 18, 979–992, doi:10.1002/adfm.200701479.

5. Decandia, G.; Palumbo, F.; Treglia, A.; Armenise, V.; Favia, P.; Baruzzi, F.; Unger, K.; Perrotta, A.; Coclite, A.M. Initiated chemical vapor deposition of crosslinked organic coatings for controlling gentamicin delivery. Pharmaceutics 2020, 12, doi:10.3390/pharmaceutics12030213.

6. Karandikar, P.; Gupta, M. Fabrication of ionic liquid gel beads via sequential deposition. Thin Solid Films 2017, 635, 17–22, doi:10.1016/j.tsf.2017.01.046.

7. Chan, K.; Gleason, K.K. Initiated chemical vapor deposition of linear and cross-linked poly(2-hydroxyethyl methacrylate) for use as thin-film hydrogels. Langmuir 2005, 21, 8930–8939, doi:10.1021/la051004q.

8. Lau, K.K.S.; Gleason, K.K. Initiated Chemical Vapor Deposition (iCVD) of poly(alkyl acrylates): An experimental study. Macromolecules 2006, 39, 3688–3694, doi:10.1021/ma0601619.

9. Lau, K.K.S.; Gleason, K.K. Initiated Chemical Vapor Deposition (iCVD) of poly(alkyl acrylates): A kinetic model. Macromolecules 2006, 39, 3695–3703, doi:10.1021/ma0601621.

10. Buchberger, A.; Peterka, S.; Coclite, A.M.; Bergmann, A. Fast optical humidity sensor based on hydrogel thin film expansion for harsh environment. Sensors 2019, 19, 1–11, doi:10.3390/s19050999.

11. Lee, H.S.; Kim, H.; Lee, J.H.; Kwak, J.B. Fabrication of a conjugated fluoropolymer film using one-step iCVD process and its mechanical durability. Coatings 2019, 9, doi:10.3390/coatings9070430.

12. Muralter, F.; Perrotta, A.; Coclite, A.M. Thickness-Dependent Swelling Behavior of Vapor-Deposited Hydrogel Thin Films. Proceedings 2018, 2, 757, doi:10.3390/proceedings2130757.

13. Lau, K.K.S.; Gleason, K.K. Particle functionalization and encapsulation by initiated chemical vapor deposition (iCVD). Surf. Coatings Technol. 2007, 201, 9189–9194, doi:10.1016/j.surfcoat.2007.04.045.

14. Lau, K.K.S.; Gleason, K.K. Particle surface design using an all-dry encapsulation method. Adv. Mater. 2006, 18, 1972–1977, doi:10.1002/adma.200600896.

15. Bose, R.K.; Heming, A.M.; Lau, K.K.S. Microencapsulation of a crop protection compound by initiated chemical vapor deposition. Macromol. Rapid Commun. 2012, 33, 1375–1380, doi:10.1002/marc.201200214.

16. Baxamusa, S.H.; Im, S.G.; Gleason, K.K. Initiated and oxidative chemical vapor deposition: A scalable method for conformal and functional polymer films on real substrates. Phys. Chem. Chem. Phys. 2009, 11, 5227–5240, doi:10.1039/b900455f.

17. Jung, B.J.; Kim, J.; Kim, J.A.; Jang, H.; Seo, S.; Lee, W. PDMS-parylene hybrid, flexible microfluidics for real-time modulation of 3D helical inertial microfluidics. Micromachines 2018, 9, doi:10.3390/mi9060255.

18. Ince, G.O.; Armagan, E.; Erdogan, H.; Buyukserin, F.; Uzun, L.; Demirel, G. One-dimensional surface-imprinted polymeric nanotubes for specific biorecognition by initiated chemical vapor deposition (iCVD). ACS Appl. Mater. Interfaces 2013, 5, 6447–6452, doi:10.1021/am401769r.

19. Baxamusa, S.H.; Gleason, K.K. Initiated chemical vapor deposition of polymer films on nonplanar substrates. Thin Solid Films 2009, 517, 3536–3538, doi:10.1016/j.tsf.2009.01.032.

20. Park, S.W.; Kim, J.W.; Choi, H.J.; Shim, J.H. Vibration atomic layer deposition for conformal nanoparticle coating. J. Vac. Sci. Technol. A 2014, 32, 01A115, doi:10.1116/1.4845735.

21. Michl, T.D.; Coad, B.R.; Hüsler, A.; Vasilev, K.; Griesser, H.J. Laboratory scale systems for the plasma treatment and coating of particles. Plasma Process. Polym. 2015, 12, 305–313, doi:10.1002/ppap.201400141.

22. McInnes, S.J.P.; Michl, T.D.; Delalat, B.; Al-Bataineh, S.A.; Coad, B.R.; Vasilev, K.; Griesser, H.J.; Voelcker, N.H. "Thunderstruck": Plasma-Polymer-Coated Porous Silicon Microparticles as a Controlled Drug Delivery System. ACS Appl. Mater. Interfaces 2016, 8, 4467–4476, doi:10.1021/acsami.5b12433.

23. Unger, K.; Salzmann, P.; Masciullo, C.; Cecchini, M.; Koller, G.; Coclite, A.M. Novel Light-Responsive Biocompatible Hydrogels Produced by Initiated Chemical Vapor Deposition. ACS Appl. Mater. Interfaces 2017, 9, 17408–17416, doi:10.1021/acsami.7b01527.

24. Unger, K.; Resel, R.; Coclite, A.M. Dynamic Studies on the Response to Humidity of Poly (2-hydroxyethyl methacrylate) Hydrogels Produced by Initiated Chemical Vapor Deposition. Macromol. Chem. Phys. 2016, 217, 2372–2379, doi:10.1002/macp.201600271.

25. Mansurnezhad, R.; Ghasemi-Mobarakeh, L.; Coclite, A.M.; Beigi, M.H.; Gharibi, H.; Werzer, O.; Khodadadi-Khorzoughi, M.; Nasr-Esfahani, M.H. Fabrication, characterization and cytocompatibility assessment of gelatin nanofibers coated with a polymer thin film by initiated chemical vapor deposition. Mater. Sci. Eng. C 2020, 110, 110623, doi:10.1016/j.msec.2019.110623.

26. Geldart, D. Types of Gas Fluidization. Powder Technol. 1973, 7, 285–292.

27. Kappeler, D.; Heimbeck, I.; Herpich, C.; Naue, N.; Höfler, J.; Timmer, W.; Michalke, B. Higher bioavailability of magnesium citrate as compared to magnesium oxide shown by evaluation of urinary excretion and serum levels after single-dose administration in a randomized cross-over study. BMC Nutr. 2017, 3, 1–12, doi:10.1186/s40795-016-0121-3.

28. Lindberg, J.S.; Zobitz, M.M.; Poindexter, J.R.; Pak, C.Y.C. Magnesium bioavailability from magnesium citrate and magnesium oxide. J. Am. Coll. Nutr. 1990, 9, 48–55, doi:10.1080/07315724.1990.10720349.

29. State, D.J.; de Lei, M.; Wood, B. One hundred years of devastation. Lancet 1997, 350, 437–439.

30. Ranacher, C.; Resel, R.; Moni, P.; Cermenek, B.; Hacker, V.; Coclite, A.M. Layered Nanostructures in Proton Conductive Polymers Obtained by Initiated Chemical Vapor Deposition. Macromolecules 2015, 48, 6177–6185, doi:10.1021/acs.macromol.5b01145.

31. Christian, P.; Tumphart, S.; Ehmann, H.M.A.; Riegler, H.; Coclite, A.M.; Werzer, O. Controlling Indomethacin Release through Vapor-Phase Deposited Hydrogel Films by Adjusting the Cross-linker Density. Sci. Rep. 2018, 8, 1–12, doi:10.1038/s41598-018-24238-w.

32. Werzer, O.; Tumphart, S.; Keimel, R.; Christian, P.; Coclite, A.M. Drug release from thin films encapsulated by a temperature-responsive hydrogel. Soft Matter 2019, 15, 1853–1859, doi:10.1039/C8SM02529K.

33. Christian, P.; Ehmann, H.M.A.; Coclite, A.M.; Werzer, O. Polymer Encapsulation of an Amorphous Pharmaceutical by initiated Chemical Vapor Deposition for Enhanced Stability. ACS Appl. Mater. Interfaces 2016, 8, 21177–21184, doi:10.1021/acsami.6b06015.

34. Simek, M.; Grünwaldova, V.; Kratochvil, B.; Comparison of Compression and Material Properties of Differently Shaped and Sized Paracetamols. KONA Powder and Particle Journal 2016, 34, 197-206, doi: 10.14356/kona.2017003

35. Pandiarajan, S.; Krishnakumar, R.V.; Muthuselvi, C. Vapor Diffusion Growth and Characterization of Aspirin—Perchloric Acid Vibrational Spectroscopy. Elixir Vib. Spec. 2017, 95, 40673–40678.

36. Bash, E. The Hydrolysis of Aspirin. PhD Propos. 2015, 1, 696–699, doi:10.1017/CBO9781107415324.004.

II.6 Applications of iCVD Synthesized Smart Hydrogels

Smart hydrogels synthesized via iCVD have already been utilized in several applications, some of them will be presented here.

A prominent sector within the application of smart responsive hydrogels is the field of coatings for controlled drug release. Sayin et al. demonstrated, that the release of chemotherapeutic agent Rose Bengal loaded into polyvinyl alcohol nanofibers, can be drastically altered by a thin layer of poly (4-vinylpyridine-co-ethylene glycol dimethacrylate), p(4VP-co-EGDMA) deposited via iCVD.[32] While the release of the uncoated fiber is not pH dependent and completely finishes within 2 hours, the coated fibers release is retarded and pH dependent. At pH 4 after 3 hours 50 % of the loaded Rose Bengal is released while at pH 9 already 100 % is released. Within this study also cell proliferation was tested on uncoated and coated samples, showing an increase of cell apoptosis for coated samples, verifying the therapeutic efficiency against tumor cells.

The possibility of iCVD to dryly deposit a responsive hydrogel, namely poly N-isopropylacrylamide crosslinked with di(ethyleneglycol) divinyl ether, on three spin coated pharmaceutics, Phenytion, Indomethacin and Clotrimazol, was demonstrated by Werzer et al.[18] While the swelling of the hydrogel at 20 °C was about 30 % of thickness increase, the hydrogel shrinks to its initial dry thickness state back when the temperature is elevated to 50 °C. The identified LCST was 29 °C. Within the performed temperature dependent drug release tests, the hydrogel has proved to act temperature dependent as a barrier that hinders the drug to dissolve in time. At elevated temperature (37 °C), where the hydrogel is in a shrunken state, the permeability of the coating is higher and the release is faster compared to the release at lower temperature (25° C), where the hydrogel is in its swollen state. Interestingly, it was also shown that in different pH milieus the release was also dependent on the pharmaceutics within the coating.

The ability of smart hydrogels to also act as an actuator was investigated by the group of Im et al.,[33] showing, that Janus microstrip, which is a layer of two faces of different distinct physical or chemical properties, of one side poly hydroxyethyl methacrylate and acrylic acid as active hydrogel groups and on the other side divinylbenzene as the rigid backside, exhibits a pH responsive curvature. While in this study iCVD was utilized to coat a non-responsive part onto a smart responsive hydrogel, it also emphasizes the use of iCVD as a technique when dealing with smart hydrogels as substrates. Upon exposure to higher pH levels, the hydrogel swells and tries to expand creating a tensile force to the rigid side. In the equilibrium state the strip is reversibly bended or even rolled up.

In an additional work on Janus membranes, ICVD was utilized as a coating technique to deliver the smart hydrogel, done by the group of Ince.[34] In their study they showed, that a porous anodic aluminum oxide template coated via iCVD on one side with poly (methylacrylic acid-co-ethylene glycol dimethacrylate), p(MAA-co-EGDMA), and the other with poly (4-vinylpyridine-co-ethylene glycol dimethacrylate), p(4VP-co-EGDMA), can act as an on-off gate for switchable controlled release. The two materials on opposite sides are pH responsive. Exposed to pH 3 the p(MAA-co-EGDMA) structure is in its shrunken state and the pores are opened, while at pH 9, in the swollen state, the pores are closed and keeping the molecules on one side. The other side of the Janus membrane acts exactly opposite: p(4VP-co-EGDMA) at pH 3 is in its swollen state and acts as a barrier while at pH 9 the pores are open. Diffusion experiments with a protein, bovine serum albumin, demonstrated a pH switchable opening and closing of the gate with the ability to actively trap proteins inside the Janus membrane and release them on the opposite side.

Another very interesting domain of smart hydrogels is as active material in sensors/actuators. Muralter et. al investigated temperature responsive poly(N-vinylcaprolactam) cross-linked by di(ethylene glycol) divinyl ether.[35] While at 10 °C the swollen hydrogel was 3 times the thickness compared to dry state, at 30 °C the thickness was only 1.5 the times of dry state with an evaluated LCST of 16 °C. The sensor/actuator was maintained by coating the hydrogel onto a poly-dimethylsiloxane substrate and cutting a flower-like shape out of it. When exposed to temperature or humidity the flower exhibited a visible reversible bending of the flower's petals.

Another example of a humidity sensor based on a hydrogel deposited via iCVD was done by Buchberger et al.[36] With a sensor design that allows only the hydrogel to be in contact with the investigated gas, these sensors are also explicitly applicable in harsh environments. A thin hydrogel made of p(HEMA) deposited on a 2 mm thick sapphire substrate is facing into a gas pipe. On the other side the sapphire glass gets illuminated by a laser or a broad band light under an incident angle. Due to the change in thickness caused by swelling of the hydrogel the reflected intensity changes due to interference phenomena.

II.7 References

1. Flory, P. J. & Rehner, J. Statistical mechanics of cross-linked polymer networks I. Rubberlike elasticity. *J. Chem. Phys.* **11**, 512–520 (1943).

2. Flory, P. J. Thermodynamics of high polymer solutions. *J. Chem. Phys.* **10**, 51–61 (1942).

3. Huggins, M. L. Solutions of long chain compounds. *J. Chem. Phys.* **9**, 440 (1941).

4. Quesada-Pérez, M., Maroto-Centeno, J. A., Forcada, J. & Hidalgo-Alvarez, R. Gel swelling theories: The classical formalism and recent approaches. *Soft Matter* **7**, 10536–10547 (2011).

5. Mark, J. E. *Physical Properties of Polymers Handbook. Physical Properties of Polymers Handbook* (Springer New York, 2007). doi:10.1007/978-0-387-69002-5.

6. Jones, R. A. L. Soft Condensed Matter Oxford Master Series in Physics: Amazon.de: Jones, Richard A.L.: Fremdsprachige Bücher. *Oxford University Press* https://www.amazon.de/Condensed-Matter-Oxford-Master-Physics/dp/0198505892 (2002).

7. Fornasiero, F., Krull, F., Prausnitz, J. M. & Radke, C. J. Steady-state diffusion of water through soft-contact-lens materials. *Biomaterials* **26**, 5704–5716 (2005).

8. Porter, T. L., Stewart, R., Reed, J. & Morton, K. Models of hydrogel swelling with applications to hydration sensing. *Sensors* **7**, 1980–1991 (2007).

9. Blanco, A., González, G., Casanova, E., Pirela, M. E. & Briceño, A. Mathematical Modeling of Hydrogels Swelling Based on the Finite Element Method. *Appl. Math.* **04**, 161–170 (2013).

10. Bouklas, N. & Huang, R. Swelling kinetics of polymer gels: Comparison of linear and nonlinear theories. *Soft Matter* **8**, 8194–8203 (2012).

11. Saunders, J. R., Abu-Salih, S., Khaleque, T., Hanula, S. & Moussa, W. Modeling theories of intelligent hydrogel polymers. *J. Comput. Theor. Nanosci.* **5**, 1942–1960 (2008).

12. Koryta, J. Diffusion. Mass Transfer in Fluid Systems. *J. Electroanal. Chem. Interfacial Electrochem.* **194**, 169–170 (1985).

13. Berens, A. R. & Hopfenberg, H. B. Diffusion and relaxation in glassy polymer powders: 2. Separation of diffusion and relaxation parameters. *Polymer (Guildf).* **19**, 489–496 (1978).

14. Richter, A. *et al.* Review on Hydrogel-based pH Sensors and Microsensors. *Sensors* **8**, 561–581 (2008).

15. Gupta, P., Vermani, K. & Garg, S. Hydrogels: From controlled release to pH-responsive drug delivery. *Drug Discovery Today* vol. 7 569–579 (2002).

16. Tufani, A. & Ozaydin Ince, G. Smart membranes with pH-responsive control of macromolecule permeability. *J. Memb. Sci.* ***537***, 255–262 (2017).

17. Echeverria, C., Fernandes, S., Godinho, M., Borges, J. & Soares, P. Functional Stimuli-Responsive Gels: Hydrogels and Microgels. *Gels* **4**, 54 (2018).

18. Werzer, O., Tumphart, S., Keimel, R., Christian, P. & Coclite, A. M. Drug release from thin films encapsulated by a temperature-responsive hydrogel. *Soft Matter* **15**, 1853–1859 (2019).

19. Muralter, F., Perrotta, A. & Coclite, A. M. Thickness-Dependent Swelling Behavior of Vapor-Deposited Hydrogel Thin Films. *Proceedings* **2**, 757 (2018).

20. Nitschke, M. *et al.* Thermo-responsive poly(NiPAAm- *co* -DEGMA) substrates for gentle harvest of human corneal endothelial cell sheets. *J. Biomed. Mater. Res. Part A* **80A**, 1003–1010 (2007).

21. Shimura, R. *et al.* Fabrication of thermo-responsive cell-culture membranes with Poly(N-isopropylacrylamide) by electron-beam graft polymerization. *Radiat. Phys. Chem.* **171**, (2020).

22. Huang, J., Wang, X., Chen, X. & Yu, X. Temperature-sensitive membranes prepared by the plasma-induced graft polymerization of N-isopropylacrylamide into porous polyethylene membranes. *J. Appl. Polym. Sci.* **89**, 3180–3187 (2003).

23. Gramm, S., Komber, H. & Schmaljohann, D. Copolymerization kinetics of N-isopropylacrylamide and diethylene glycol monomethylether monomethacrylate

determined by online NMR spectroscopy. *J. Polym. Sci. Part A Polym. Chem.* **43**, 142–148 (2005).

24. Petruczok, C. D., Armagan, E., Ince, G. O. & Gleason, K. K. Initiated chemical vapor deposition and light-responsive cross-linking of poly(vinyl cinnamate) thin films. *Macromol. Rapid Commun.* **35**, 1345–1350 (2014).

25. Jochum, F. D. & Theato, P. Temperature- and light-responsive smart polymer materials. *Chem. Soc. Rev.* **42**, 7468–7483 (2013).

26. Zhao, Y. L. & Fraser Stoddart, J. Azobenzene-based light-responsive hydrogel system. *Langmuir* **25**, 8442–8446 (2009).

27. Baxamusa, S. H., Im, S. G. & Gleason, K. K. Initiated and oxidative chemical vapor deposition: A scalable method for conformal and functional polymer films on real substrates. *Phys. Chem. Chem. Phys.* **11**, 5227–5240 (2009).

28. Coclite, A. M. *et al.* 25th Anniversary Article: CVD polymers: A new paradigm for surface modification and device fabrication. *Adv. Mater.* **25**, 5392–5423 (2013).

29. Alf, M. E. *et al.* Chemical vapor deposition of conformal, functional, and responsive polymer films. *Adv. Mater.* **22**, 1993–2027 (2010).

30. Tenhaeff, W. E. & Gleason, K. K. Initiated and oxidative chemical vapor deposition of polymeric thin films: ICVD and oCVD. *Adv. Funct. Mater.* **18**, 979–992 (2008).

31. Lau, K. K. S. & Gleason, K. K. Initiated Chemical Vapor Deposition (iCVD) of Poly(alkyl acrylates): A Kinetic Model. (2006) doi:10.1021/ma0601621.

32. Sayin, S. *et al.* Electrospun Nanofibers With pH-Responsive Coatings for Control of Release Kinetics. *Front. Bioeng. Biotechnol.* **7**, 1–12 (2019).

33. Oh, M. S. *et al.* Control of Reversible Self-Bending Behavior in Responsive Janus Microstrips. *ACS Appl. Mater. Interfaces* **8**, 8782–8788 (2016).

34. Tufani, A. & Ozaydin Ince, G. Protein gating by vapor deposited Janus membranes. *J. Memb. Sci.* **575**, 126–134 (2019).

35. Muralter, F., Greco, F. & Coclite, A. M. Applicability of Vapor-Deposited Thermoresponsive Hydrogel Thin Films in Ultrafast Humidity Sensors/Actuators. *ACS Appl. Polym. Mater.* **2**, 1160–1168 (2020).

36. Buchberger, A., Peterka, S., Coclite, A. M. & Bergmann, A. Fast optical humidity sensor based on hydrogel thin film expansion for harsh environment. *Sensors (Switzerland)* **19**, 1–11 (2019).

Chapter III

Characterization Methods

The following chapter will focus on the most important analyzation methods used within the publications of this thesis, namely X-ray reflectivity, Fourier transform infrared spectroscopy, spectroscopic ellipsometry and electrochemical impedance spectroscopy.

III.1 X-Ray Reflectivity

X-Ray reflectivity (XRR) is a surface sensitive technique to investigate morphology properties like film thickness, surface and interface roughness as well as electron density of thin films. An incident X-ray beam strikes the sample and gets reflected in specular direction. Depicted in figure 12 the arrangement of incident wave vector $\boldsymbol{k_i}$, reflected wave vector $\boldsymbol{k_r}$, scattering vector $\boldsymbol{q}$, the incident angle θ and the scattering angle 2θ, is illustrated. Morphology analysis of thin organic and inorganic films on various substrates were already successfully performed with XRR.

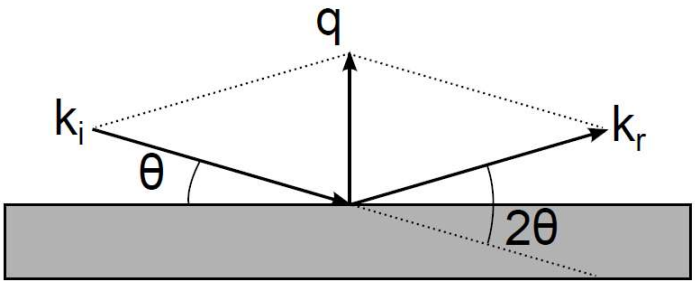

Figure 12: X-ray reflectivity in specular conditions with $\boldsymbol{k_i}$, the incident wave vector, $\boldsymbol{k_r}$, the reflected wave vector, $\boldsymbol{q}$, the scattering vector, θ, the incident angle and 2θ, the angle between $\boldsymbol{k_i}$ and $\boldsymbol{k_r}$

The theoretical formulation of XRR is taken out of the book *X-Ray and Neutron Reflectivity* by J. Daillant and A. Gibaud,[1] and the book *Thin film analysis by X-ray scattering* by M. Birkholz.[2] To explain the method, the propagation properties of X-rays through materials have to be considered. The real part of the refractive index n_{real} of an arrangement of N atoms can be derived by assuming an ensemble of harmonic oscillators with a resonance frequency ω_i. With ρ_e- the electron density, m_e- the electrons mass, e the electrons charge, ε_0 the electric constant, s_i the

weight of the oscillator and ω the exciting electromagnetic waves' frequency, n_{real} can be written as:

$$n_{real} = 1 + \frac{\rho_{e^-}}{2\pi m_{e^-}} \frac{e^2}{4\pi\epsilon_0} \sum \frac{s_i}{\omega_i^2 - \omega^2} \qquad III - 1$$

The frequencies of X-rays are far beyond the domain of resonance frequencies of solids ($\omega^2 >> \omega_i^2$) which is from the infrared up to the ultraviolet spectrum. The classical electron radius r_{e^-}, which is a fundamental quantity that defines a length of electrons interacting with electromagnetic waves is given as (c, the speed of light):

$$r_{e^-} = \frac{1}{4\pi\varepsilon_0} \frac{e^2}{m_{e^-} c^2} = 2.818 \cdot 10^{-15} m \qquad III - 2$$

This simplifies the real part of the refractive index to:

$$n_{real} = 1 - \frac{\overbrace{\rho_{e^-} \lambda^2 r_{e^-}}^{\delta}}{2\pi} \qquad III - 3$$

The refractive index imaginary part β, which is related to the attenuation of light while propagating through a material μ via:

$$\beta = \frac{\lambda}{4\pi} \mu \qquad III - 4$$

Which finally defines the refractive index N of X-rays within solid matter. The real part $1-\delta$ is slightly below 1 with typical values of $\delta \approx 10^{-6}$.

$$N = 1 - \delta + i\beta \qquad III - 5$$

The propagation of electromagnetic waves changes direction when passing an interface from two media of different real parts of refractive indexes, n_1 and n_2. The incident beams angle α_i (measured from the beam to the surface), the transmitted beams angle α_t and the real part of the refractive index is related via Snells' law.

$$\frac{n_1}{n_2} = \frac{\cos\alpha_t}{\cos\alpha_i} \qquad \text{III - 6}$$

Because X-ray reflectivity operates only at small angle, $\cos(\alpha)$ can be simplified to $1-\alpha^2/2$. Further the first media is typically air with $n_1 = 1$. Inserting the real part of the refractive index of equation III - 3 into Snells' law the angle of the transmitted beam can be written as followed:

$$\alpha_t = \sqrt{\alpha_i^2 - 2\delta} \qquad \text{III - 7}$$

If $\alpha_i^2 < 2\delta$, the angle of transmitted beam is imaginary, and the beam cannot propagate into the material and gets totally reflected. The critical angle α_c is defined as the angle above which transmission occur and it can be linked to the real part of the refractive index and therefore also the electron density via equation III - 7. Typical values for α_c for materials illuminated by a copper $K\alpha$ tube ($\lambda = 1.54$ Å) are between 0.1° and 0.4°.

$$\alpha_c = \sqrt{2\delta} \qquad \text{III - 8}$$

Above α_c the electromagnetic wave partially transmit trough the interface and propagate into the material. Close above α_c, the intensity drops with the fourth power of the scattering vector $I \sim q^4$, which is called the Porod slope.[3] Due to surface- and interface- roughness (σ_{rms}, root mean square), the intensity decreases more rapidly.[4]

$$I_{rough} = I_{ideal} e^{-q^2\sigma_{rms}^2} \qquad \text{III - 9}$$

$$q = \frac{4\pi}{\lambda}\sin(\theta) \qquad \text{III - 10}$$

For a sample with several thin films upon each other, the Fresnel coefficient can be calculated iteratively and multiplied with the influence of the roughness. The resulting intensity of an X-ray reflectivity measurement above the critical angle has an overlaying oscillation with the angle 2θ, which is called Kiessig fringes and can be explained by the interference of the reflection of the X-ray beams at the different interfaces.[5] Thin films of different materials have already been investigated with XRR methods.[6,7]

An example of three X-ray reflectivity measurements of a thin film of poly(hydroxyethyl methacrylate) thin films of thicknesses of 50 nm, 100 nm and 200 nm deposited on a native silicon wafer is depicted in figure 13. The measurements were plotted among each other for visual comparison. At the plateau from 2θ of 0.3° to 0.4° two critical angles can be spotted which can be related to the electron density of the polymer thin film and the silicon oxide. Above the critical angle the intensity drops and fringes appear which are related to the film thickness. The 50 nm thick polymer film exhibits the broadest fringes while the 200 nm thick film the fringes are smaller.

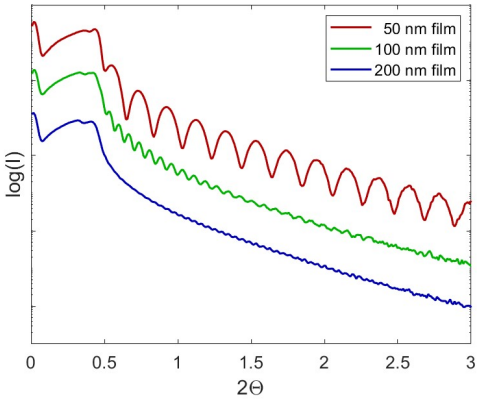

Figure 13: Shifted X-ray reflectivity scans of thin hydrogel films of different thicknesses on silicon wafers.

For measurement of responsive hydrogel thin films, X-ray reflectivity scans can be taken consecutively while exposing the hydrogel to a certain stimulus. One challenging task of the realization of such measurements in the lab is to provide and receive information of a stimulus within a typically closed goniometer. Within this thesis, a domed goniometer stage was equipped with a humidity sensor as depicted in figure 14. Humidity was either generated by a small vessel with water inside the dome or by bubbling nitrogen gas through water and afterwards mixing it with dry nitrogen again to set a specific humidity level. An example of X-ray reflectivity measurements on responsive poly(hydroxyethyl methacrylate) hydrogels exposed to humidity is plotted in figure 15. At 2θ of 0.4°, the critical angle of the sample exposed to humidity shifts slightly to higher value indicating an increase of electron density. Above the critical angle the Porod slope of both measurements are similar, meaning, that the humidity has only little impact to the roughness of the surface. The Kiessig fringes become narrower when the hydrogel is exposed to humidity, which implies an increase of the hydrogels film thickness.

Figure 14: X-Ray diffraction goniometer with doomed heating stage equipped with a humidity sensor.

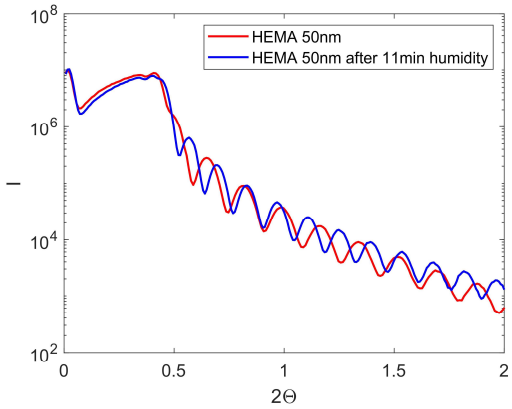

Figure 15: X-ray reflectivity scans of hydrogel thin film during exposure of humidified air.

III.2 Fourier-Transform Infrared Spectroscopy

Fourier-transform infrared spectroscopy (FTIR) is an extensive technique that measures the absorption of an incident IR beam propagated through a material. In the mid-infrared region (4000 cm^{-1} – 400 cm^{-1}), which is commonly explored within an FTIR scan, vibration and rotation modes of chemical structures cause absorption, which can be directly linked to the corresponding compound, depicted in Figure 16.

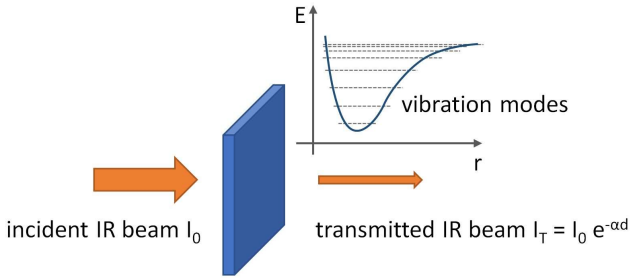

Figure 16: During an infrared spectroscopy scan, the transmitted beam gets absorbed due to rotation or vibration modes of chemical compounds by the law of Beer-Lambert.

In the case of synthesizing polymers FTIR can be utilized to analyze the retention of functional groups, the change from monomer to polymer spectrum, which can be typically seen with the absence of the vinyl bond that is present in the monomer species but is lost in the polymer, and especially when measuring co-polymers, the ratio of different monomer units incorporated in the polymer.

According to Beer-Lambert the optical attenuation coefficient μ along the depth z, which is a material constant that characterize how easy a wave signal is weakened, can be written as a sum of N single attenuating species n_i, present in a concentration of σ_i.

$$\mu(z) = \sum_{i=1}^{N} \sigma_i n_i(z) \qquad III - 11$$

Typically, the attenuation coefficient of polymers synthesized by iCVD does not vary with z and the intensity transmitted I_T can be related to the incident intensity I_0, the attenuation coefficient and the sample thickness d as follows:

$$I_T(d) = I_0 e^{-\mu d} \qquad III - 12$$

Especially when analyzing the ratio of different monomer species within polymers, from this law and the approximation, that the difference of volume that is occupied by monomer species in co-polymer and homo-polymer is negligible, follows, that the absorption results by a co-polymer synthesized with different monomer species can be seen as a sum of absorptions caused by homo-polymers of these species weighted by their concentration within the co-polymer. As an example, figure 17 shows a spectrum (red line) of a co-polymer of methacrylic-acid MAA and ethylglycol-di-methacrylate EGDMA. The analysis within this picture was performed by first subtracting a base-line and further calculating the concentrations of MAA and EGDMA with the provided spectra of homo-polymers. The program used was elaborated by Tatzreiter et al.[8]

The broad peak at 1750 cm^{-1} corresponds to C=O stretching vibration, present in MAA and EGDMA. In the homo-polymers (green and blue lines) the C=O peaks are slightly shifted. The C=O stretching vibration is also dependent on the groups attached to the carbon. A typical vinyl bond absorption band would be present at about 1650 cm^{-1} caused by C=C stretching. The absorption in this region is neglectable small, confirming a nearly complete polymerization. Further peaks from 1500 cm^{-1} to 1350 cm^{-1} belong to CH_2 and CH_3 bending, the peak from 1300 cm^{-1} to 1200 cm^{-1} corresponds to C-O-C and C-O and the last peak from 1200 cm^{-1} to 1100 cm^{-1} is caused by C-C bonding.

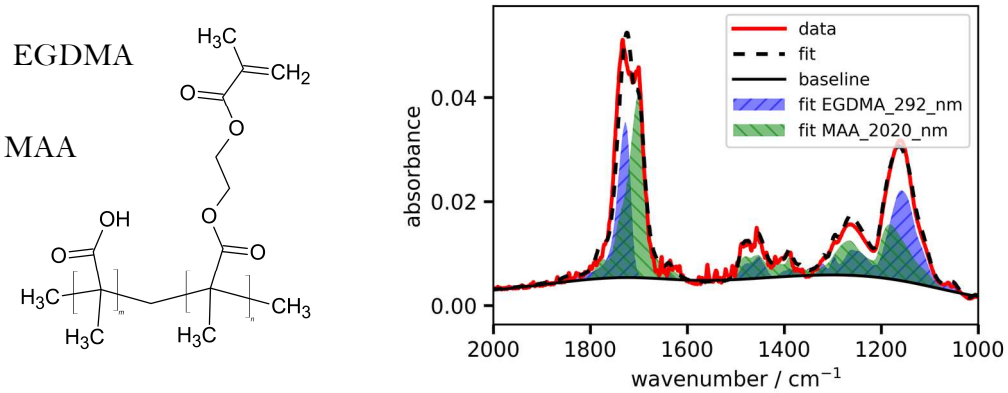

Figure 17: Representation of analysis of a poly(MAA-co-EGDMA) copolymer. The measured data of two functional groups in red can be derived by a sum of the individual ones weighted by the number of monomers present in the copolymer.

III.3 Spectroscopic Ellipsometry

With spectroscopic ellipsometry material properties of thin films, such as the reflective index, the film thickness and the roughness, are obtained by measuring the change in polarization as a function of the wavelength of the incident linearly polarized light beam to the reflected light beam. The fundamental equation for spectroscopic ellipsometry is that the ratio of transverse electric component r_p and transverse magnetic component r_s is equal to an amplitude component ψ and a phase difference Δ.

$$\frac{r_p}{r_s} = tan(\psi) \cdot e^{i\Delta} \qquad III - 13$$

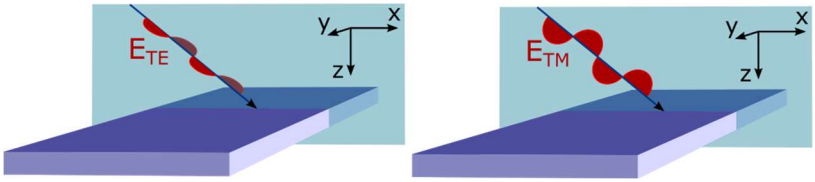

*Figure 18: transverse electric (TE): The **E**-field is parallel to the surface and normal to the (x,z)-plane. Transverse magnetic (TM): The **E**-field is in the (x,z)-plane and the **H**-field is normal to the (x,z)-plane.*

The equation was taken out of the book *Fundamentals of Photonic Crystal Guiding* by M. Skorobogatiy and J. Yang.[8] To derive r_s and r_p, in a first step, light propagation can be written as a superposition of a vertical (transverse electric) and parallel (transverse magnetic) to the surface polarized part. These fields can be described as two planar waves, with one pointing in the direction of propagation and one in the opposite. Within the first step, the materials are considered as dielectric, transparent and without rough surfaces. Starting with the transverse electric polarization, with A and B being the expansion coefficient of the electric field within the jth layer.

$$\mathrm{E}_y^j(x,y,z) = e^{ik_x x}\left(A_j e^{ik_z^j(z-z_j)} + B_j e^{-ik_z^j(z-z_j)}\right) \qquad III - 14$$

Because of Ampères law, which formulates that an, in time varying, electric field induces a magnetic field,

$$\mathbf{H} = -\frac{i}{\omega}\nabla \times \mathbf{E} \qquad III - 15$$

the magnetic field can therefore be written as:

$$\mathrm{H}_x^j(x,y,z) = -e^{ik_x x}\frac{k_z^j}{\omega}\left(A_j e^{ik_z^j(z-z_j)} - B_j e^{-ik_z^j(z-z_j)}\right) \qquad \textit{III - 16}$$

$$\mathrm{H}_z^j(x,y,z) = e^{ik_x x}\frac{k_z^j}{\omega}\left(A_j e^{ik_z^j(z-z_j)} + B_j e^{-ik_z^j(z-z_j)}\right) \qquad \textit{III - 17}$$

At the interface of two materials, the horizontal component of the electric field and the vertical component of the magnetic field have to be conserved:

$$\mathrm{E}_y^j(x,y,z) = \mathrm{E}_y^{j-1}(x,y,z) \qquad \textit{III - 18}$$

$$\mathrm{H}_x^j(x,y,z) = \mathrm{H}_x^{j-1}(x,y,z) \qquad \textit{III - 19}$$

With this boundary conditions a matrix equation can be derived, with $M_{j-1,j}$ the so called transfer matrix.

$$M_{j-1,j}\begin{pmatrix}A_{j-1}\\B_{j-1}\end{pmatrix} = \begin{pmatrix}A_j\\B_j\end{pmatrix} \qquad \textit{III - 20}$$

$$M_{j-1,j} = \frac{1}{2}\begin{pmatrix}\left(1+\frac{k_z^{j-1}}{k_z^j}\right)e^{ik_z^{j-1}d_{j-1}} & \left(1-\frac{k_z^{j-1}}{k_z^j}\right)e^{-ik_z^{j-1}d_{j-1}}\\ \left(1-\frac{k_z^{j-1}}{k_z^j}\right)e^{ik_z^{j-1}d_{j-1}} & \left(1+\frac{k_z^{j-1}}{k_z^j}\right)e^{-ik_z^{j-1}d_{j-1}}\end{pmatrix} \qquad \textit{III - 21}$$

With this matrix, the change of expansion coefficients *A* and *B* of the transverse electric component propagating from one material to another can be derived. For the transverse magnetic part, the same approach can be applied, starting now with A_j and B_j being the expansion coefficient of the magnetic field.

$$\mathrm{H}_y^j(x,y,z) = e^{ik_x x}\left(A_j e^{ik_z^j(z-z_j)} + B_j e^{-ik_z^j(z-z_j)}\right) \qquad \textit{III - 22}$$

The Faradays law, which is the inverse of Amperes law, describes the relation of an in- time-varying-magnetic field to the induced electric field,

$$\mathbf{E} = \frac{i}{\omega\epsilon(r)}\boldsymbol{\nabla}\times\mathbf{H} \qquad \textit{III - 23}$$

and the relation $k_x^2+(k_z^j)^2=\omega^2\varepsilon_j$ the electric field can be written as:

$$\mathrm{E}_x^j(x,y,z) = -e^{ik_x x}\frac{k_z^j}{\omega\varepsilon_j}\left(A_j e^{ik_z^j(z-z_j)} - B_j e^{-ik_z^j(z-z_j)}\right) \qquad \textit{III - 24}$$

$$\mathrm{E}_z^j(x,y,z) = e^{ik_x x}\frac{k_z^j}{\omega\varepsilon_j}\left(A_j e^{ik_z^j(z-z_j)} + B_j e^{-ik_z^j(z-z_j)}\right) \qquad \textit{III - 25}$$

At the interface the vertical component of the electric field and the horizontal component of the magnetic field have to be continuous.

$$\mathrm{E}_x^j(x,y,z) = \mathrm{E}_x^{j-1}(x,y,z) \qquad \textit{III - 26}$$

$$\mathrm{H}_y^j(x,y,z) = \mathrm{H}_y^{j-1}(x,y,z) \qquad \textit{III - 27}$$

Ending up again with a matrix equation:

$$M_{j-1,j}\begin{pmatrix}A_{j-1}\\B_{j-1}\end{pmatrix} = \begin{pmatrix}A_j\\B_j\end{pmatrix} \qquad \textit{III - 28}$$

$$M_{j-1,j} = \frac{1}{2}\begin{pmatrix}\left(1+\frac{k_z^{j-1}\epsilon_j}{k_z^j\epsilon_{j-1}}\right)e^{ik_z^{j-1}d_{j-1}} & \left(1-\frac{k_z^{j-1}\epsilon_j}{k_z^j\epsilon_{j-1}}\right)e^{-ik_z^{j-1}d_{j-1}}\\ \left(1-\frac{k_z^{j-1}\epsilon_j}{k_z^j\epsilon_{j-1}}\right)e^{ik_z^{j-1}d_{j-1}} & \left(1+\frac{k_z^{j-1}\epsilon_j}{k_z^j\epsilon_{j-1}}\right)e^{-ik_z^{j-1}d_{j-1}}\end{pmatrix} \qquad \textit{III - 29}$$

The advantage of this formalism is, that samples typically consists of several layers. Each interface of one layer to another can be represented with a transfer matrix. Light propagating through materials can be simply ascribed as a multiplication of transfer matrices in the correct order.

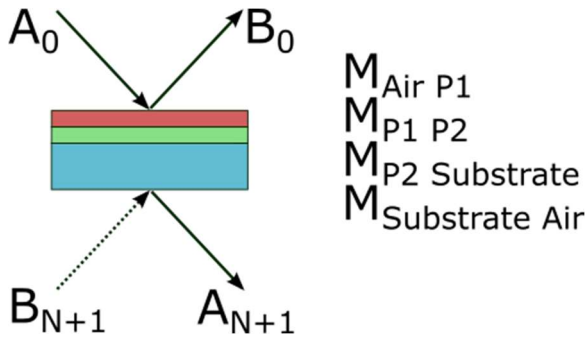

Figure 19: In an ellipsometry setup, the incident beam irradiates a sample of different layers while the illumination from the backside can be neglected $B_{N+1}=0$. The reflected beam and the transmitted beam can be derived by calculating the expansion coefficients B_0 and A_{N+1} by a transfer matrix multiplication.

In figure 19, an example of an ellipsometry measurement can be seen, with $A_0 \equiv 1$, the incident beam and B_0, the measured beam. Aside the image, the transfer matrices for this system are cited. Within spectroscopic ellipsometry measurements, there is no illumination from the backside, so $B_{N+1}=0$, the matrix multiplication reads as follows:

$$\begin{pmatrix} A_{N+1} \\ 0 \end{pmatrix} = M_{sub,air} M_{P2,sub} M_{P1,P2} M_{air,P2} \begin{pmatrix} 1 \\ B_0 \end{pmatrix} \qquad \text{III - 30}$$

$$\begin{pmatrix} A_{N+1} \\ 0 \end{pmatrix} = \begin{pmatrix} m_{11} & m_{12} \\ m_{21} & m_{22} \end{pmatrix} \begin{pmatrix} 1 \\ B_0 \end{pmatrix} \qquad \text{III - 31}$$

$$B_0 = -\frac{m_{21}}{m_{22}} \qquad \text{III - 32}$$

$$A_{N+1} = -\frac{m_{11}m_{22} - m_{12}m_{21}}{m_{22}} \qquad \text{III - 33}$$

The reflected beams intensity $|B_0|^2$ is the measured quantity in ellipsometry, and it is dependent on the thickness d of each layer j and the refractive index of the materials $n_j=\varepsilon_j^{1/2}$. As an example, a reflection of a single surface can be ascribed with one transfer matrix for the transverse electric polarized part and one transfer matrix for the transverse magnetic polarized part and calculating B_0 with equation III - 21 and equation III - 29. The results are the Fresnel coefficients:

$$B_{0,TE} = \frac{k_z' - k_z''}{k_z' + k_z''} \qquad \text{III - 34}$$

$$B_{0,TM} = \frac{k_z'\epsilon_2 - k_z''\epsilon_1}{k_z'\epsilon_1 + k_z''\epsilon_2} \qquad \text{III - 35}$$

Or with $k \propto n \cdot cos(\varphi)$, and $n^2 = \varepsilon$, $B_{0,TE} \equiv r_s$ and $B_{0,TM} \equiv r_p$ a more common form of the Fresnel equation can be derived:

$$r_s = \frac{n_1 cos(\varphi_1) - n_2 cos(\varphi_2)}{n_1 cos(\varphi_1) + n_2 cos(\varphi_2)} \qquad III - 36$$

$$r_p = \frac{n_2 cos(\varphi_1) - n_1 cos(\varphi_2)}{n_2 cos(\varphi_1) + n_1 cos(\varphi_2)} \qquad III - 37$$

For materials with absorptions according to the law of Beer-Lambert the electromagnetic wave needs to be multiplied by a damping factor $e^{-2\pi\alpha z/\lambda}$, with α the attenuation constant along the depth z.

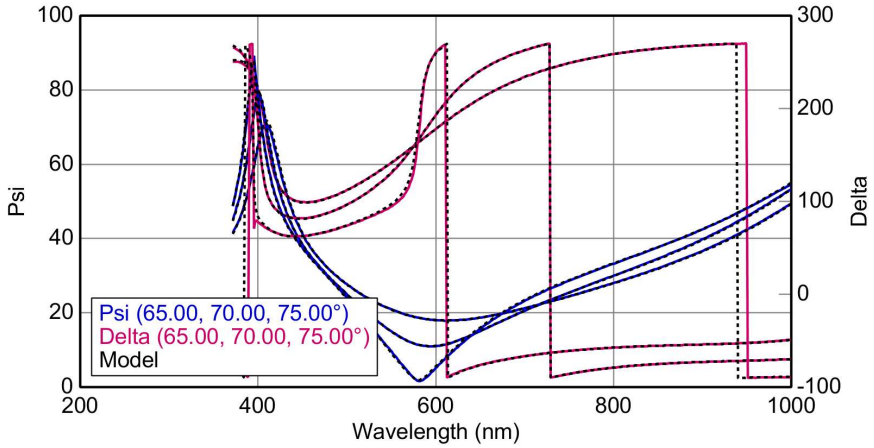

Figure 20: Spectroscopic ellipsometry measurements of a 250 nm thin hydrogel film on silicon wafer.

A representative data set of a performed spectroscopic ellipsometry measurement on a poly-hydroxy-ethyl-methacrylate thin film can be seen in figure 20. The parameters ψ and Δ are plotted versus the wavelength in the region from 300 nm to 1100 nm collected at the three angles 65°, 70° and 75°. The thin film thickness and the optical constants cannot be obtained directly but need to be fitted. A typical routine would be a designed representative model of the sample consisting of a substrate of well-known optical properties and the thin film with a thickness d. For the hydrogels used within this thesis, which are isotropic, transparent and have a normal dispersion within the region observed, a possible and well-established ansatz between the

refractive index n and the wavelength λ is the Cauchy equation. With A and B being fitting parameter.

$$n(\lambda) = A + \frac{B}{\lambda^2} + \frac{C}{\lambda^4} \qquad \textit{III - 38}$$

In terms of responsive hydrogels, ellipsometry measurements can be done continuous while in-situ exposing the hydrogel to its stimulus. Typically, a chamber or special stage designed for the ellipsometer is needed to apply temperature, light, humidity or solution-based stimuli to the sample.

Within this thesis a Woollam M2000 ellipsometer with a normal stage, a liquid stage and a temperature stage was used. The temperature stage was further complemented to a self-designed humidity chamber and a chamber that can provide humidity, temperature and light in terms of multi-stimuli responsive tests.

III.4 Electrochemical Impedance Spectroscopy

Electrochemical impedance spectroscopy is a powerful technique to analyze electrochemical properties of materials. Typical applications are the characterization of corrosion protective layers or batteries. The principle is based on an applied sinusoidal electrical signal and the measured response (see figure 21) at frequencies from 1 Hz to 1 MHz. If the applied signal has a constant voltage amplitude the measurement is called potentiostatic, if the signal has a constant current amplitude it is called galvaniostatic. In a potentiostatic measurement the voltage U and the current I in the time t can be written with ω, the angular frequency and φ, the phase shift between the voltage and the current:

$$U(t) = U_0 \cos(\omega t) \qquad \textit{III - 39}$$

$$I(t) = I_0 \cos(\omega t + \varphi) \qquad \textit{III - 40}$$

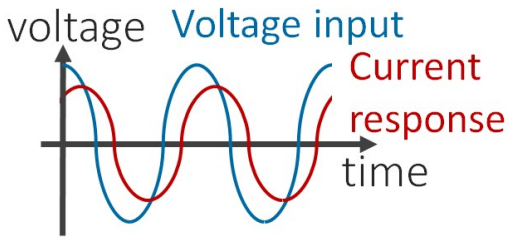

Figure 21: Sinusoidal voltage signal and responding current within an electrochemical impedance spectroscopy scan.

The impedance is defined as the relation between the voltage and the current.

$$Z(t) = \frac{U(t)}{I(t)} = \frac{\overset{Z_0}{\widetilde{U_0}}}{I_0} \frac{\cos(\omega t)}{\cos(\omega t + \varphi)} \qquad III - 41$$

Which can be transformed into the frequency domain:

$$Z(\omega) = Z_0(\cos(\varphi) + i\, sin(\varphi)) = Z_0 e^{i\varphi} \qquad III - 42$$

There exist two main graphical representations of electrochemical impedance spectroscopy. One is the Nyquist plot, which presents the real part of equation III - 42 versus the imaginary part. The other are the two Bode plots, which show Z_0 and φ versus the frequency. A representing equivalent circuit needs to be modeled to interpret electrochemical impedance measurement.

In the domain of smart hydrogels, electrochemical impedance can measure the dielectric response towards certain stimuli by in-situ taking scans while exposing the hydrogel to external changes of the environment.

III.5 References

1. Daillant, J. & Gibaud, A. X-ray and neutron reflectivity: Principles and applications. vol. 770 (Springer, 2009).

2. Birkholz, M., Fewster, P. F. & Genzel, C. Thin film analysis by X -ray scattering. (Wiley-VCH and John Wiley, distributor], 2006).

3. Porod, G. Die Röntgenkleinwinkelstreuung von dichtgepackten kolloiden Systemen. Kolloid-Zeitschrift **124**, 83–114 (1951).

4. Névot, L. & Croce, P. Caractérisation des surfaces par réflexion rasante de rayons X. Application à l'étude du polissage de quelques verres silicates. Rev. Phys. Appliquée **15**, 761–779 (1980).

5. Kiessig, H. Interferenz von Röntgenstrahlen an dünnen Schichten. Ann. Phys. **402**, 769–788 (1931).

6. Unger, K. et al. Distributed Bragg Reflectors: Morphology of Cellulose Acetate and Polystyrene Multilayers. Proc. Ict. 2014.

7. Werzer, O., Matoy, K., Strohriegl, P. & Resel, R. Temperature treatment of semiconducting polymers: An X-ray reflectivity study. Thin Solid Films **515**, 5601–5605 (2007).

8. Tazreiter, M., Christian, P., Schennach, R., Grießer, T. & Coclite, A. M. Simple method for the quantitative analysis of thin copolymer films on substrates by infrared spectroscopy using direct calibration. Anal. Methods **9**, 5266–5273 (2017).

Chapter IV

Scientific Publications

Within this section, two scientific peer-reviewed publications by the author of this thesis will be presented with the permission from the publisher.

Dynamic Studies on the Response to Humidity of Poly (2-hydroxyethyl methacrylate) Hydrogels Produced by Initiated Chemical Vapor Deposition

---

(link: https://doi.org/10.1002/macp.201600271)

Novel Light-Responsive Biocompatible Hydrogels Produced by Initiated Chemical Vapor Deposition

---

(link: https://doi.org/10.1021/acsami.7b01527)

Additionally, a manuscript of a third study will be presented, which is still in preparation and not published yet.

Temporary Tattoo pH Sensor with pH Responsive Hydrogel via Initiated Chemical Vapor Deposition

---

IV.1 Dynamic Studies on the Response to Humidity of Poly (2-hydroxyethyl methacrylate) Hydrogels Produced by Initiated Chemical Vapor Deposition

Macromolecular Chemistry and Physics

Dynamic Studies on the Response to Humidity of Poly (2-hydroxyethyl methacrylate) Hydrogels Produced by Initiated Chemical Vapor Deposition

Katrin Unger, Roland Resel, Anna Maria Coclite

First published: 22 August 2016 | https://doi.org/10.1002/macp.201600271 | Citations: 18

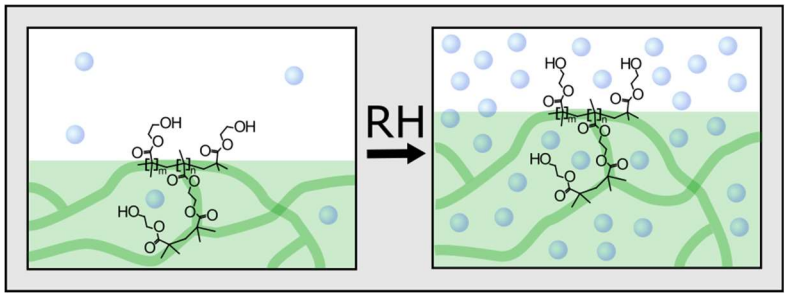

Humidity-responsive hydrogels are synthetized by initiated chemical vapor deposition, with defined crosslinking ratios. The swelling in a humid environment is measured in situ by X-ray reflectivity and related to the mesh size and the solubility of the polymer. It is found that the intermixing between the water vapor and the hydrogels changes with the relative humidity due to molecular rearrangements in the hydrogel's meshes.

Reference: Katrin Unger, Roland Resel, Anna Maria Coclite; Dynamic Studies on the Response to Humidity of Poly (2-hydroxyethyl methacrylate) Hydrogels Produced by Initiated Chemical Vapor Deposition. *Macromol. Chem. Phys.* **217**, 2372–2379 (2016).
https://doi.org/10.1002/macp.201600271

IV.1.1 Preface

The work of this publication was conducted at the Graz University of technology as the first part of the Marie Curie International Incoming Fellowship (project 626889) named Smart multi Stimuli-responsive Supports for controlled cell growth by Anna Maria Coclite. The author of this thesis performed the sample preparation, characterization and wrote the manuscript. Roland Resel helped regarding the interpretation of data and preparing the manuscript. Anna Maria Coclite supervised the project and helped in the manuscript preparation. The article is reproduced identical in text and illustration to that in the scientific publication with permission.

IV.1.2 Abstract

The swelling of 2-hydroxyethyl methacrylate (HEMA) hydrogels, commonly synthesized by solution polymerization, has been widely studied for its practical and fundamental importance. While a good understanding of polymer-liquid interactions has been established within the Flory-Huggins framework, little is known about polymer-water vapor interactions. In this study, the swelling of pHEMA films in response to water and humidity is investigated by means of X-ray reflectivity and spectroscopic ellipsometry. The hydrogels are synthesized by initiated chemical vapor deposition, using ethylene glycol dimethacrylate (EGDMA) as a crosslinking agent. In water, copolymers of p(HEMA-co-EGDMA) are stable for an EGDMA fraction above 17%. In a humid atmosphere, even samples with no EGDMA are stable. On increasing the EGDMA fraction, both the swellability in water and in humid environments decreases. The swelling in both environments is related to the mesh size and solubility of the hydrogel, using the Flory-Huggins theory. The mesh size (average length between two crosslinks) decreases with increasing EGDMA fraction, as expected. The interaction parameter between water vapor and the polymer decreases with increasing relative humidity and reaches 1 ± 0.1 at RH > 75%.

IV.1.3 Introduction

Hydrogels are water-unsolvable polymer networks, which absorb and retain water. Their mechanical properties and swellability are highly desirable for various applications including biocompatible sensors, matrices for incorporating pharmaceuticals, and scaffolds for cell culture.[1–3] The hydrophilic groups in the hydrogel are responsible for water absorption. To guarantee stability in water, the hydrophilic polymer chains need to be physically or chemically crosslinked.[4] Properties like the surface tension, the swellability, and the elasticity are crucially

dependent on the crosslink ratio.[5,6] In a humid environment, hydrogels require no or just a few crosslinks, while in an aqueous environment a stronger polymer network is needed to maintain stability. Synthesizing hydrogels with solution-based methods is often problematic due to the incorporation of the solvent in the hydrogel matrices. Especially biocompatible polymers need to be free of residual solvents. A solvent-free technique to produce hydrogel thin films is initiated chemical vapor deposition (iCVD).[7] This technique is based on radical polymerization, in which free radicals react with non-radical monomer units to form long polymer chains.[8,9] The free-radicals are formed by thermal decomposition of a sacrificial molecule, called the initiator. The initiator and monomer species enter the iCVD chamber as vapors. The initiator is decomposed by interacting with a relatively hot filament (150–300 °C). At these temperatures, only the labile bonds present in the initiator (e.g., the O–O bond in tert-butyl peroxide) break. The monomer decomposition temperatures are generally higher than 500 °C; therefore the monomer does not decompose at the filament temperature. Several review papers explain the polymerization mechanism of the iCVD method in more detail.[10,11] The chemical composition of polymers can be tuned by changing the monomer fraction, while other process parameters, such as the filament temperature and the substrate tempera- ture, affect the kinetics of the polymerization process.[12] In addition to control over the crosslinking density and chemical composition, the iCVD can widen the applicability of hydrogels by adding other interesting features, such as the possibility of fabricating them in an ultrathin (<50 nm) film form of uniform thickness on geometrically complex surfaces (e.g., conformal coatings), in the complete absence of trace solvents or plasticizers. The hydrogels were investigated with spectroscopic ellipsometry and X-ray reflectivity (XRR). Both techniques are non-destructive and require minimal sample preparation. XRR measures the differences in electron density. Each interface within the sample causes reflection and transmission, and as a consequence produces an interference pattern called Kiessig fringes.[13] The quantities measurable by XRR are the thickness (in the range of 0.5–200 nm), the surface roughness, and the total electron density. In situ XRR studies are commonly used to measure thin film morphology changes due to temperature or humidity.[14–18] Spectroscopic ellipsometry is the method of choice for the determination of the optical properties of thin films, such as the refractive index and the extinction coefficient. Thicknesses up to several micrometers are measurable. Both experimental techniques require suitable modeling and fitting tools to extract the above-mentioned information. The most intensively studied hydrogel is the polymer of 2-hydroxyethyl methacrylate (pHEMA).[6,19–21] Polymers of HEMA need to be crosslinked to be stable in water, e.g., chemically with ethylene glycol-dimethacrylate (EGDMA). Homogeneous ultrathin (<50 nm) polymer films of water stable crosslinked hydrogels have been synthesized by iCVD and they were investigated regarding their interaction with water.[6,19,20]

The water content absorbed by pHEMA can be as high as in living tissues, which makes it suitable for biochemical applications, such as contact lenses or coronal replacements.[21]

The absorption of water can be related to the mesh size (i.e., the length scale of two sequential crosslinks in the polymer matrix) with the equilibrium swelling theory of Flory and Rehner.[22,23] The mesh size and the characteristic interaction parameter, χ, can be determined by swelling measurements. The interaction parameter of pHEMA with water has already been investigated.[24,25] The interaction parameter of pHEMA with water vapor has been measured so far only for solution-synthesized pHEMA hydrogels with a low density, and it was shown to decrease from 1.5 to 1, in the relative humidity range 20–90%.[26] The interaction of pHEMA and water vapor changes with the relative humidity, because the pendant chains at the polymer-air interface can rearrange depending on the water vapor concentration.[29] Due to its polarity, water tends to form strong H-bonds, within itself or with the polymer, as has been observed for other polymer films, such as poly(3-alkylthiophene), exposed to humidity.[30] This turns into the formation of clusters or plasticization of the polymer matrix. In particular, at low relative humidity (RH), pHEMA hydrogels tend to produce a glassy skin at the film-air interface that prevents the film from swelling.[25] This is of crucial interest, especially for pHEMA-based soft contact lenses or membranes.[26–28] In the absence of data, research groups tend to use the Flory-Huggins interaction parameter pHEMA with water, while actually performing measurements in humidity.[24,25,31] Therefore, a systematic investigation of the dependency of χ on the relative humidity is extremely important and urgently needed, particularly for vapor-phase synthetized pHEMA. In the present investigation, the interaction between water, as well as water vapor, and crosslinked p(HEMA) hydrogel films obtained by iCVD is studied. In particular, we related the swelling in aqueous and humid environments to the mesh size and calculated the interaction parameter, χ, between the water vapor and the hydrogels.

IV.1.4 Experimental Part

Film Preparation

Co-polymer films of 2-hydroxyethyl methacrylate (HEMA, Aldrich 97%) and ethylene glycol-dimethacrylate (EGDMA, Aldrich 98%) were deposited on silicon wafers in a custom-built initiated Chemical Vapor Deposition (iCVD) reactor, described elsewhere.[32] The monomers and the tert-Butyl peroxide (TBPO, Aldrich 98%), which acts as initiator, were used without further purification. HEMA and EGDMA were heated up to 75°C and 80°C, respectively. The TBPO was kept at room temperature and was fed in the reactor at a flow rate of 1 sccm. While the HEMA flow rate was kept at 0.8 sccm (except for the pure EGDMA sample), the EGDMA flow rate increased for the different depositions stepwise from 0 sccm to 0.15 sccm to obtain a gradient in the cross-linking degree. The flow rate of EGDMA was kept small compared to the one of HEMA, because EGDMA has a rather small saturation pressure (0.012 mTorr at 25°C) compared to HEMA (0.159 mTorr at 25°C), therefore more EGDMA molecules tend to get adsorbed on the surface.[6,33] During the deposition, the working pressure was maintained at 350 mTorr. Nitrogen was fed into the reactor at a flow rate of 3 sccm. The substrate and the filament temperatures were 20°C and 300°C, respectively. The film thickness was in-situ monitored via laser interferometry. The depositions were stopped at a thickness of approximately 100 nm. The deposition rates achieved in these conditions were ranging between 5 nm/min and 12 nm/min.

Characterization

Fourier Transform Infrared (FTIR) spectroscopy (Bruker IFS 66v/S) was performed to verify the polymerization and the retention of functional groups. The spectra were recorded in transmission mode in the region 400 – 4000 cm^{-1} with a resolution of 4 cm^{-1}. The spectrometer was evacuated to a pressure of 5 mbar and a constant flow of nitrogen was used to cool the mirror. All the spectra were baseline corrected and normalized with the thickness. The height of the peak at 1727 cm^{-1}, which corresponds to the C=O stretching, was used to extract the EGDMA fraction in the polymer.

The film thickness was measured by X-ray reflectivity. The goniometer used was a *PANalytical Empyrean* system with radiation produced by a copper tube (λ = 1.54 Å). The primary side the reflectometer was equipped with a 1/32° slit, a 10 mm beam mask, a multilayer mirror and an automatic beam attenuator. On the secondary side, a receiving slit of 0.1 mm and a Soller slit of 0.02 rad were placed before the point detector, *PANalytical PIXEL3D*. The sample stage was a domed DHS 900 by Anton Paar.[34] For the in-situ swelling measurements, the dome was equipped with a SHT15 humidity sensor to monitor the relative humidity and the temperature.

The humidity was increased by introducing a small vessel filled with pure water under the dome. XRR scans were performed in the region of 2θ 0.024° - 1.00° with a step size of 0.008° before exposing the sample to the water vapor and every minute during the humidity ramp. After 15 min the dome was purged for 3 min with CO_2 to lower the humidity. The XRR scans are characterized by a plateau of total reflection up to the critical angle of the material, θ_c. The sample contains three materials (Si - SiO_2 - polymer) which all contribute with their individual critical angle, θ_c. The critical angle $\theta_{substrate}$, measured at the half of the plateaus maximum, at 0.22°, is typical of the silicon and silicon dioxide. The distance of two serial fringe positions gives the information on the film thickness The film thickness (d) was calculated with Eq. 1, knowing the critical angle of the polymer (θ_{pol}), the angle position of two sequential fringe peaks (θ_1 and θ_2), and the X-ray wavelength.[35]

$$\lambda = 2d\left(\sqrt{cos^2\theta_{pol} - cos^2\theta_2} - \sqrt{cos^2\theta_{pol} - cos^2\theta_1}\right) \quad (1)$$

For the in situ swelling measurements, the dome was equipped with a SHT15 humidity sensor to monitor the relative humidity and the temperature. The humidity was increased by introducing a small vessel filled with pure water under the dome. This induced a fast RH increase in the first five minutes (≈9 % min^{-1}) and a slower rate thereafter (≈1 % min^{-1}). After 15 min the dome was purged for 3 min with CO_2 to decrease the humidity. Correspondingly, the humidity decreased quickly with a rate of ≈15 % min^{-1} in the first minute and then kept constant. A plot of the humidity ramp is shown in figure 1. The XRR scans were recorded before exposing the sample to the water vapor and every minute during the humidity ramp.

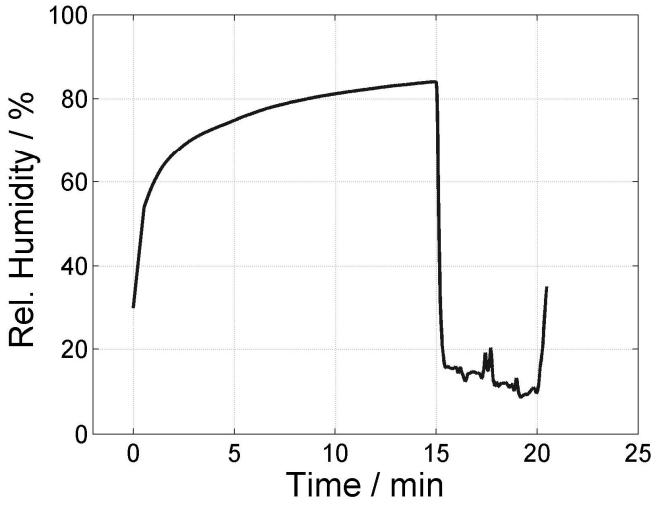

Figure 1: Plot of the relative humidity ramp to which the hydrogels were exposed.

The film thickness and the swelling in water was measured with spectroscopic ellipsometry (J. A. Woollam ESM-300). A liquid cell (J. A. Woollam) was used to hold the pure water in a tight seal. Because of the geometry of the cell, only spectra with an incident angles of 75° were measured. The sampled spectral region was between 370 nm and 1000 nm. The data were collected with a time resolution of 2 s. In the dried state, the measured data were modeled with a 3-layers system containing silicon and native silicon dioxide (2.1 nm) as substrate and a Cauchy layer for the thin film polymer. In water, the polymer layer was modeled with the effective material approximation (EMA), which models the material as a mixed composition of two components with defined optical parameters. The thickness and the materials ratio are the fitting parameters. This is a typical procedure for transparent swollen hydrogels.[33]

IV.1.5 Results and Discussion

The initiated chemical vapor deposition (iCVD) was used to synthetize copolymers of HEMA and EGDMA, p(HEMA-co-EGDMA), with different chemical composition. Infrared absorption spectra were used to analyze the chemical composition of the p(HEMA-co-EGDMA) samples. The infrared absorption spectra are plotted in figure 2. The absorption band due to the OH stretching is visible at 3460–3000 cm^{-1}. The multiple absorptions at 2954–2850 cm^{-1} can be assigned to the symmetric and antisymmetric stretching of the CHx bonds. The footprint region starts with a prominent strong peak at 1728 cm^{-1} caused by C=O stretching. Another strong peak at 1152 cm^{-1} can be assigned to the C–OH stretching. The C=O stretching at 1728 cm^{-1} can be ascribed to the contribution of both HEMA and EGDMA units. Since HEMA has just one C=O bond and EGDMA two, the EGDMA homopolymer spectrum shows a C=O peak which has approximately double the intensity of the HEMA homopolymer spectrum. The height of the C=O peak was used to calculate the EGDMA fraction in the copolymer, as indicated in figure 2. Already a relatively small EGDMA flow rate of 0.025 sccm leads to an EGDMA fraction in the polymer of 17%. This high reactivity, compared to HEMA, can be attributed to the two vinyl bonds of EGDMA, as well as to the smaller saturation pressure of EGDMA.

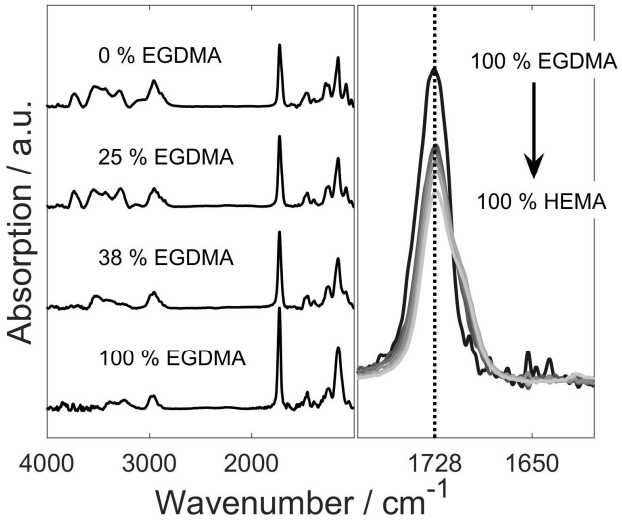

Figure 2: left: Infrared absorption spectra overview of four samples; right: enlarged area of the C=O stretching of all p(HEMA-co-EGDMA) samples

X-ray reflectivity (XRR) investigations showed that the thicknesses of the samples ranged between 106 and 137 nm. The surface roughness for all the samples was between 0.42 and 0.51 nm.The critical angle of pHEMA homopolymer, $\theta_{pol,}$ was 0.170 ± 0.002°. This value of critical angle gave an electron density of 0.41 ± 0.01 $e^-/Å^3$. Considering that the electron density of a single HEMA species is 70 e^-/molecule, we can calculate the molecular density; this results in 5.9 HEMA units per nm^3. Knowing also the HEMA molecular weight (130 g/mol), we can determine the polymer weight density. The so obtained value was 1.26 ± 0.09 g/cm^3. Literature values for the density of pHEMA vary between 1.15 g/cm^3 (Sigma Aldrich) and 1.274 g/cm^3, depending the synthetic route.[36,37] It has been indeed demonstrated that solution-synthesized pHEMA forms homogeneous and transparent hydrogels, with density comparable to the one calculated for our iCVD polymers, when it is solution-synthesized with a water content below 40%. The density, instead, drops when the hydrogel is prepared with a higher water amount. In the latter case, sponge-like macroporous and opaque low-density structures are observed.[21]

The effect of the cross-linking degree on the swelling of the hydrogels in relative humidity was as well measured by X-ray reflectivity (XRR). figure 3 shows several XRR scans of the sample with 17% EGDMA. The topmost curve was measured under ambient condition. The relative humidity was increased for 15 min from 30% (ambient condition) up to 84% and afterwards abruptly lowered to 13%, as shown in figure 1. The same humidity ramp was used for all the samples. The change in the Kiessig fringe positions is caused by thickness changes induced by changes in the relative humidity. The fringes shifted with increasing humidity to the left, which

implies an increase in thickness of the film. After 15 min the humidity was lowered to 13% and the fringes moved back to their initial position indicating that the swelling is reversible and the de-swelling is faster than 1 min. A change in the critical angle of the polymer could not be observed with increasing humidity since the electron density of water (0.33 e– Å^{-3}) is too similar to the polymer electron density.

The trend of the thickness increase $\Delta d/d_0$ (where d0 is the thickness under ambient conditions and Δd is the change of thickness after exposure to humidity) in time is plotted in Figure 4 and fitted with an exponential function. [26] The hydrogels response depends on the crosslinking degree. Without any crosslinker, pHEMA swells the most (+30%). With increasing amounts of EGDMA, the pHEMA hydrogels swell less. Samples with more than 25% EGDMA showed poor swelling upon exposure to humidity, with less than a 3% thickness increase. All the samples showed a fast deswelling (<1 min) when the RH was decreased to 13%, after 15 min.

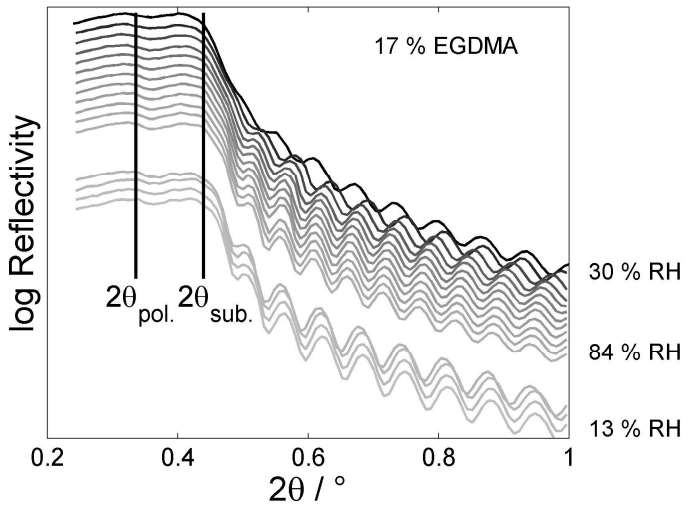

Figure 3: In situ X-ray reflectivity scans during humidity treatment of the hydrogel p(HEMA-co-EGDMA), with 17% EGDMA, as representative. In the first 15 min, the relative humidity (RH) increased from 30 to 84%. After that, the humidity was lowered to 13%. $2\theta_{pol.}$ and $2\theta_{sub.}$ are the critical angles of the polymer and the substrate, respectively. The curves are shifted for clarity.

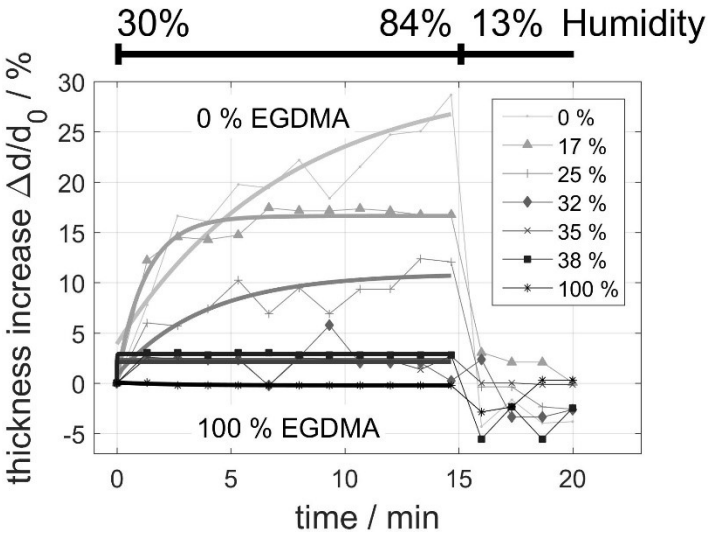

Figure 4: Thickness increase during humidity exposure of samples with different amount of EGDMA. The thickness was measured by X-ray reflectivity. The topmost curve belongs to the sample with 0% EGDMA while the lowermost corresponds to the sample with 100% EGDMA.

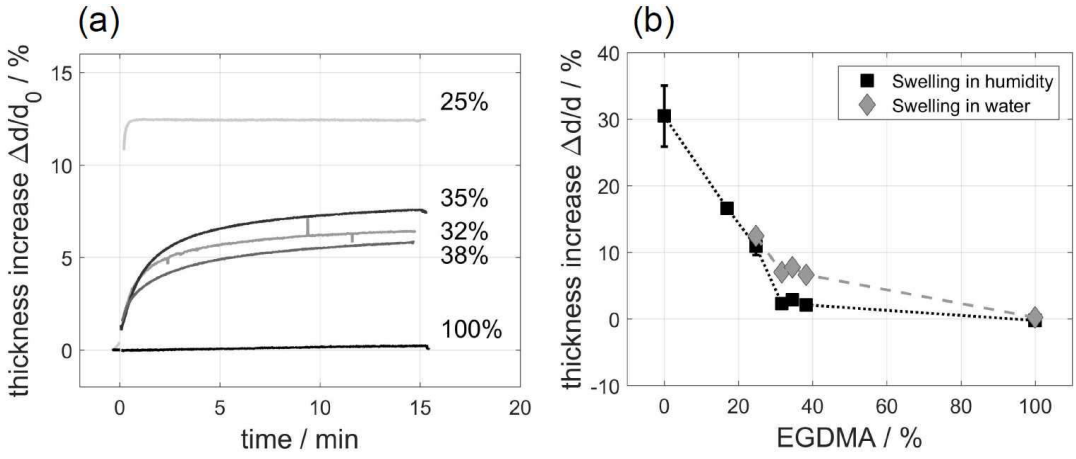

Figure 5: (a) Spectroscopic ellipsometry data on the thickness increase in time of p(HEMA-co-EGDMA) hydrogels with different amounts of EGDMA upon immersion in water. (b) Thickness increase versus the EGDMA fraction in humidity and in water.

For comparison, the thickness increase in water was measured by in situ spectroscopic ellipsometry. The p(HEMA-co-EGDMA) film with 0% EGDMA dissolved completely, while the one with 17% dissolved partially. The thickness increase in time, for the samples with more than 25% EGDMA, is plotted in figure 5a. The stable sample with the lowest fraction of EGDMA (25%) swells the most, with 12% water uptake. The sample with 38% EGDMA swells by about 7% and the pure EGDMA sample shows no swelling. Other iCVD hydrogels showed higher

swelling when crosslinked with other molecules, e.g., ethylenglycoldiacrylate (EGDA),[33] but differences in swelling ratios depending on the length of crosslinked chain are expected.[38] The swelling in water and in humid air of p(HEMA-co-EGDMA) is shown in figure 5b. The p(HEMA-co-EGDMA) films swell slightly more in water than in humid air. In humidity, samples with more than 32% EGDMA fraction swell less than 3%. Only the sample with 25% EGDMA fraction swells in humidity (+11%) as well as in water (+12%) with a thickness increase of more than 10%. In order to exclude possible misleading results due to the lifting of the physisorbed film from the substrate by water, we repeated some experiments on films that were covalently bonded to the substrate.[39] The covalent bonding was achieved by pre-treating the silicon substrate with oxygen plasma to remove any organic impurities and to increase the surface hydroxyl concentration. Subsequent exposure of the treated Si substrate to tricholorovinylsilane vapor produced covalently bound vinyl groups on the surface. The pretreated substrate was then subjected to the iCVD process. The swelling amplitude observed on the covalently bonded films was the same as the swelling performances of the physisorbed films ±1%. The Flory-Rehner theory links the mesh size of a polymer network with the swelling in water d/d0, where d0 is the thickness before the water treatment and d is the thickness in water in the thermodynamic equilibrium.[22,23] For a hydrogel on a silicon wafer, the average molecular weight between two cross-links Mc can be calculated using equation (2)[6]

$$\frac{1}{\bar{M}_c} = -\frac{2}{M_m}\frac{ln\left(1-\frac{d_0}{d}\right)+\frac{d_0}{d}+\chi\left(\frac{d_0}{d}\right)^2}{2\frac{d}{d_0}-\frac{d_0}{d}} \qquad (2)$$

where M_m is the molecular weight of the monomer HEMA (130 g mol^{-1}) and χ is the Flory-Huggins interaction parameter of pHEMA with water. This parameter is known in the literature (0.84) and was determined with swelling and elasticity measurments in liquid water.[24] The mesh size of the polymer network can be calculated by knowing the C–C bond length l (0.154 nm) using equation (3).

$$\xi = \left(\frac{d_0}{d}\right)^{-\frac{1}{3}} l \left(\frac{2\bar{M}_c}{M_m}\right)^{\frac{1}{2}} c_n^{\frac{1}{2}} \qquad (3)$$

where c_n is the characteristic HEMA ratio (6.9), which accounts for the deviation of HEMA to an ideal polymer chain model due to steric hindrance and bond rotation.[40] The mesh size, calculated with the swelling results taken from ellipsometry, is plotted in figure 6 as a function of the EGDMA fraction.

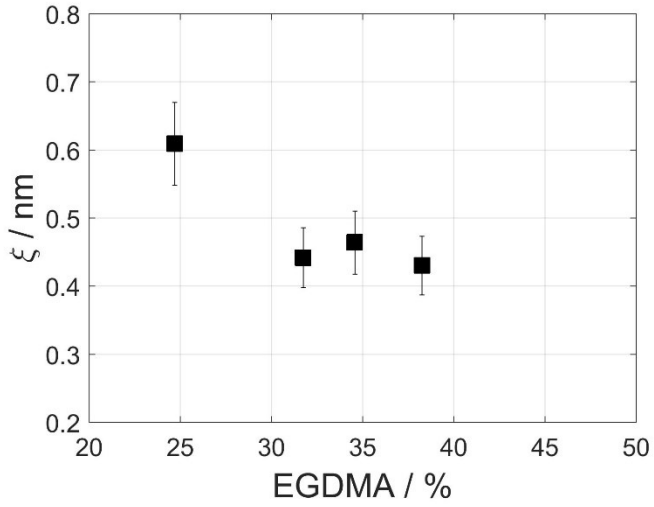

Figure 6: Polymer network mesh size ξ in liquid water versus the EGDMA fraction calculated with Flory theory of cross-linked hydrogels.

It varies from 0.6 to 0.4 nm, depending on the fraction of EGDMA incorporated in the polymer. Similar mesh sizes were obtained for iCVD hydrogels of HEMA crosslinked with EGDMA by Tufani et al.[41] They obtained mesh sizes from 0.34 to 0.75 nm, depending on the crosslink ratio. Hydrogels with such small mesh sizes can be used for the diffusion of small dye molecules.[6,41] The Flory-Rehner theory holds for crosslinked hydro-gels, while the water vapor sorption of linear or slightly crosslinked polymers can be described by the Flory-Hug- gins theory. For linear or slightly crosslinked hydrogels, the amount of water vapor sorption due to the relative humidity (RH) depends on the swelling d/d_0 and the Flory- Huggins parameter χ, as described in Equation (4).[30]

$$\ln(RH) = \ln\left(1 - \frac{d_0}{d}\right) + \frac{d_0}{d} + \chi\left(\frac{d_0}{d}\right)^2 \quad (4)$$

Generally, the Flory-Huggins interaction parameter, χ, gives an indication of the interaction between polymer and solvent. The larger the interaction parameter χ, the less solvent molecules tend to penetrate into the film and swelling is reduced. If $\chi < 0.5$, the solvent can easily dis- solve the polymer (good solvent), while if $\chi > 0.5$, the solvent poorly dissolves the polymer (bad solvent).[42] When a solvent diffuses into a polymer, the chains rearrange to a new configuration depending on the temperature and on the solvent concentration. The Flory-Huggins interaction parameters, calculated from equation (4), for the copolymers p(HEMA-co-

EGDMA) with 0 and 17% EGDMA, are plotted against the relative humidity in figure 6. These two samples are water soluble, which fit the requirements for this theory. The d/d0 values were taken from figure 4. Due to the rapid increase of relative humidity in the first minute and the low time resolution of the XRR investigation, the d/d0 values were measured only in the range of humidity 65–84%. In order to access the trend of the Flory-Huggins parameter also below 65%, we calculated the d/d0 values by fitting the thickness increase as a function of time as in figure 4. The Flory-Huggins parameter trend calculated from this fit is labeled as "predicted" in figure 7. Two regions can be distinguished depending on the relative humidity in figure 7. For relative humidity values smaller than 75%, the predicted χ decreases quickly: from 2.8 to 1.1 for pHEMA and from 3.7 to 1.2 in the case of the copolymer with 17% EGDMA. PHEMA hydrogels have been reported to produce a glassy skin at the membrane- air interface below 75% RH which protects the film from swelling.[25] The decrease of the predicted χ below 75% observable in figure 6 seems to indicate that also our hydrogels tend to form a similar protection layer against swelling. When the humidity is low, the hydrophilic OH- terminated pendant chains of HEMA preferably orient inwards, to minimize the surface energy. This kind of chain organization results in an apolar surface that swells less. Above 75% RH, both the predicted χ and the χ calculated over the experimental data reach a plateau around 1 ± 0.1. This means that the water vapors can penetrate the hydrogel, but still do not dissolve the polymer. This could be explained with a chain rearrangement in which the hydrophilic OH-terminated pendant chain of HEMA orients outwards the interface between the polymer and humid air. The literature value of χ for pHEMA and water is 0.84.[24] The value of 1 ± 0.1 obtained for χ of pHEMA and water vapor (>75%) in this study is correspondingly reasonable. The sample with 17% EGDMA shows a higher interaction parameter χ compared to the pHEMA sample. The difference in χ shrinks with increasing humidity and converges at 75% RH, suggesting that the influence of EGDMA lowers with increasing humidity. The permeability of water vapor through the hydrogel can have important consequences in pharmaceutical research, e.g., for drug delivery systems, or in packaging applications. In particular, the slow swelling at low RH can be favorable to enhance the delivery of poorly-water soluble drugs and stabilize them in an amorphous state in which they are more soluble and more bioavailable.[43] The swelling at high RH or in water can be used for the controlled delivery of the drug.

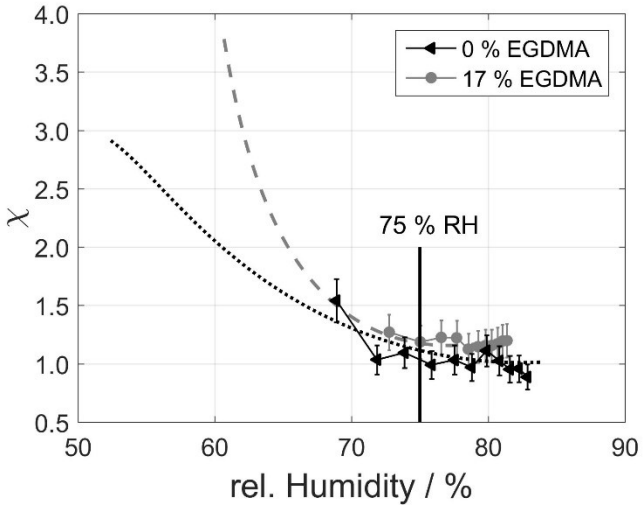

Figure 7: *Flory-Huggins interaction parameter χ for p(HEMA-co- EGDMA) hydrogel with 0 and 17% EGDMA as a function of the relative humidity. Symbols were calculated using the measured thickness increases reported in figure 4. Dotted lines (predicted values) were calculated from the fitting of the thickness increases reported in figure 4.*

IV.1.6 Conclusion

Hydrogels of p(HEMA-co-EGDMA) copolymers were synthesized by initiated chemical vapor deposition with the aim of studying the response of iCVD hydrogels to humidity. Different crosslinking degrees were obtained by varying the monomer gas flow rates during the deposition. The density of the hydrogel films, as calculated from X-ray reflectivity, was comparable to the density of hydrogels obtained by solution synthesis. The swelling in humidity was measured by in situ X-ray reflectivity. None of the samples dissolved upon exposure to relative humidity up to 84 ± 2%. Pure pHEMA swelled the most with a thickness increase of 30%. Samples with more than 25% EGDMA showed less than 3% thickness increase due to humidity. The more EGDMA, the less swelling was observed. For samples with low crosslinking degrees (low EGDMA), the water vapor sorption data were interpreted with the Flory-Huggins equation. The Flory interaction parameter, χ, describes the intermixing of water vapor and the polymer. Increasing the relative humidity to 75%, the parameter χ decreases for pure pHEMA from 2.8 to 1.1 and reaches a constant value of 1 ± 0.1 at RH > 75%. The parameter χ for the sample with 17% EGDMA showed a similar trend: it decreases quickly from 3.7 to 1.2 with increasing RH below 75% RH and remains constant at 1.2 ± 0.1 above 75% RH. The high χ values obtained at low humidity can be interpreted as evidence for the formation of a glassy skin at the hydrogel-air interface that prevents the water vapor from penetrating the hydrogel structure. In comparison,

the swelling in water was measured with spectroscopic ellipsometry. The samples with less than 17% EGDMA fraction dissolved. Also in this case, the more EGDMA incorporated in the film, the smaller the thickness increase observed. The mesh size was calculated by applying the Flory theory on crosslinked hydro- gels. The larger the mesh size of a hydrogel polymer net- work, the easier water or other molecules can penetrate into it. The mesh size varied from 0.4 to 0.6 nm, upon lowering the EGDMA fraction.

Acknowledgements

This research was supported by a Marie Curie International Incoming Fellowship (project 626889) within the 7th European Community Framework Programme.

IV.1.7 References

(1) Buenger, D., Topuz, F., Groll, J. Hydrogels in sensing applications. *Progress in Polymer Science* **2012**, *37*, 1678–1719.

(2) Qiu, Y., Park, K. Environment-sensitive hydrogels for drug delivery. *Advanced Drug Delivery Reviews* **2012**, *64*, 49–60.

(3) van Vlierberghe, S., Dubruel, P., Schacht, E. Biopolymer-based hydrogels as scaffolds for tissue engineering applications: a review. *Biomacromolecules* **2011**, *12*, 1387–1408.

(4) Hennink, W., van Nostrum, C. Novel crosslinking methods to design hydrogels. *Advanced Drug Delivery Reviews* **2002**, *54*, 13–36.

(5) Wong, Rachel Shet Hui, Ashton, M., Dodou, K. Effect of Crosslinking Agent Concentration on the Properties of Unmedicated Hydrogels. *Pharmaceutics* **2015**, *7*, 305–319.

(6) Yagüe, J. L., Gleason, K. K. Systematic control of mesh size in hydrogels by initiated chemical vapor deposition. *Soft Matter* **2012**, *8*, 2890.

(7) Coclite, A. M., Howden, R. M., Borrelli, D. C., Petruczok, C. D., Yang, R., Yagüe, J. L., Ugur, A., Chen, N., Lee, S., Jo, W. J., Liu, A., Wang, X., Gleason, K. K. 25th anniversary article: CVD polymers: a new paradigm for surface modification and device fabrication. *Advanced materials (Deerfield Beach, Fla.)* **2013**, *25*, 5392–5423.

(8) Lau, Kenneth K. S., Gleason, K. K. Initiated Chemical Vapor Deposition (iCVD) of Poly(alkyl acrylates): An Experimental Study. *Macromolecules* **2006**, *39*, 3688–3694.

(9) Lau, Kenneth K. S., Gleason, K. K. Initiated Chemical Vapor Deposition (iCVD) of Poly(alkyl acrylates): A Kinetic Model. *Macromolecules* **2006**, *39*, 3695–3703.

(10) Reeja-Jayan, B., Kovacik, P., Yang, R., Sojoudi, H., Ugur, A., Kim, D. H., Petruczok, C. D., Wang, X., Liu, A., Gleason, K. K. A Route Towards Sustainability Through Engineered Polymeric Interfaces. *Adv. Mater. Interfaces* **2014**, *1*, 2196–7350.

(11) Petruczok, C. D., Armagan, E., Ince, G. O., Gleason, K. K. Initiated Chemical Vapor Deposition and Light-Responsive Cross-Linking of Poly(vinyl cinnamate) Thin Films. *Macromol Rapid Commun* **2014**, *35*, 1345–1350.

(12) Ozaydin-Ince, G., Gleason, K. K. Transition between kinetic and mass transfer regimes in the initiated chemical vapor deposition from ethylene glycol diacrylate. *J. Vac. Sci. Technol. A* **2009**, *27*, 1135.

(13) Kiessig, H. Interferent von Röntgenstrahlen an dünnen Schichten. *Annalen der Physik* **1931**.

(14) Werzer, O., Matoy, K., Strohriegl, P., Resel, R. Temperature treatment of semiconducting polymers: An X-ray reflectivity study. *Thin Solid Films* **2007**, *515*, 5601–5605.

(15) Flesch, H.-G., Mathijssen, Simon G. J., Gholamrezaie, F., Moser, A., Neuhold, A., Novák, J., Ponomarenko, S. A., Shen, Q., Teichert, C., Hlawacek, G., Puschnig, P., Ambrosch-Draxl, C., Resel, R., de Leeuw, Dago M. Microstructure and Phase Behavior of a Quinquethiophene-Based Self-Assembled Monolayer as a Function of Temperature. *J. Phys. Chem. C* **2011**, *115*, 22925–22930.

(16) Mondal, M. H., Mukherjee, M. Effect of Annealing Induced Polymer Substrate Attachment on Swelling Dynamics of Ultrathin Polymer Films. *Macromolecules* **2008**, *41*, 8753–8758.

(17) Galvin, C. J., Dimitriou, M. D., Satija, S. K., Genzer, J. Swelling of polyelectrolyte and polyzwitterion brushes by humid vapors. *Journal of the American Chemical Society* **2014**, *136*, 12737–12745.

(18) Salditt, A., Li, C., Spaar, A., Mennicke, U. X-ray reflectivity of solid-supported, multilamellar membranes. *The European Physical Journal E* **2002**.

(19) Ince, G. O., Armagan, E., Erdogan, H., Buyukserin, F., Uzun, L., Demirel, G. One-dimensional surface-imprinted polymeric nanotubes for specific biorecognition by initiated chemical vapor deposition (iCVD). *ACS applied materials & interfaces* **2013**, *5*, 6447–6452.

(20) Kaya, A., Demiryürek, R., Armağan, E., Ozaydin-Ince, G., Sezen, M., Koşar, A. Boiling heat transfer enhancement in mini/microtubes via polyhydroxyethylmethacrylate (pHEMA) coatings on inner microtube walls at high mass fluxes. *J. Micromech. Microeng.* **2013**, *23*, 115017.

(21) Zhang, Y., Li, Y., Du, Y., Shi, Z., Cui, Z. An Overview of the Material and Structure of the Porous Scaffold for Artificial Cornea. *J. Nanoeng. Nanomanuf.* **2014**, *4*, 279–288.

(22) Flory, P. J. Statistical Mechanics of Swelling of Network Structures. *J. Chem. Phys.* **1950**, *18*, 108.

(23) Flory, P. J., Rehner, J. Statistical Mechanics of Cross-Linked Polymer Networks I. Rubberlike Elasticity. *J. Chem. Phys.* **1943**, *11*, 512.

(24) Hoch, G., Chauhan, A., Radke, C. J. Permeability and diffusivity for water transport through hydrogel membranes. *Journal of Membrane Science* **2003**, *214*, 199–209.

(25) Fornasiero, F., Krull, F., Prausnitz, J. M., Radke, C. J. Steady-state diffusion of water through soft-contact-lens materials. *Biomaterials* **2005**, *26*, 5704–5716.

(26) Rodríguez, O., Fornasiero, F., Arce, A., Radke, C. J., Prausnitz, J. M. Solubilities and diffusivities of water vapor in poly(methylmethacrylate), poly(2-hydroxyethylmethacrylate), poly(N-vinyl-2-pyrrolidone) and poly(acrylonitrile). *Polymer* **2003**, *44*, 6323–6333.

(27) Fornasiero, F., Krull, F., Radke, C. J., Prausnitz, J. M. Diffusivity of water through a HEMA-based soft contact lens. *Fluid Phase Equilibria* **2005**, *228-229*, 269–273.

(28) Bahar, I., Erbil, H. Y., Baysal, B. M., Erman, B. Determination of polymer-solvent interaction parameter from swelling of networks: the system poly(2-hydroxyethyl methacrylate)-diethylene glycol. *Macromolecules* **1987**, *20*, 1353–1356.

(29) Elbs, H., Krausch, G. Ellipsometric determination of Flory-Huggins interaction parameters in solution. *Polymer* **2004**, *45*, 7935–7942.

(30) Jaczewska, J., Raptis, I., Budkowski, A., Goustouridis, D., Raczkowska, J., Sanopoulou, M., Pamuła, E., Bernasik, A., Rysz, J. Swelling of poly(3-alkylthiophene) films exposed to solvent vapors and humidity: Evaluation of solubility parameters. *Synthetic Metals* **2007**, *157*, 726–732.

(31) Fornasiero, F., Tang, D., Boushehri, A., Prausnitz, J., Radke, C. J. Water diffusion through hydrogel membranes. *Journal of Membrane Science* **2008**, *320*, 423–430.

(32) Ranacher, C., Resel, R., Moni, P., Cermenek, B., Hacker, V., Coclite, A. M. Layered Nanostructures in Proton Conductive Polymers Obtained by Initiated Chemical Vapor Deposition. *Macromolecules* **2015**, *48*, 6177–6185.

(33) Chan, K., Gleason, K. K. Initiated chemical vapor deposition of linear and cross-linked poly(2-hydroxyethyl methacrylate) for use as thin-film hydrogels. *Langmuir the ACS journal of surfaces and colloids* **2005**, *21*, 8930–8939.

(34) Resel, R., Tamas, E., Sonderegger, B., Hofbauer, P., Keckes, J. A heating stage up to 1173 K for X-ray diffraction studies in the whole orientation space. *J Appl Crystallogr* **2003**, *36*, 80–85.

(35) Hecht E., Zając A. *Optics*, 2nd ed.; Addison-Wesley Pub. Co.: Reading, Mass., 1987, p347.

(36) *Poly(2-hydroxyethyl methacrylate) BioReagent, powder, suitable for cell culture | Sigma-Aldrich.* http://www.sigmaaldrich.com/catalog/product/sigma/p3932?lang=de&region=AT. Accessed 15 December 2015.

(37) Ellis B., Smith R. *Polymers: a Properties Database*; Chapman & Hall/CRC Press, Sheffield University, UK, 2000.

(38) Mabilleau, G., Stancu, I. C., Honoré, T., Legeay, G., Cincu, C., Baslé, M. F., Chappard, D. Effects of the length of crosslink chain on poly(2-hydroxyethyl methacrylate) (pHEMA) swelling and biomechanical properties. *Journal of biomedical materials research. Part A* **2006**, *77*, 35–42.

(39) S. Krishnamoorthy, R. Pugin, J. Brugger, H. Heinzelmann, C. Hinderling, Adv. Mater. **2008**, 20, 1962.

(40) N. A. Peppas, H. J. Moynihan, L. M. Lucht, School of Chemical Engineering **1985**.

(41) A. Tufani, G. O. Ince, J. Appl. Polym. Sci. **2015**, 132, 1097.

(42) J. E. Mark J., Physical Properties of Polymer Handbook, 2nd ed., Springer, New York **2006**.

(43) P. Zahedi, P. I. Lee, Eur. J. Pharmaceutics and Biopharmaceutics **2007**, 65, 320.

IV.2 Novel Light-Responsive Biocompatible Hydrogels Produced by Initiated Chemical Vapor Deposition

ACS APPLIED MATERIALS & INTERFACES

Novel Light-Responsive Biocompatible Hydrogels Produced by Initiated Chemical Vapor Deposition

Katrin Unger[†], Paul Salzmann[†], Cecilia Masciullo[§], Marco Cecchini[§], Georg Koller[‡], and Anna Maria Coclite[*†]

Cite this: *ACS Appl. Mater. Interfaces* 2017, 9, 20, 17408−17416
Publication Date: May 5, 2017
https://doi.org/10.1021/acsami.7b01527

Reference: Katrin Unger, Paul Salzmann, Cecilia Masciullo, Marco Cecchini, Georg Koller, and Anna Maria Coclite; Novel Light-Responsive Biocompatible Hydrogels Produced by Initiated Chemical Vapor Deposition. ACS Appl. Mater. Interfaces 9, 17408−17416
DOI: 10.1021/acsami.7b01527

IV.2.1 Preface

The work of this publication was conducted at the Graz University of Technology as the second part of the Marie Curie International Incoming Fellowship (project 626889) named Smart multi Stimuli-responsive Supports for controlled cell growth by Anna Maria Coclite. The author of this thesis performed together with Paul Salzmann the sample preparation, characterization and partially the data evaluation. Georg Koller performed the XPS analysis and Cecilia Masciullo and Marco Cecchini tested the hydrogels cytocompatibility with Rat Embryo Fibroblast cells. Anna Maria Coclite supervised the project and wrote the manuscript. The article is reproduced from the publication identical in text and illustration with permission.

IV.2.2 Abstract

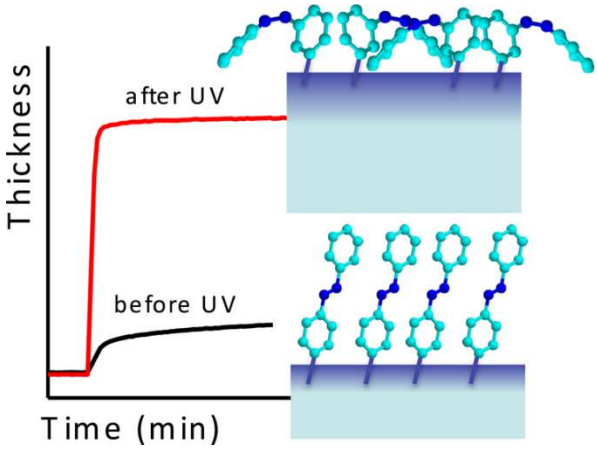

A novel multi-responsive hydrogel has been synthetized by initiated chemical vapor deposition (iCVD). Hydrogels are known for their dynamic swelling response to aqueous environments. A chemical functionalization of the hydrogel surface was performed to add other stimuli-responsive functionalities and obtain a smart material that responds to two stimuli: light irradiation and exposure to aqueous environment. Modifying the hydrogel surface with solution-based methods is often problematic due to the damages caused by the permeation of solvents in the hydrogel. This issue is completely bypassed by the use of solvent-free techniques. Cross-linked polymers of 2-hydroxyethyl methacrylate (HEMA) were functionalized with azobenzene groups, as confirmed by IR spectroscopy and X-ray photoelectron spectroscopy (XPS). Through photoisomerization of the azobenzene, the polarity within the hydrogel is modified and as a consequence the affinity to water. Light irradiation modifies the degree of swelling within thin hydrogel films from 13% before exposure to UV light to 25% after exposure. The possibility of controlling the degree and rate of swelling by light irradiation was never reported before on these timescales and can have exceptional implications for light-induced drug delivery or light-controlled microfluidic systems. The light-responsive hydrogels showed also biocompatibility, which makes them suitable for a great variety of applications as biomaterials.

IV.2.3 Introduction

Stimuli-responsive materials are characterized by dynamic switching of their properties depending on external stimuli.[1] Responsive elements may be anisotropic deformation, non-linear stress-strain behavior, thermal and/or optical changes to the elastic modulus of the material framework. Recently, numerous synthetic examples of responsive surfaces have emerged, which rely on conformational change in the polymer network, or pattern change.[2] Very interesting and appealing seems to be the combination of several stimuli to tune the properties of the materials in manifold ways. There are not many examples of multi-stimuli responsive thin films, because they require precise control on the coordination among surface chemistry and response. Light- and temperature- responsiveness have been combined to reversibly change the solubility of polyacrylamide containing azo-benzene groups.[3-4]

Among the other types of stimuli, light is non-invasive, it does not require contact, has high accurate positioning and a low thermal effect. All these advantages open up interesting fields of application for light-responsive materials, spanning from biotechnology to microelectronics. Most commonly, photochromic molecules are used to tune the properties within light-responsive polymers. These well-known organic dyes undergo a reversible isomerization upon irradiation. This process is usually accompanied with a polarity change as well as a color change in the chromophoric units. Such phenomena can be observed in chemical compounds like azobenzene (Scheme 1), spiropyran, salicylideneaniline etc. Consequently, a light-responsive polymer containing photochromic units would change its solubility, reversibly, through an irradiation process as long as the irradiation is being applied.

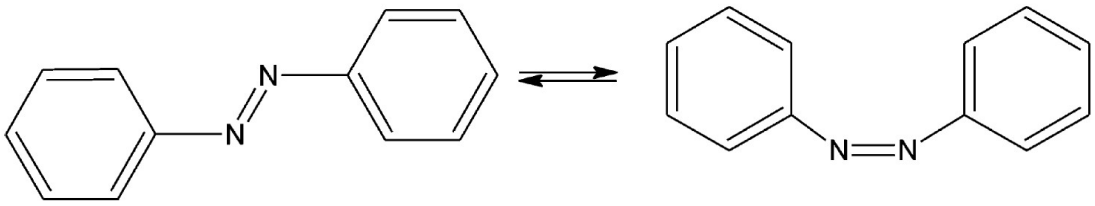

Scheme 1. Isomerization of the Azobenzene: Prior to irradiation, azobenzene is in the more stable trans-configuration. After irradiation with UV light at 365 nm, the excited cis-azobenzene appears.

Hydrogels are known for their dynamic swelling response to aqueous environments. The hydrogel swelling in water results in changes in the mechanical properties[5], protein adsorption capabilities[6] and hydrophilicity of the polymer[7]. The elastic modulus of a pHEMA (poly 2, hydroxyethyl methacrylate) hydrogel has been demonstrated to decrease from 881 MPa in the

dryed state to 2 MPa in the hydrated state.[8] The fast and reversible changes in the thickness of hydrogels were used in impedance sensors to control the passage of the analyte or for controlled drug delivery systems.[9] Owing to their high water content in the swollen state, porosity and soft consistency, hydrogels have many characteristics similar to those of living tissue.[10] In particular, the pHEMA is well known as a synthetic biocompatible material useful for contact lens applications.[11]

The aim of this study was to develop a light-responsive hydrogel, coupling responsiveness to both light and aqueous environment. For this purpose, the surface of a crosslinked pHEMA hydrogel was functionalized with azobenzene groups. The isomerization of the azobenzene upon illumination induces a polarity change as a direct consequence of the change in the dipole moment from 0 Debye for the trans-isomer to 3 Debye for the cis-isomer. Based on the significant polarity change induced by the isomerization, we investigated the possibility to control the water uptake in the hydrogel film. Achieving a precise control over the water uptake through light irradiation can be used to induce controlled and reversible changes in the stiffness and elasticity of the hydrogel. The chemical structure of the hydrogels and the combined response to light and aqueous environment makes these materials absolutely unique.

The light-responsive hydrogels were obtained by initiated Chemical Vapor Deposition (iCVD). A peculiar feature of iCVD is that delicate surfaces, such as hydrogels or molecular layers, can be easily functionalized without damages to the structure.[12] The iCVD technique is a surface polymerization method with high tolerance towards functional groups, which are critical to achieve the desired response.[13] It follows the mechanism of a free-radical polymerization. The initiator and monomer species enter the iCVD chamber as vapors. The initiator is decomposed by interaction with a relatively hot filament (150-300°C). These temperatures are enough to selectively break only labile bonds present in the initiator structure, (e.g. the O-O bond in the tert-butyl peroxide, TBPO). The monomer decomposition temperatures are > 500°C, therefore the monomer fully retains its chemical structure. In analogy to solution-phase synthesis, in the iCVD, the initiator radicals activate the chain growth polymerization of the monomer. The mechanism of polymerization is well detailed in ref [14-15]. The result is a surface of well-defined chemical composition having a high density of functionalities. The iCVD process requires only modest energy input and operates at low surface temperatures (~20°C to ~60°C). Keeping the surface at low temperature, promotes the adsorption of the monomers. Despite the benign reaction conditions of iCVD, high deposition rates can often be achieved (>200 nm/min).

Previously, we have studied the response to humidity (i.e. degree of swelling) of cross-linked hydrogels deposited by iCVD from hydroxyethylmethacrylate (HEMA) and ethylenglycoldimethacrylate (EGDMA).[16] Now these hydrogels were top-functionalized with a

layer of poly-pentafluorophenylacrylate (p-PFPA). Since the pentafluorophenyl group of PFPA is a good leaving group, the layer of p-PFPA can be used as a platform for subsequent functionalization with a multitude of amine containing compounds. Here we report the results obtained by functionalizing the hydrogels with aminoazobenzene and by studying the effect of the density of azobenzene groups on the combined response to light and water.

IV.2.4 Experimental Section

Hydrogel synthesis. Polymer coatings of 2-Hydroxyethyl methacrylate (HEMA, 97%, Aldrich, Germany) and Ethylene glycol dimethacrylate (EGDMA, 98%, Aldrich, Germany) with a top layer of Pentafluorophenyl Acrylate (PFPA, 98%, TCI, Germany) were deposited on Silicon wafers in a custom-build iCVD chamber, using *tert*-butyl peroxide (TBPO, 98%, Aldrich, Germany) as initiator. The depositions were performed at a pressure of 350 mTorr. The substrate temperature was kept at 20 ± 3°C by a chiller/heater system (Thermo Scientific Accel 500 LC). The thermal decomposition of the initiator was induced by a filament array of nickel-chromium wires (Goodfellow, UK), heated to 270 ± 5°C. The HEMA, EGDMA and PFPA monomers were kept at 75, 80 °C and 60°C, respectively, and flown into the reactor through a heated mixing line. The flow rates were adjusted via needle valves. The initiator was kept at ambient temperature and was introduced separately into the chamber. The various polymers were obtained using constant flow rates: TPBO 1 ± 0.02 sccm, HEMA 0.8 ± 0.05 sccm, EGDMA 0.05 ± 0.01 sccm, PFPA 5.3 ± 1 sccm and N_2 3.0 ± 0.1 sccm. The N_2 was used as patch flow. The polymer of HEMA and EGDMA (p-HEMA-co-EGDMA) was deposited up to a nominal thickness of 200 nm, monitored *in situ* by laser interferometry (He–Ne Laser with λ = 633 nm, Thorlabs, USA). Then, the flow of HEMA and EGDMA were turned off and the PFPA one was opened, while the TBPO and N_2 were constantly flowing in. Different deposition times of the p-PFPA layer were used, which turned in different nominal thicknesses of the PFPA layer, estimated again from laser interferometry. For comparison, also a sample deposited flowing continuously PFPA together with HEMA and EGDMA (p-HEMA-co-EGDMA-co-PFPA) was deposited using the same conditions and flow rates reported above, to a thickness of 243 nm. A post-deposition functionalization was performed on all the samples, to substitute the pentafluorophenyl groups with azobenzene moieties. For this purpose, the samples were immersed for 24h in a 20 mM solution of 4-Aminoazobenzene (Sigma Aldrich) in ethanol and then rinsed with ethanol and water to eliminated unreacted chemicals.

Hydrogels Characterization. The chemical composition and structure of the polymers were evaluated by Fourier transform infrared (FT-IR) spectroscopy (Bruker IFS 66v/S) in

transmission. The atomic composition of the polymers was determined by X-ray photoelectron spectroscopy (XPS). The spectra were acquired using non-monochromatic Mg K-alpha radiation (1253 eV). The pass energy was 50 eV for survey scans and 20 eV for high resolution scans. The take-off angle was 55°. The analysis of the data was performed using Casa XPS.

The UV-Vis absorption spectra of the samples containing azobenzene were measured with a spectrometer (Shimadzu UV-1800) equipped with a double beam system (190 to 1100 nm range, light source change at 300 nm). The UV-Vis spectra were measured before and after illumination at 390 ± 5 nm with a UV LED (4 LEDs in series, 3.3 V, 20 mA) to measure the isomerization trans-cis. After this, the samples were illuminated with green LED (4 LEDs in series, 3.3 V, 10 mA, at 495 ± 20 nm) and positioned in the spectrometer to measure the kinetics of the stimulated cis-trans isomerization.

The film thickness and the swelling in water and humidity were measured with spectroscopic ellipsometry (J. A. Woollam ESM-300). A liquid cell (J. A. Woollam) was used to hold the pure water in a tight seal. Because of the geometry of the cell, only spectra with an incident angles of 75° were measured. The sampled spectral region was between 370 nm and 1000 nm. In the dry state, the measured data were modeled with a 3-layers system containing silicon and native silicon dioxide (2.1 nm) as substrate and a Cauchy layer for the thin film polymer. In water, the polymer layer was modeled with the effective material approximation (EMA), which models the material as a mixed composition of two components with defined optical parameters. The thickness and the materials ratio were the fitting parameters. This is a typical procedure for transparent swollen hydrogels.[17] The increase in thickness upon water immersion was measured for 4-5 min with a time resolution of 2 s, before and after sample illumination with a LED light. The swelling in humidity was measured by flowing water vapor at RH=85%. Also in this case the data were collected with a time resolution of 2s. In order to demonstrate the reversibility of the isomerization of azobenzene and of its consequence on the swelling degree, humidity and illumination cycles were performed in-situ during the thickness measurements. First the sample was exposed to humidity without illumination, then the humidity was decreased to 50% and the sample was illuminated with the UV LED for 6 min. During illumination, the humidity was increased again to 82%. Next, the humidity was decreased to 50% and the sample was exposed to the green LED for 1 min. Green light stimulates the transition cis-trans of the azobenzene. After exposure to the green LED, the sample was exposed to humidity at 82% and the cycles of humidity and UV/green light illumination were repeated over a period of 100 min.

Water Contact Angle measurements were measured using a goniometer CAM200 (KSV Instruments, Finland). Static contact angles were evaluated on 1 μL droplets. Advancing and receding angles were measured with the sessile drop method by depositing a droplet of 1 μL on

the surface, then increasing the volume to 4 μL, and finally decreasing it. Advancing angles were measured as the maximum angles observed during the droplet growth. Receding contact angles were measured in correspondence of the drop profile just before the contact surface reduction. Each WCA value was averaged from measurements of five drops, distributed along the surface.

Cell culture and viability tests. In order to perform biocompatibility tests, the hydrogels were deposited directly on WillCo plates and sterilized for 10 minutes under UV tissue culture hood.[18] Rat Embryo Fibroblast cell line (REF cells)[19] were seeded on top of three different types of hydrogels at density of 10×10^3 cells cm^{-2} and cultured under standard cell culture conditions. REF cells were grown in Dulbecco's modified eagle medium (DMEM) supplemented with 10% Fetal Bovine Serum (FBS), 5% 4×10^{-3} M L-glutamine, 5% of antibiotics and 5% Sodium Pyruvate (100mM, Thermofisher Scientific, #11360070). REF cell viability was evaluated at 3 h (D0), 24h (D1), 72h (D3) and 92h (D4) after seeding was measured by the 2-(2-methoxy-4-nitrophenyl)-3-(4-nitrophenyl)-5-(2,4-disulfophenyl)-2H-tetrazolium-monosodium salt (WST-8) assay, according to the manufacturer instructions (Sigma, #96992). REF cells were incubated in a 10% WST-8 solution (in medium) in a CO_2 incubator for 3 hours. The supernatant was carefully aspirated, transferred to a new plate, and the absorbance of each well was observed by a plate reader at a wavelength of 450 nm. The absorbance of formazan produced was directly proportional to the number of living cells.

Bright field Microscopy. REF cells were seeded at the same concentration on the three types of hydrogels grown on top of WillCo dishes (GWST-3522) and then imaged at four different times (3h-96h). An Eclipse Ti inverted microscope (Nikon, Japan) equipped with a perfect focus system, an incubating chamber (Okolab, Italy) and a CCD ORCA R2 (Hamamatzu, Japan) was used with an 40x oil objective (N.A.: 1.30).

Statistical analysis. All the experiments were repeated at least three times independently for each condition. Data are reported as the average value ± the standard error of the mean (mean ± SEM). Data were statistically analysed by using GraphPad Prism commercial software (GraphPad Prism, 6.05 version). The mean values obtained in each repeated experiment were assumed to be normally distributed about the true mean. One-way ANOVA (Dunnett's multiple comparison test) analysis was used, unless differently stated, to compare light-responsive hydrogels to the plate control condition. Statistical significance refers to results where $P < 0.05$ was obtained.

IV.2.5 Results and Discussion

The light-responsive hydrogels were obtained by iCVD starting from the deposition of a copolymer of 2, hydroxyethyl methacrylate and ethylenglycoldimethacrylate (p-HEMA-co-EGDMA), followed by the deposition of a top layer of a polymer of pentafluorophenylacrylate (p-PFPA). Different thicknesses of p-PFPA were investigated. Only the duration of the top p-PFPA layer deposition was increased while maintaining constant all the flow rates, meaning that only the p-PFPA thickness at the surface was sequentially increased. The nominal thicknesses of the p-PFDA top-layers are reported in Table 1, as expected longer top p-PFPA deposition times produced a thicker p-PFPA layer on the hydrogels.

Table 1: Deposition Time and Nominal Thicknesses of the p-PFPA Top Layer Deposited on the p-HEMA-co-EGDMA. The estimated error on the nominal thickness is ±20 nm.

time (min)	**thickness (nm)**
2	20
5	50
7	80
10	150
15	200

The controllability of the PFPA contents in the copolymers can be observed from the chemical analysis, made by FT-IR and XPS, reported in figure 1. Figure 1a compares the FTIR spectra of the bare hydrogel p-HEMA-co-EGDMA with three p-HEMA-co-EGDMAs top-coated with p-PFDA of varying thickness. The labeled thickness in figure 1a are the nominal thicknesses of the top p-PFPA layer, therefore "0 nm" corresponds to the bare p-HEMA-co-EGDMA. The spectrum of the copolymer HEMA-co-EGDMA contains three main vibrational modes. The most intense of these peaks is centered at ~ 1727 cm^{-1} and can be attributed to the C=O stretching. The C- H stretching and bending appear in the ranges of 3000 - 2850 cm^{-1} and 1500 - 1350 cm^{-1}, respectively. The peak centered at ~ 1260 cm^{-1} can be assigned to the stretching vibrational mode of C-O. The spectra of the copolymers top-coated with p-PFPA show some new absorption bands characteristics of the PFPA structure. The narrow and weak peak that appears at 1774 cm^{-1} can be associated with the stretching of the C=O within the pentafluorophenyl esteric group. The fluorinated phenyl ring has a characteristic sharp and intense peak at 1522 cm^{-1}. The C- F vibrations absorption can be observed at 1000 cm^{-1}. The intensities of those peaks increase

with the thicknesses of the p-PFPA top-layer. This clearly demonstrates that the composition in the copolymers was systematically controlled by iCVD.

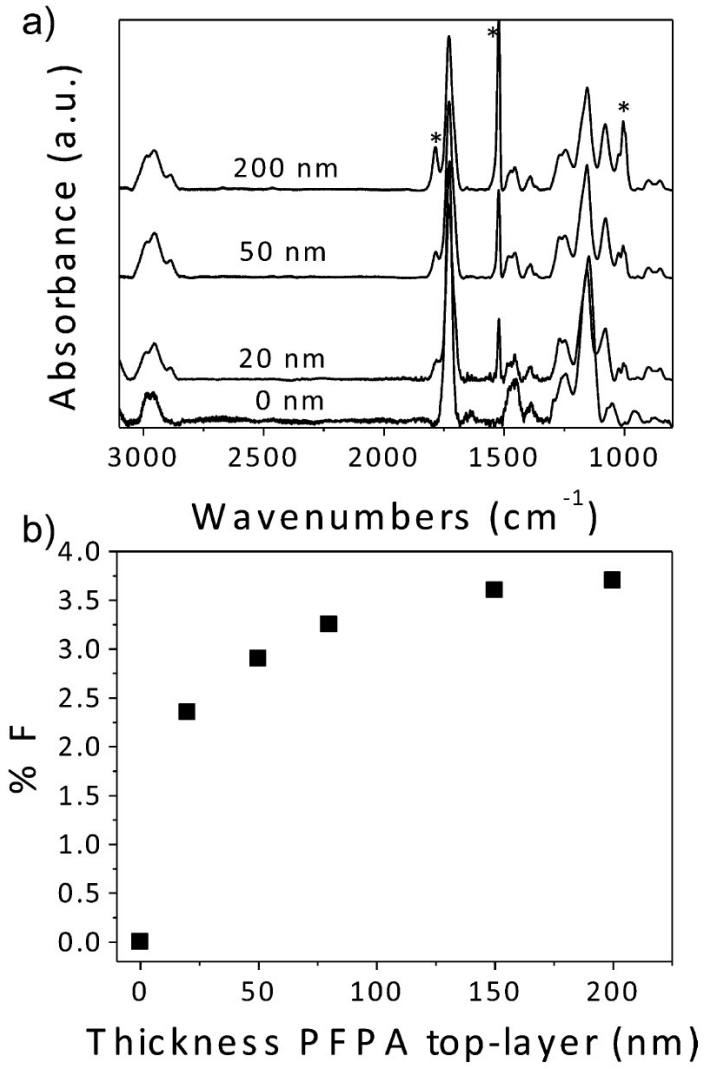

Figure 1. (a) FT-IR spectra and (b) XPS data of the p-HEMA-co-EGDMA samples with different thicknesses of p-PFPA top layer. The labels indicate the thickness of the p-PFPA top-layer. The label "0 nm" refers to the bare p-HEMA-co-EGDMA, which has been added for comparison. In panel a, the asterisks indicate the main p-PFPA absorptions. In panel b, the %F is the surface elemental percentage as calculated from XPS. Error bars have been omitted for clarity, as the standard deviation of the atomic percentage is <1.

layers, the percentage of F measured by XPS should have been 31% for all the samples, since the p-PFPA layer is always thicker than 10 nm. The discrepancies between this value and the F percentages measured by XPS could be due to the fact that during the shifting from one composition (p-HEMA-co-EGDMA) to the other (p-PFPA), there is a certain overlap of

monomer vapors. In fact, the concentration of a species in the reactor chamber does not go to zero immediately after the relative valve closure and this has probably created graded interfaces from one composition to the other. The atomic percentages of F from XPS survey scan spectra can be used to estimate the percentage of PFPA in the top-layer. This goes from 7.5% in the 20 nm p-PFPA top-layer to 12% in the 200 nm top-layer.

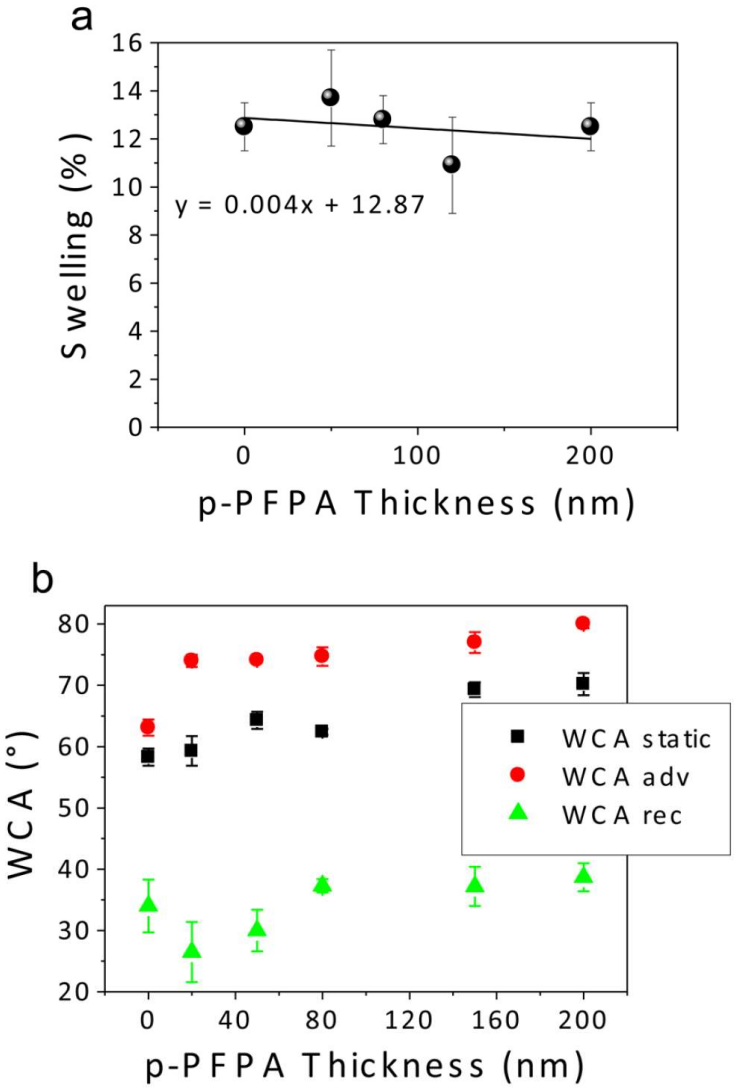

Figure 2. (a) Swelling in water of the hydrogels top-coated with different thicknesses of p-PFPA. (b) Static, advancing (adv), and receding (rec) water contact angles measured for the hydrogels top-coated with different thicknesses of p-PFPA.

An important characteristic of the hydrogels is their ability to swell in water. As demonstrated also by Montero et al.[20], retaining the swelling properties of the hydrogels while incorporating surface-active components (i.e. the PFPA) is extremely important. Figure 2

displays the percentage of thickness increase (i.e. swelling) for the copolymers top-coated with different p-PFPA thicknesses. It can be observed that with increasing the PFPA thickness, the swelling decreases very slightly with a slope of 0.004 and an intercept of 12.87%. For sake of comparison, a homogeneous copolymer p-HEMA-co-EGDMA-co-PFPA was produced with PFPA units incorporated throughout the whole hydrogel thickness. This hydrogel shows a thickness increase upon water immersion of 5.5 %, which is statistically lower than the swelling measured on the bare p-HEMA-co-EGDMA hydrogels and the ones coated with p-PFPA top-layer. The homogeneous copolymer does not retain the swelling properties of the p-HEMA-co-EGDMA because of the hydrophobicity of the PFPA units. On the contrary, when the PFPA units are placed only on the surface of the hydrogel, the water that penetrates the p-PFPA top-layer can swell the hydrogel to its characteristic swelling percentage. In order to further investigate the interaction between water and the top-functionalized hydrogels, water contact angles were measured in static and dynamic mode. igure 2b shows that the static and advancing contact angles increase with the thickness of p-PFPA top-layer from 58° to 70° and from 63° to 80°, respectively. These increases are due to the increasing density of hydrophobic fluorinated groups, in good agreement with the increase in % F shown in figure 1. The receding contact angles show instead a flatter trend: they increase slightly from 34° to 38°. The large difference in values and trends of the advancing and receding angles can be related to the chemical composition heterogeneities, reorientation, and mobility of the polymer chains on the surface.[21-22] It is well known that, when the surface of a polymer is exposed to air, the hydrophobic groups are oriented towards the interface polymer-air, in order to minimize the surface energy. When a drop of water is deposited on the surface the chain reorganize in order to expose the hydrophilic groups at the interface water-polymer. The advancing contact angle can be considered as a probe of a dry surface, since the front of the drop moves towards the dry areas. As a consequence, when more hydrophobic groups are present on the surface the advancing contact angle is larger. Also the surface of the bare pHEMA hydrogel shows a relatively high static and advancing contact angle, which may seem in contrast to the characteristic of this material to absorb water in its meshes. The receding contact angle can be considered a probe of a wet surface: the front of the water droplet is moved inwards. During this movement the chains re-arrange at the interface, exposing the hydrophilic sites of the pHEMA hydrogel towards the droplet. Therefore, the equilibrium water content of a hydrogel is probably more relatable to the receding contact angles than to the advancing ones, since during the swelling measurements the samples are immersed in water and therefore chain rearrangement takes place. A similar conclusion was also demonstrated by Holly et al.[23] Due to this chain rearrangement, the receding contact angles and the swelling ratio seem not to be affected by the presence of the p-PFPA top-layer.

The samples were then immersed in a 4-aminoazobenzene/ethanol bath for 24 h. With this post-deposition reaction, the pentafluorophenyl groups were substituted by the light-responsive azobenzene groups, as shown in Scheme 2.

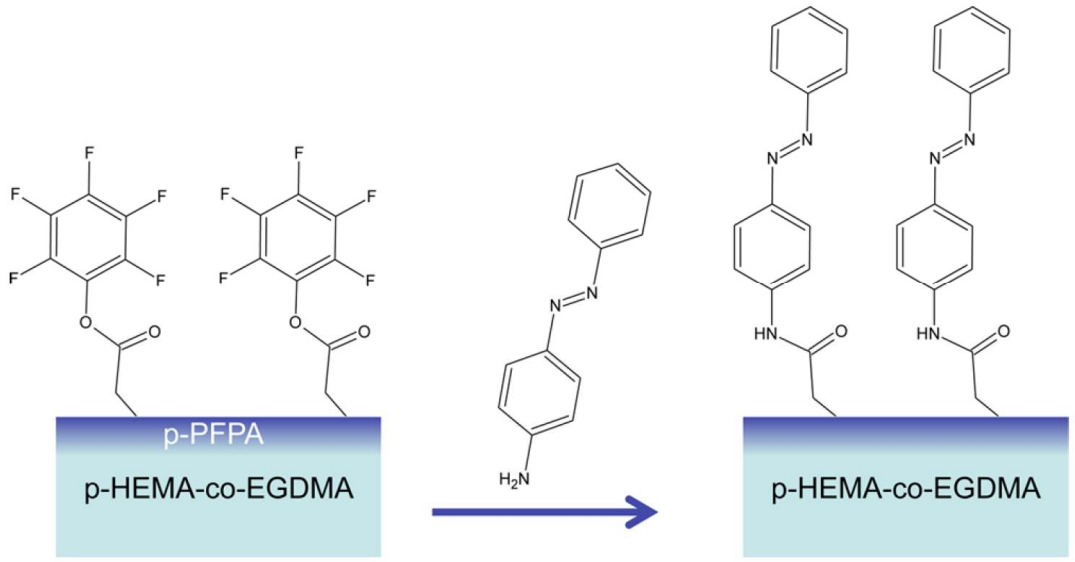

Scheme 2: Post-Deposition Functionalization of the Hydrogels to Covalently Bind Light-Responsive Azobenzene Groups

Figure 3 shows the FT-IR spectra of the homogeneous copolymer that has PFPA incorporated throughout the hydrogel matrix before and after the functionalization. After functionalization, a peak is expected to appear at 1630-1690 cm^{-1}, attributed to the C=O vibration in the newly formed amide group. The FTIR spectrum of the functionalized hydrogel shows a weak absorption, in this area, which would confirm the bonding with azobenzene. All the peaks relative to the PFPA show smaller intensities in the spectra of the functionalized hydrogels compared to the spectra of the as deposited ones. The conversion of PFPA to azobenzene is more evident in the XPS data reported in figure 3b. The decrease in % F is much stronger for the hydrogels top-coated with PFPA than for the homogenous copolymer that has PFPA incorporated throughout the hydrogel matrix. This suggests that the functionalized homogeneous copolymer contains a significant fraction of unreacted PFPA. This phenomenon can be explained by the inability of the aminoazobezene to diffuse through the film and it justifies our choice of adding the PFPA only on the top of the hydrogels. XPS measurements confirmed that the yield of conversion of PFPA groups in azobenzene groups was always above 60% as calculated by dividing the difference in PFPA % before and after azobenzene bath by the initial percentage of PFPA. The appearance of the surface nitrogen peak after the functionalization

reflects the presence of azobenzene moieties on the hydrogel surface. Considering the %N in an aminoazobenzene molecule and the one measured by XPS on our films, it is possible to roughly estimate the surface percentage of azobenzene, whose values are reported in Table 2. The surface contamination of N, detectable by XPS and due to the exposure of the samples in air, was not taken into account in these estimations. A thicker p-PFPA top-layer contains a higher density of pentafluorophenyl groups that can react with the aminoazobenzene. As it can be seen from Table 2, thicker p-PFPA top-layer give higher surface percentage of azobenzene after functionalization, with an estimated maximum of 37%. Probably the size of the azobenzene moieties limits the surface coverage that can be obtained during the functionalization.

Table 2. Thickness of the PFPA Top-Layer and Corresponding Estimated Surface Percentage of Azobenzene after Functionalization. An estimated error of ±1% has to be considered, coming from the N contamination that could be present on the surface by exposure to air.

Thickness PFPA top-layer (nm)	Surface % azobenzene after functionalization
20	4
50	6
80	8
150	12
200	37
homo	11

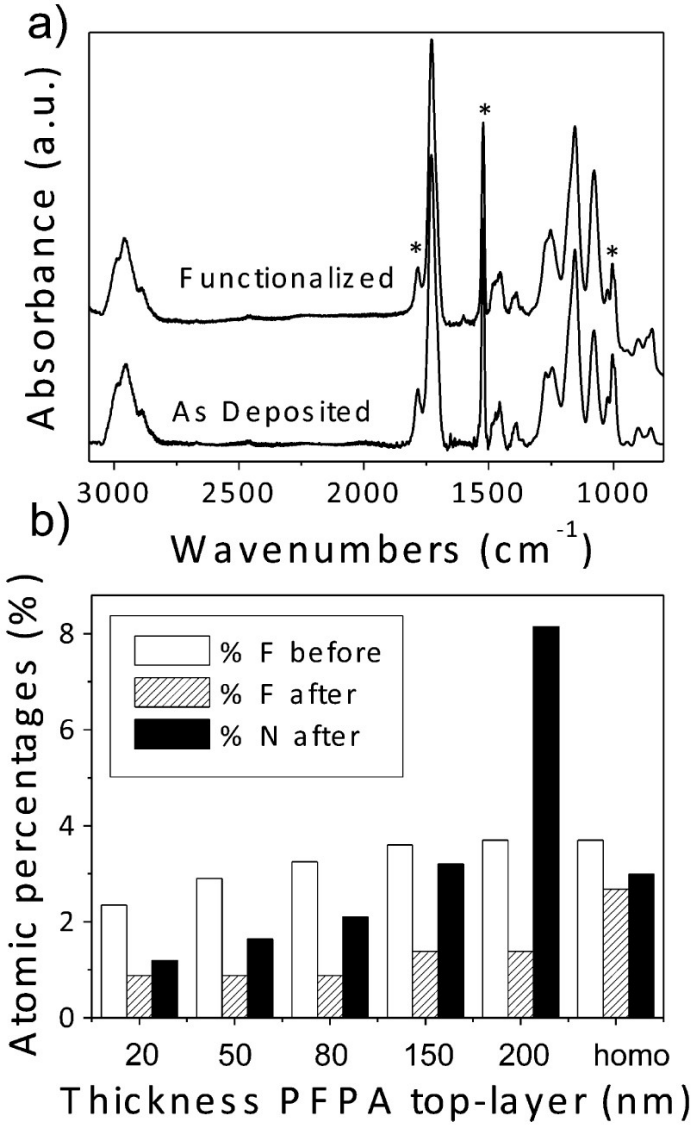

Figure 3. Chemical analysis of the hydrogels before and after functionalization in the 4-aminoazobenzene bath. (a) FTIR spectra of the hydrogels with homogeneous fraction of PFPA through the whole matrix. The peak indicated with an arrow in figure a corresponds to the C=O vibration in the amide group formed after functionalization of the hydrogels with azobenzene, the asterisks indicate the main PFPA absorptions. (b) Surface atomic percentages of F and N as measured from XPS for all the samples. The label "homo" refers to the sample with homogeneous content of PFPA. Error bars have been omitted for clarity as the standard deviation of the atomic percentage is below 1%.

The UV/Vis spectrum of the hydrogel with 8% of azobenzene is shown in Fig. 4, as an example for the retention of the light-induced isomerization kinetics of the azobenzene immobilized on the surface of the hydrogels. Prior irradiation all azobenzene groups were in the trans-isomer, which has a characteristic absorption band at ≈ 380 nm. This band is associated with the $\pi \rightarrow \pi^*$ electronic excitation.[24] After irradiation of the sample with UV light at 390 ± 5 nm for 1 min, the absorption band at 380 nm decreased in intensity. The relaxation of the excited azobenzenes back into the trans-configuration occurs spontaneously under visible light with half time of 30 min.[4] The further exposure of the sample to green (i.e. visible) light at 495 ± 20 nm for 1 min led to the stimulated cis - trans relaxation in much shorter time. The spectrum recorded after green light exposure shows that the absorbance around 380 nm is almost completely recovered after only 1 min.

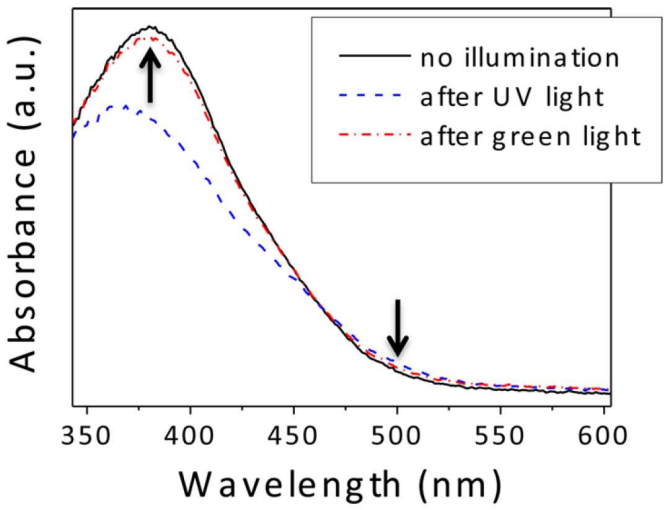

Figure 4. UV−vis spectra of the sample with 8 surface % of azobenzene, taken as representative. The spectra were measured prior illumination and upon UV light and visible-light irradiation.

The light-responsive swelling was demonstrated by investigating the combined response to light and aqueous or humid environments. Figure 5 shows the swelling upon immersion in water for the azobenzene-functionalized hydrogels, prior and upon UV irradiation. The hydrogels containing azobenzene show higher swelling in water, upon UV irradiation, to a maximum of +10% in the case of the sample with 12% of azobenzene. The increase in swelling demonstrates that the trans-cis isomerization of the azobenzene units can be used to control the water uptake of the hydrogels. The cis-isomer has a 3 Debye dipole moment and is therefore more hydrophilic than the trans, whose dipole is null.[24] This makes the hydrogel matrix more prone to the water sorption. The sample that had PFPA homogeneously copolymerized with HEMA and EGDMA

through the whole thickness, is the one that swells the least either before and after UV irradiation and especially less than the hydrogel made of p-HEMA-co-EGDMA (labeled with 0%). This is probably due to the presence of hydrophobic unconverted PFPA units, which probably hinder the swelling also after UV light irradiation. Figure 5b shows the thickness increase upon immersion in water before and after UV exposure, as measured in-situ by ellipsometry, on the sample with 12% azobenzene, as representative. The slope of the thickness increase upon immersion in water, is higher upon exposure of the sample to UV light. This means that the isomerization of the azobenzene does not only result in more but also in faster swelling. To further investigate the interaction between water and the hydrogels before and after UV-exposure, the water contact angles were measured and are reported in figure 5 c and d.

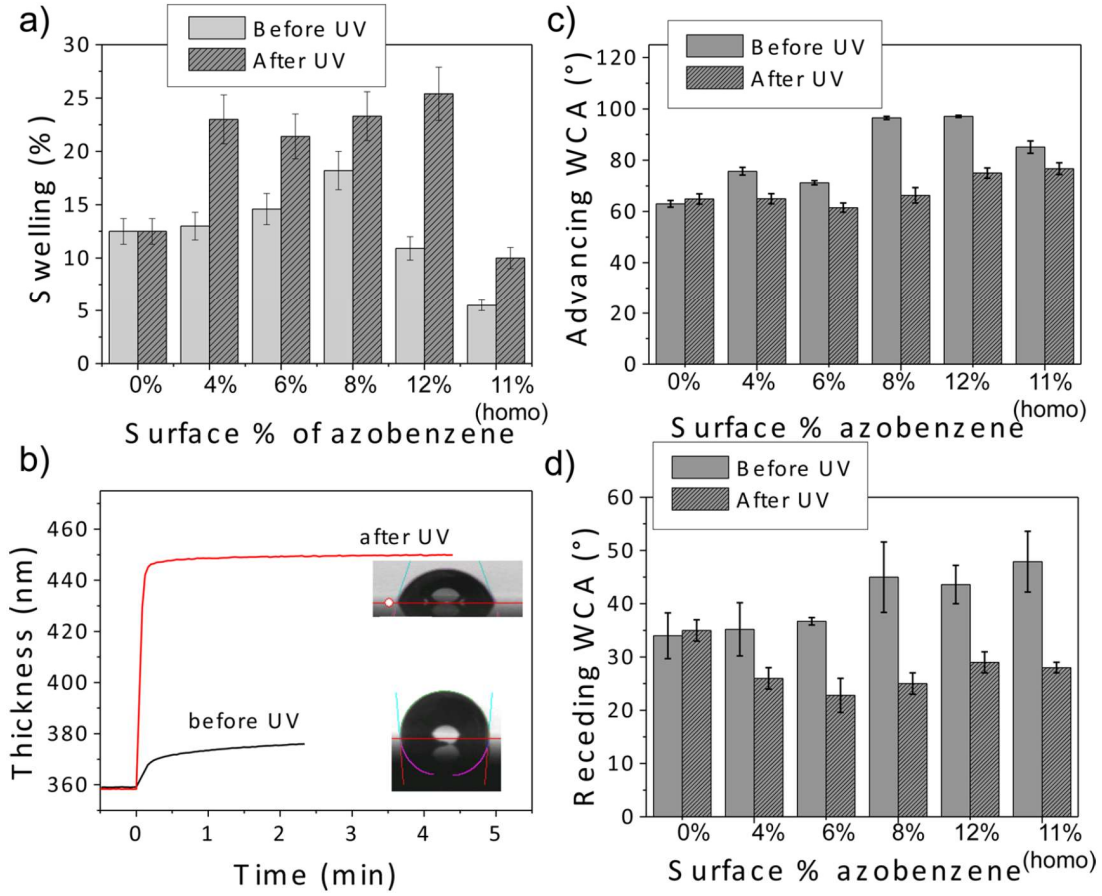

Figure 5. (a) Plot of the increase in thickness (swelling) upon immersion in water of the hydrogels containing different surface percentages of azobenzene. The swelling was measured before and after UV exposure. (b) Profile of the thickness increase for the sample with 12% azobenzene. The insets in b show the picture of a water droplet profile on the surface of the sample, prior and upon illumination. (c, d) Advancing and receding WCAs, respectively, measured on the hydrogels before and after light exposure.

By comparison between the WCAs before UV irradiation and the ones reported in figure 2b, it can be observed that the samples show higher advancing angles after the functionalization. Nevertheless, the receding angles remain very similar to the one measured for the bare p-HEMA-co-EGDMA. The high advancing contact angles prior UV irradiation can be ascribed to the hydrophobicity of the trans-azobenzene isomer and the unreacted perfluorinated groups. Similarly to what observed in figure 2, it seems like the high surface hydrophobicity does not hinder the swelling and the sticking of the water, indeed low receding contact angles were measured also prior illumination. Upon illumination, both the advancing and receding angle drastically decreased confirming that the surfaces become polar and prone to allow the passage of water. For sake of comparison, also the sample containing no azobenzene was illuminated with UV. As expectable, in this case the angles did not change significantly.

As demonstrated in figure 4, the isomerization of the azobenzene is completely reversible: upon illumination of the sample with visible light, all azobenzene units go back to the trans-configuration. Correspondingly, also the swelling after illumination of the hydrogels with visible light is expected to go back to its original percentage. In order to observe this reversible dynamics, we measured the thickness increase in-situ during humidity and illumination cycles. The relative humidity inside the small volume of the ellipsometric cell can be continuously increased and decreased, without having to stop the measurement and dry the sample, as it would have been required for measurements in aqueous environment. figure 6 shows the thickness measured on the sample with 12% of azobenzene. The humidity was increased and decreased over 10 cycles from 82% to 50%. For the first three cycles, the sample was not illuminated. The thickness in this timeframe increased and decreased following the humidity stimulus, showing the reversibility of the polymer swelling upon exposure to humid air. Afterward in each humidity cycle, the sample was exposed first to UV light and then to visible light. The humidity and the light exposure affected a reversible change in the swelling of the hydrogels. The maxima of swelling, corresponding to the maxima of RH, were higher upon UV light exposure and went back to almost the original position upon exposure to green light. It is noteworthy noticing that after several humidity and illumination cycles the thickness oscillated always in the same range: from 362 nm at RH=50% to 375 nm at RH=82% upon UV-exposure. This reversibility speaks also for the stability of the hydrogel meshes in the time frame of the experiments. The swelling of the hydrogel in humid air is expected to be smaller than the thickness increase registered in water (figure 5b), because less water molecules are inducing the polymer chains reorientation that is necessary to expose the hydrophilic groups to the surface and induce the swelling.[16]

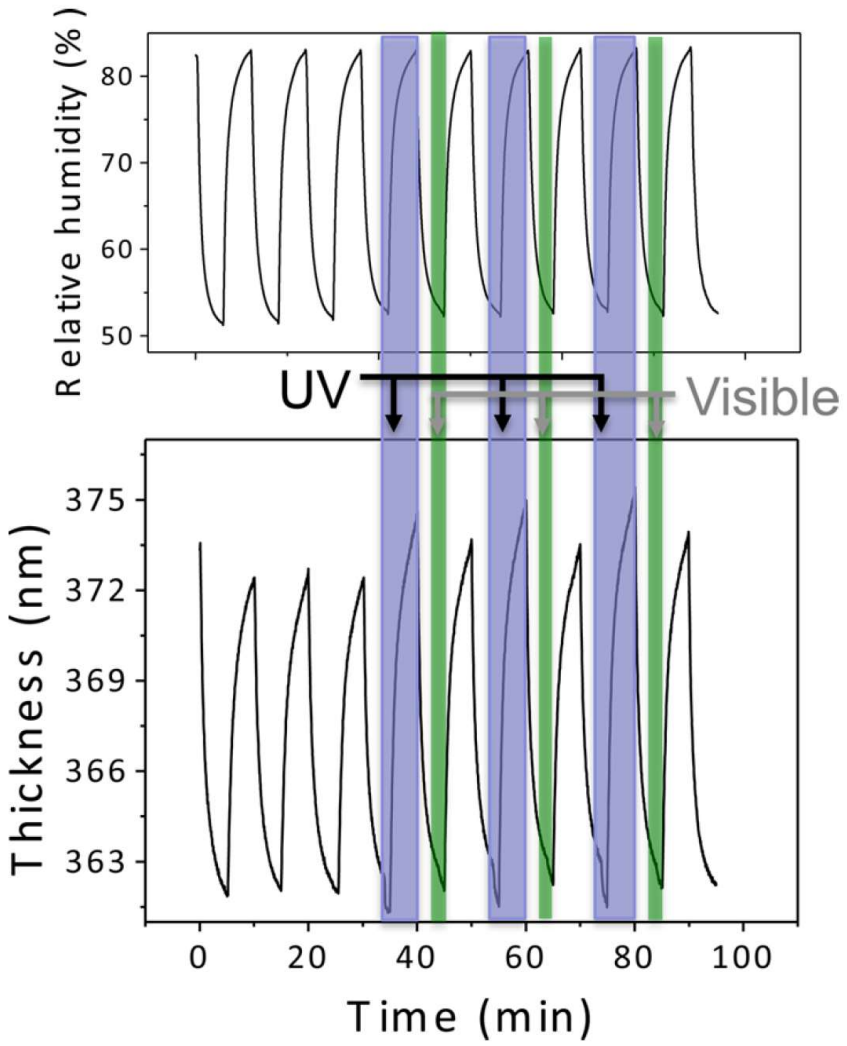

Figure 6. Plot of the hydrogel thickness in time, upon exposure to humid air and to UV–visible light cycles. The hydrogel, taken as representative, had 12% of azobenzene on the surface. The thick blue areas indicate the period of time in which the hydrogels were exposed to UV light and the thin green areas the time frames of visible light exposure. On top, the corresponding relative humidity oscillations are plotted as a function of time.

In order to investigate also a possible use for biomedical applications, we have tested the cytocompatibility of the hydrogels functionalized with azobenzene (i.e. homo, 12% and 8%) with Rat Embryo Fibroblast (REF) cells, which were also previously grown on pHEMA substrates.[25] REF cells cultured on the novel hydrogels preserved their morphological phenotype, as shown in the bright field microscopy images reported in Fig. 7a: their natural spindle-shape was indeed retained, with a branched cytoplasm surrounding the elliptical nucleus. After 3 hours from seeding (D0), the cells were mostly scattered on the surface of the hydrogels. Conversely, after 24 hours (D1), the substrates showed to be crowded by REF cells, and from 72h after seeding, the

REFs locally formed clusters, maintaining their normal shape and proliferating until 96h (D4). This healthy behaviour was confirmed by the viability tests reported in Fig.7b. After three hours from seeding (D0), the REF cells found difficulties to adhere on the hydrogel surfaces rather than the plate control, in fact the intensity of WST signal produced by viable cells was lower. The fibroblasts started to adhere on top of the light-responsive hydrogels after 24h (D1) from seeding, suggesting that REF cells were able to recover the initial decrease in viability, since the number of viable cells present on all type of hydrogels was comparable with the control plate.

This positive trend was maintained until the final time point of this experiment, i.e. t = 96h. Here, REFs cells increased their viability over 150% respect to the plate value at D0.

All of these evidences let us to conclude that the light-responsive hydrogels are not cytotoxic for this cell line, namely the interaction with the biomaterial did not cause cell death or alterations of the cell morphotype.

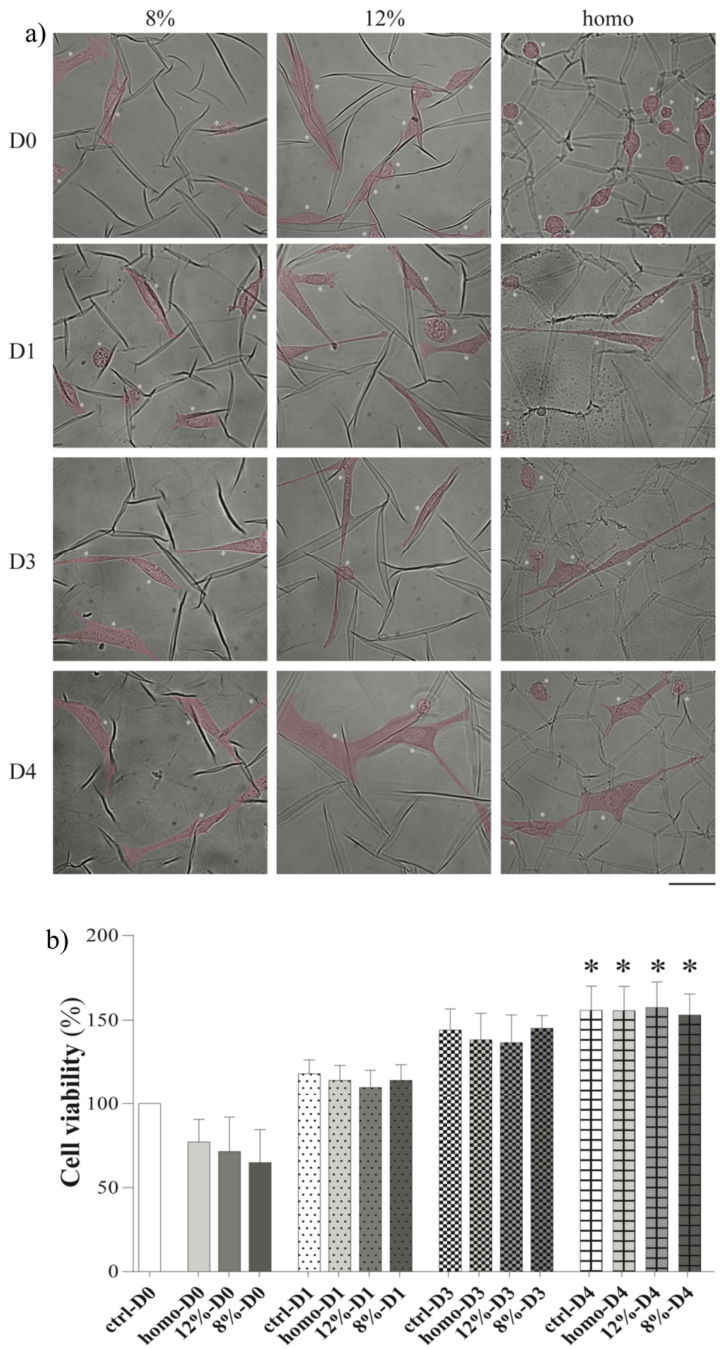

*Figure 7. (a) Bright-field images of rat embryo fibroblasts (REFs) (highlighted with a red-shadow mask and white stars) cultured on top of light-responsive hydrogels with three different surfaces percentage of azobenzene, 8%, 12%, and the homotype, at 3 h (D0), 1 day (D1), 3 days (D1), and 4 days (D4) after seeding. Scale bar: 50 μm. (b) Cell viability vs substrate at different time points as result of the WST essay, mean ± SEM, *P < 0.05, one-way ANOVA, Dunnett's multiple comparisons test vs plate control at 3 h from seeding (ctrl-D0).*

IV.2.6 Conclusion

The goal of this study was to obtain a light responsive hydrogel, whose water uptake could be controlled and reversibly changed by light irradiation. For this purpose, the surface of a crosslinked pHEMA hydrogel was functionalized with azobenzene moieties. The surface functionalization of hydrogels is not a trivial task, since solvents can penetrate, swell and in some cases dissolve the material. In this study, the hydrogel surface was modified by using a vapor-based deposition technique that allowed to create a top-coat bearing pentafluorophenyl groups. The latters were easily reacted with amino groups to tether azobenzene groups at the surface. The azobenzene units undergo a photoisometization upon UV light exposure, which produces an increase in the dipole moment of the molecule. The hydrogels, whose surface had the azobenzene units in the most polar cis-isomer (upon UV exposure) showed higher swelling degree and rate compared to the hydrogels whose surface had the azobenzene in the trans-isomer configuration. The light-responsive swelling was demonstrated in water and in humid environments. Since both the swelling and the photoisomerization of the azobenzene are reversible processes, the hydrogels were also exposed to humidity and light exposure cycles. When the humidity increased the hydrogels swelled to a different percentage depending also on the UV or visible light exposure, verifying the idea that cis-azobenzene immobilized on the surface enhances the water sorption in the hydrogels due to its higher polarity, while trans-azobenzene moieties leave the swelling properties of the hydrogels almost unchanged.

The hydrogel biocompatibility was also tested. REF cells showed the same growth rate and morphotype that was showed by the same cell line on the control plate.

The demonstrated synthesis of biocompatible light-responsive hydrogels will certainly open up new fields of application in which the reversible stimuli responsiveness of the material can be used for biotechnology, light-controlled cell growth or light-controlled drug delivery[26].

Acknowledgements

This research was supported by a Marie Curie International Incoming Fellowship (project 626889) within the 7th European Community Framework Programme. We thank Dr. Ilaria Tonazzini for support in fibroblast experiments.

IV.2.7 References

(1) Dameron, A. A.; Seghete, D.; Burton, B. B.; Davidson, S. D.; Cavanagh, A. S.; Bertrand, J. A.; George, S. M., Molecular Layer Deposition of Alucone Polymer Films Using Trimethylaluminum and Ethylene Glycol. Chem Mat. 2008, 20 (10), 3315-3326.

(2) Yoshida, M.; Lahann, J., Smart Nanomaterials. ACS Nano 2008, 2 (6), 1101-1107.

(3) Jochum, F. D.; Theato, P., Temperature- and Light-Responsive Smart Polymer Materials. Chem Soc Rev 2013, 42 (17), 7468-7483.

(4) Jochum, F. D.; Theato, P., Temperature and Light Sensitive Copolymers Containing Azobenzene Moieties Prepared via a Polymer Analogous Reaction. Polymer 2009, 50 (14), 3079-3085.

(5) Refojo, M. F.; Leong, F. L., Poly(methyl acrylate-co-hydroxyethyl acrylate) Hydrogel Implant Material of Strength and Softness. J Biomed Mater Res 1981, 15 (4), 497-509.

(6) Baxamusa, S. H.; Gleason, K. K., Random Copolymer Films with Molecular-Scale Compositional Heterogeneities that Interfere with Protein Adsorption. Adv. Funct. Mat. 2009, 19 (21), 3489-3496.

(7) Alf, M. E.; Hatton, T. A.; Gleason, K. K., Initiated Chemical Vapor Deposition of Responsive Polymeric Surfaces. Thin Solid Films 2011, 519, 4412-4414.

(8) Mabilleau, G.; Stancu, I. C.; Honore, T.; Legeay, G.; Cincu, C.; Basle, M. F.; Chappard, D., Effects of the Length of Crosslink Chain on Poly(2-hydroxyethyl methacrylate) (pHEMA) Swelling and Biomechanical Properties. J Biomed Mater Res A 2006, 77 (1), 35-42.

(9) Pena-Francesch, A.; Montero, L.; Borros, S., Tailoring the LCST of Thermosensitive Hydrogel Thin Films Deposited by iCVD. Langmuir 2014, 30 (24), 7162-7167.

(10) Caló, E.; Khutoryanskiy, V. V., Biomedical Applications of Hydrogels: A Review of Patents and Commercial Products. Eur. Polym. J. 2015, 65, 252-267.

(11) Wichterle, O.; LÍM, D., Hydrophilic Gels for Biological Use. Nature 1960, 185 (4706), 117-118.

(12) Montero, L.; Gabriel, G.; Guimera, A.; Villa, R.; Gleason, K. K.; Borros, S., Increasing Biosensor Response through Hydrogel Thin Film Deposition: Influence of Hydrogel Thickness. Vacuum 2012, 86 (12), 2102-2104.

(13) Coclite, A. M.; Howden, R. M.; Borrelli, D. C.; Petruczok, C. D.; Yang, R.; Yague, J. L.; Ugur, A.; Chen, N.; Lee, S.; Jo, W. J.; Liu, A.; Wang, X.; Gleason, K. K., 25th Anniversary Article: CVD Polymers: a New Paradigm for Surface Modification and Device Fabrication. Adv Mater 2013, 25 (38), 5392-5423.

(14) Lau, K. K. S.; Gleason, K. K., Initiated Chemical Vapor Deposition (iCVD) of Poly(alkyl acrylates): A Kinetic Model. Macromolecules 2006, 39 (10), 3695-3703.

(15) Lau, K. K. S.; Gleason, K. K., Initiated Chemical Vapor Deposition (iCVD) of Poly(alkyl acrylates): An Experimental Study. Macromolecules 2006, 39 (10), 3688-3694.

(16) Unger, K.; Resel, R.; Coclite, A. M., Dynamic Studies on the Response to Humidity of Poly (2-hydroxyethyl methacrylate) Hydrogels Produced by Initiated Chemical Vapor Deposition. Macromol. Chem. Phys. 2016, 217 (21), 2372-2379.

(17) Chan, K.; Gleason, K. K., Initiated Chemical Vapor Deposition of Linear and Cross-Linked Poly(2-hydroxyethyl methacrylate) for Use as Thin-Film Hydrogels. Langmuir 2005, 21 (19), 8930-8939.

(18) Caliari, S. R.; Burdick, J. A., A Practical Guide to Hydrogels for Cell Culture. Nat Methods 2016, 13 (5), 405-414.

(19) Bergert, M.; Lendenmann, T.; Zundel, M.; Ehret, A. E.; Panozzo, D.; Richner, P.; Kim, D. K.; Kress, S. J.; Norris, D. J.; Sorkine-Hornung, O.; Mazza, E.; Poulikakos, D.; Ferrari, A., Confocal Reference Free Traction Force Microscopy. Nat Commun 2016, 7, 12814.

(20) Montero, L.; Baxamusa, S. H.; Borros, S.; Gleason, K. K., Thin Hydrogel Films With Nanoconfined Surface Reactivity by Photoinitiated Chemical Vapor Deposition. Chem. Mat. 2009, 21 (2), 399-403.

(21) Wenzel, R. N., Resistance of Solid Surfaces to Wetting by Water. Ind. Eng. Chem. 1936, 28, 988-994.

(22) Cassie, A. B. D.; Baxter, S., Wettability of Porous Surfaces. Trans. Faraday Soc. 1944, 40, 0546-0550.

(23) Holly, F. J.; Refojo, M. F., Wettability of Hydrogels. I. Poly (2-hydroxyethyl methacrylate). J Biomed Mater Res 1975, 9 (3), 315-326.

(24) Wagner, S.; Leyssner, F.; Kordel, C.; Zarwell, S.; Schmidt, R.; Weinelt, M.; Ruck-Braun, K.; Wolf, M.; Tegeder, P., Reversible Photoisomerization of an Azobenzene-Functionalized Self-Assembled Monolayer Probed by Sum-Frequency Generation Vibrational Spectroscopy. Phys Chem Chem Phys 2009, 11 (29), 6242-6248.

(25) Lydon, M. J.; Minett, T. W.; Tighe, B. J., Cellular Interactions with Synthetic Polymer Surfaces in Culture. Biomaterials 1985, 6 (6), 396-402.

(26) Yadav, S.; Deka, S. R.; Verma, G.; Sharma, A. K.; Kumar, P., Photoresponsive Amphiphilic Azobenzene-PEG Self-Assembles to Form Supramolecular Nanostructures for Drug Delivery Applications. Rsc Advances 2016, 6 (10), 8103-8117.

IV.3 Temporary Tattoo pH Sensor with pH Responsive Hydrogel via Initiated Chemical Vapor Deposition

Katrin Unger, Francesco Greco, Anna Maria Coclite*

Keywords: temporary tattoo, sensor, wearable device, biomonitoring, skin pH, initiated Chemical Vapor Deposition, epidermal, pH responsive hydrogel

IV.3.1 Preface

The presented work in this article was conducted at the Graz University of Technology. The author of this thesis elaborated and designed the project and received funding for the proposal named "All-polymer tattoo pH sensors" in the "Women in Science" fellowship program. Further she performed the sample preparation, the characterization, data analysis and wrote the manuscript. Francesco Greco and Anna Maria Coclite supervised the project and helped to prepare the manuscript. The following article is still in preparation and not submitted yet.

IV.3.2 Abstract

In the expanding field of physiological pH skin sensors, thin temporary tattoo-based devices have gained attention because of ultra-conformal adhesion while providing excellent water vapor transmission. Here, a pH sensor tattoo made of temporary tattoo paper, screen printed PEDOT:PSS electrodes and pH responsive hydrogel deposited via initiated chemical vapor deposition, is proposed. The tattoo sensor is easily transferred on skin maintaining full functionality and shows excellent conformability to topographical features of epidermis. The investigation of the morphology of all layers within the sensor verifies full control of the desired width of electrodes, thickness of hydrogel and deposition shielded areas. The hydrogel layer exhibits a reversible pH responsive swelling of 24 % to 37 %, with respect to the dry state, at pH 4 to pH 6, respectively. Impedance spectroscopy identifies the phase shift at 10 Hz and 1000 Hz as excellent pH-related property of the sensor which can be only ascribed to the presence of the hydrogel. The sensor ability to operate with non-sophisticated read-out hardware and software was also demonstrated.

IV.3.3 Introduction

Wearable flexible body sensors for *in situ* physiological measurements have become of major interest in healthcare because of the possibility to monitor permanently the patients state of health providing the chance to prematurely detect deterioration and act at early stage of diseases.[1–7] Body fluids such as sweat, saliva or tears contain various chemical substances that provide insight about the state of health.[8–10] Sweat is of particular interest as it is accessible via the body surface, readily available and its composition can be directly linked to that of blood.[11–14] Sweat is a complex mixture of several ion species, ammonium, glucose and lactate among others, and provides rich source of information about the physiological state of the body.

The pH of eccrine sweat is slightly acid with a pH value in the range from 4.5 to7 forming together with sebum the acid mantel of the skin, which acts as a natural barrier against bacteria, viral infections and other contaminants that might penetrate the skin. The combination of the acid skin with the alkaline blood equips the body with a great defense against bacteria pathogens. Different exogenous (skin disease, hormones, electrolyte loss) or endogenous (alkaline cosmetics, drugs) factors can disrupt the epidermal pH, leading to a dehydrated, broken and vulnerable skin.[15–17] Skin-worn pH sensors were already successfully implemented in patches[14,18–20], wristbands[13,21,22], textiles[23,24] or temporary tattoos[25,26]. Due to their thinness (< 1µm thickness), tattoo sensors have the great benefit of smoothly follow the grooves and ridges of the skin topography -just as a second skin-, while providing excellent water vapor transport properties, letting the skin "breath".[27–29] The combination of maximizing the sensor/skin actual contact area and the removal of perspiration is highly needed. Indeed average sweat production in an adult is in the range of 1 - 20 µl $min^{-1}mm^{-2}$at rest, but it rises several orders of magnitude during exercise.[10,30] To maintain these features the fabrication methods and processing of such tattoo sensors must be well chosen. In 2012 the first tattoo-based electrochemical sensor for skin-contact application was proposed by the group of Wang *et.al.* by screen-printing working, reference and counter electrodes on top of a market available temporary tattoo paper.[31] Selectivity of the sensor could be adjusted by functionalization of the working electrode or by supplementary electrodes. [32–36] Solution-based methods, such as screen- or inkjet-printing are attractive fabrication processes, because they are performed under ambient condition and are easily scalable. Nevertheless, in combination with tattoo substrates these methods are mostly limited to water-based inks as otherwise the tattoo layers integrity and/or transferability get compromised. [37]

Widening the possible manufacturing methods and materials, recently also vacuum-based deposition techniques have been utilized to functionalize transferable tattoos.[25] Techniques that

necessitate high or ultrahigh vacuum are costly and time-consuming especially when thinking of the tattoo paper as substrate which is typically water-affine and has a large surface area.

On the contrary, initiated Chemical Vapor Deposition (iCVD) is a low-vacuum (<100 mTorr) and scalable technique that synthesize thin and conformal polymer coatings with high retention of functional groups on various substrates at low temperatures (20 - 60 °C).[38–40] An initiator species is added to the monomer in the vacuum chamber feed. The initiator has a labile bond that decomposes at relatively hot filament (~280 °C), producing radicals, which start the polymerization at the surface, where the monomer is adsorbed. At such temperatures, the monomer is not fragmented and retains its structure.[41,42] With this technique delicate substrates such as tissue paper[43,44], pharmaceutics[45,46] or even ionic liquids[47,48] were already successfully coated.

An interesting branch of functional polymers achievable by iCVD is that of responsive hydrogels, that absorb water depending on a certain stimulus.[49] The rich variations of the responsiveness that can be accessed via iCVD were already demonstrated for humidity[50,51], temperature[52,53], light[54,55] and pH[56,57]. pH responsive hydrogels comprise weak acidic (or basic) functional groups which can be ionized depending on the pH level. The swelling of the hydrogel versus the pH exhibits a first order phase transition with a material characteristic apparent dissociation constant pKα. Above pKα the acidic functional groups deprotonate and repel each other, resulting in a swelling of the polymer network. Below pKα the acid units can form strong hydrogen bonds among themselves and the polymer chain collapse. Not only the swelling changes drastically but also the dielectric properties within the hydrogel exhibit a drastic change at pKα. In terms of measuring the pH of the skin (4.5 - 7), hydrogels made of poly-methacrylic-acid (pMAA) seem promising candidates, as the apparent dissociation constant pKα is about 4.8. pMAA is biocompatible and was already successfully synthesized via iCVD to obtain pharmaceutical drug coatings [46] for pH dependent release properties.[57,58]

Within this study, tattoo-based substrates were screen printed with poly(3,4-ethylenedioxythiophene) : polystyrene sulfonate (PEDOT:PSS) electrodes and further conformally coated with a pH responsive hydrogel of pMAA via iCVD, (figure 1). The fabricated pH sensor tattoo is thoroughly investigated in terms of applicability, morphology and pH responsiveness concerning swelling and dielectric properties.

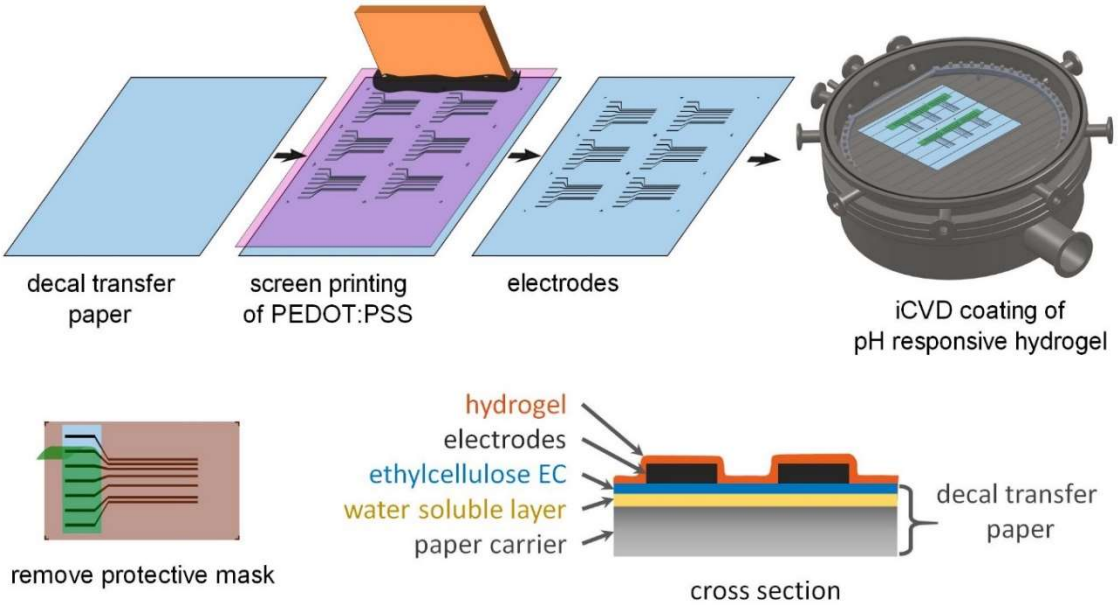

Figure 1: Fabrication steps of the pH sensor tattoo. The decal paper of a transferable temporary tattoo is used as a substrate. PEDOT:PSS electrodes are printed on the substrate via screen printing. A pH responsive hydrogel (pMAA) is deposited via iCVD. Kapton tape is utilized to mask areas from unwanted deposition. After removal of the mask the pH sensor tattoo can be transferred on skin, by applying a little pressure and wetting the back paper. A cross section is pictured of the final pH sensor tattoo with all implemented layers within, the decal paper consisting of a paper carrier, a water-soluble layer and the ethylcellulose EC layer, the polymer electrodes and the pH responsive hydrogel.

IV.3.4 pH Sensor Tattoo Structure

The temporary tattoo paper used in this study consists of a paper carrier sheet, a water soluble starch layer and a ethylcellulose layer (see cross section within figure 1), which was already used in other reports of tattoo sensors.[27] After the temporary tattoo paper was screen printed with PEDOT:PSS electrodes and further coated via initiated chemical vapor deposition (iCVD) with a co-polymer consisting of methacrylic acid (MAA) and di(ethylene glycol) divinyl ether (DEGDVE), the resulting pH sensor tattoo was thoroughly investigated concerning transferability, morphology and chemistry.

Transferability

In figure 2.a cut-out part of the sensor applied on a silicon wafer and on a silicone replica of thumb epidermis can be seen. The transfer on the wafer was performed via floating technique, which led to a structure where the ethylcellulose layer is facing the wafer while the hydrogel and the electrodes (and the Ag coating provided for SEM imaging) are facing towards the microscope. Except the outlines, where the sensor was cut with a scissor which resulted in a frayed edge, and

some small areas with particles beneath the layer, the tattoo sensor is well adhered to the wafer. Clearly the electrodes can be seen as dark grey lines. As well the transition from the coated hydrogel to the part which was shielded during the deposition is visible as a distinct line. The shielded area looks completely uncoated in the SEM image. The possibility that the sensing part of the sensor can also face outwards from a surface onto which the tattoo has been transferred lead to other possible methods of usage.

On the thumb replica the sensor was transferred by pressing the sensor facing the hydrogel layer towards the thumb replica, wetting the back paper and removing the paper carrier sheet, resulting in a contact of the hydrogel with the silicone replica while the ethylcellulose layer is facing the microscope (see figure 2.b). Again, both the electrodes and the hydrogel can be seen. All areas within the sensor tattoo, namely the hydrogel, the electrodes and the uncoated tattoo follow the topological features of the thumb replica resulting in an intimate contact between the surface of the thumb and the sensor. Therefore it can be concluded, that coating a tattoo with PEDOT:PSS electrodes via screen printing and further with a co-polymer of MAA and DEGDVE (p(MAA-DEGDVE)) by iCVD, compromise neither the transferability nor the ability to smoothly follow the underlying surface topography.

Morphology

Atomic force microscopy was utilized to investigate the surface morphology of the different coated layers of the sensor tattoo. Again, the tattoo sensor was transferred via floating technique onto a Si wafer. In figure 2.c the AFM topography image of all areas within the sensor are displayed. While the edge of the printed electrode is distinct and clearly visible, that of the hydrogel has some spikes at the border, due to irregularities at the protective mask. Indeed, during the iCVD deposition, one part of the tattoo and the electrodes were masked via a tape which was peeled off after the deposition. The removal of the tape seems to cause very localized delamination (< 1 mum lateral) and small peeling off effects (< 300 nm in height) of the hydrogel towards the layer underneath. The roughness, calculated by the root mean square error (R_{rms}), of the uncoated ethylcellulose layer was 45 nm. The hydrogel layer coated on a tattoo has a R_{rms} = 49 nm. The R_{rms} values of the electrode and the hydrogel deposited on the electrodes are 45 nm and 42 nm, respectively. The iCVD coating technique typically results in a uniform polymer thin film with a constant film thickness which preserves the roughness of the underlying layer through the polymer growth, as confirmed by these results.

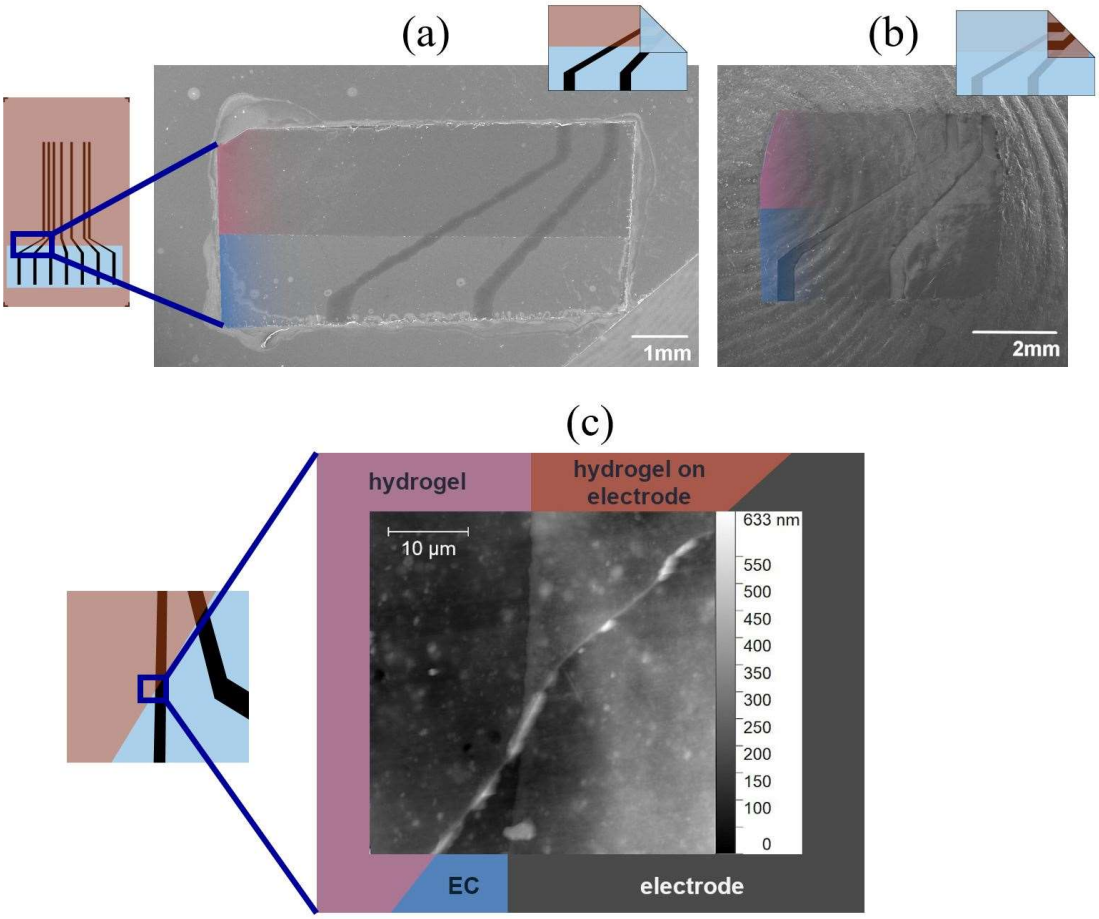

Figure 2: (a) Scanning Electron Microscopy image of a pH sensor tattoo transferred onto a Si wafer. The sensing part faces out of plane. (b) Image of the pH sensor tattoo transferred on a silicone replica of thumb skin. The sensing part faces the thumb. (c) AFM topography image of the four areas within the sensor tattoo.

Chemical Composition

To verify the retention of chemical groups of the hydrogel during the iCVD deposition FTIR spectra were analyzed (see figure 3.a and figure 3.b). The spectrum of the hydrogel p(MAA-DEGDVE) deposited on a silicon wafer has its most intense absorption band at 1720 cm^{-1} which can be attributed to C=O stretching of the functional group of MAA. Further peaks caused by C-H stretching and bending, which are typical for polymer backbones, can be found in the ranges of (3000 – 2800) cm^{-1} and (1500 – 1350) cm^{-1}, respectively. A typical vinyl absorption band would be at 1650 cm^{-1} corresponding to the C=C stretching. The hydrogel spectrum has negligible absorption at that frequency verifying a complete conversion of the monomer species to the polymer. The IR spectrum of the ethylcellulose layer of the uncoated tattoo has a broad and intense O-H stretching absorption in the range of (3500 – 3150) cm^{-1}. After the deposition with

p(MAA-DEGDVE) this peak got smaller which can be attributed to the affinity of the acid MAA group to deprotonate. Typically, the lost proton bounds to an -OH group which further became -OHH^+. Zooming into the fingerprint region, into the range of (1800 – 1600) cm^{-1}, shows that the uncoated tattoo absorbs exactly at 1720 cm^{-1}, way less than a coated tattoo. This can be explained by considering that the p(MAA-DEGDVE), which was deposited on the tattoo, also contributes to the adsorption at 1720cm^{-1} with the C=O stretching of its ester groups. Concluding, the hydrogel is present on the tattoo and the chemistry of the hydrogel is also retained on the tattoo, which did not degrade during the deposition. After rinsing the coated tattoo with artificial sweat of pH 4 and pH 6 the absorption spectrum (not plotted) shows no change, indicating, that the hydrogel did neither delaminate from the tattoo nor was chemically modified in the salty and acidic environment of artificial sweat.

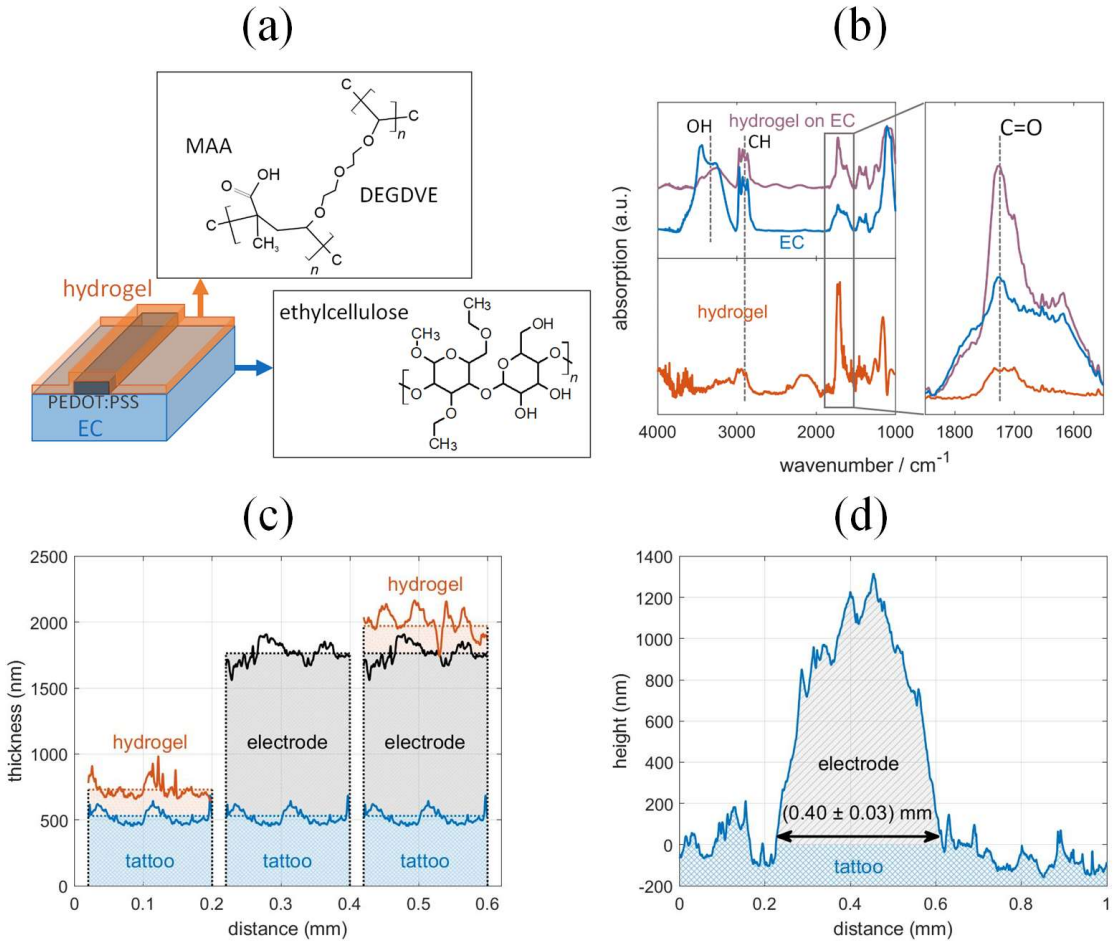

Figure 3: (a) Chemical structure of layers in the tattoo sensor: the native ethylcellulose layer releasable form a temporary tattoo paper, the screen printed PEDOT:PSS and the hydrogel. (b) FTIR spectra of the hydrogel, the EC and the EC/hydrogel. (c) Thickness profiles of the different layers stacked above each other for visualization, as obtained by stylus profilometry. (d) Height scan across a PEDOT:PSS electrode.

The thicknesses of the individual layers of the sensor tattoo with removed paper carrier were measured with profilometry. In figure 3.b the line-scans of individual layers were stacked for visualization purpose. The EC layer of the tattoo has an average height of (530 ± 50) nm which is in the typical range of production for this decal paper (400-600) nm.[27] The estimated error is the roughness' root mean square error, which fits well the value determined via atomic force microscopy (45 nm). The average thickness of an EC/hydrogel bilayer is (730 ± 54) nm which implies an increase of thickness of 200 nm compared to the bare EC, which fits perfectly the desired deposition thickness monitored via laser interferometry on the reference wafer during the deposition. The roughness value of 54 nm again matches the value determined by AFM (49 nm).

PEDOT:PSS electrodes were patterned with screen printing and had a thickness of (1230 ± 44) nm. The average thickness of the coated electrodes (PEDOT:PSS/hydrogel) rises to (1440 ± 93) nm which is again an increase of 210 nm caused by the hydrogel coating. The thickness of the deposited hydrogel is the same on the reference wafer, on the tattoo and on the electrode, meaning that the iCVD deposition kinetics does not favor none of the three surfaces. The maximum overall thickness of the sensor, i.e. in the areas composed of EC/PEDOT:PSS/hydrogel layers, is around 2 μm; this low thickness is very relevant for achieving the necessary conformability and transpirability in on-skin application.

The height profile of a cross section of an electrode without hydrogel coating is plotted in figure 3.c. The width of the electrode was measured with (0.40 ± 0.03) mm which fits the designed value of 0.4 mm well, validating the accuracy of screen-printing process. Cross sections of electrodes coated with hydrogels show no significant difference with an evaluated width of (0.41 ± 0.02) mm.

IV.3.5 pH Sensor Tattoo Responsiveness

pH Responsive Swelling

Swelling response of the hydrogel in artificial sweat with changing pH values were measured *in-situ* with spectroscopic ellipsometry. In figure 4.a, the upper plot schematizes the set pH value of the artificial sweat, which the sample was exposed to. After measuring the dry sample, the applied artificial sweat loops between pH 6 and pH 4 and during one loop also increase incrementally to evaluate the response in terms of responsiveness, repeatability and sensitivity.

In dry state the hydrogel thickness was evaluated with (203 ± 1) nm. With immersing the hydrogel in artificial sweat of pH 6, the thickness increases within 10 minutes to (277 ± 2) nm, which is a thickness increase of 36.5 % with respect to dry state. Changing the pH from 6 to 4 lead to a deswelling, resulting in a thickness increase of 24.3 % in respect to the dry state.

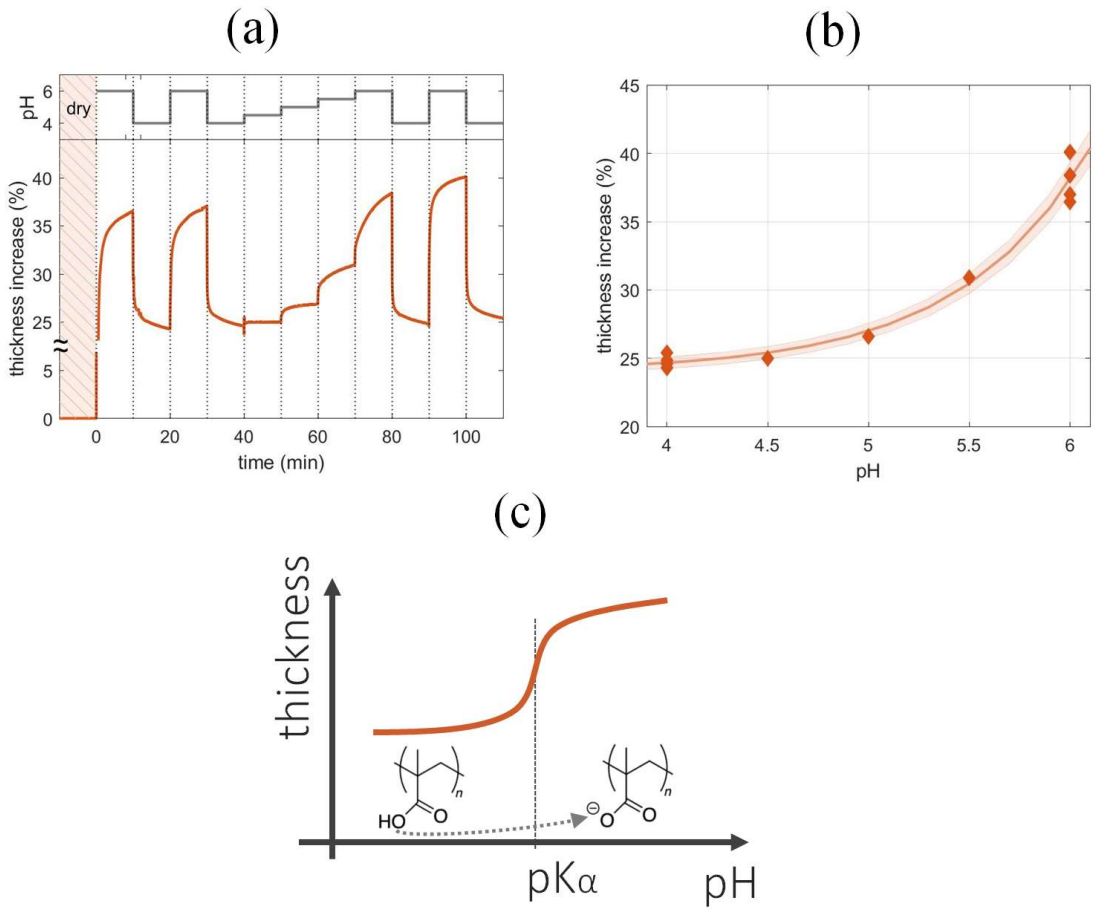

Figure 4: (a) pH responsive swelling of the hydrogel. (b) Swelling (thickness increase, %) versus pH. (c) Swelling behavior of a pH responsive hydrogel in the pH domain around the inflection point, represented by pKα of the MAA.

Generally, acid groups within pH responsive hydrogels have an association constant pKα. With a pH value above pKα the acid groups deprotonate, resulting in a repulsion of the negative left acid groups; the hydrogel opens voids where water molecules can penetrate into and swells. Below pKα, the acid groups protonate which results in a strong attraction among the acid groups and the hydrogel collapses, (figure 4.c). Polymers of MAA have pKα values from pH 4.4 to pH 6. [59] The co-polymer hydrogel p(MAA:DEGDVE) deswells when changing from pH 6 to pH 4 as a result of the protonation of the acid groups, as explained above. But at pH 4 the hydrogel is not in a complete shrunken state and has still a high swelling, implying that the hydrogel has also at pH 4 a good affinity to incorporate the artificial sweat. This can be explained by the interaction of the hydrogel with the salt as well as the attraction of the DEGDVE to water molecules.

When again looping the pH of the artificial sweat from pH 6 to pH 4, the hydrogel swells again to 37.0 % and shrinks back to 24.6 %, respectively. The swelling of the hydrogel is pH

responsive and reversible. Generally, the swelling of a pH responsive hydrogel versus the pH is a sigmoid function, with the acid's dissociation constant pKα being defined as the inflection point of the curve. Plotting the thickness increase reached within 10 min versus the pH value (figure 4.b), the trend appears exponential implying that the pKα value of the synthesized hydrogel is not within the range from pH 4 to pH 6 but above. The thickness measured at pH=6 increased with time: (see Supporting Information). Such deviation may be explained considering some kinetics effects during the measurement. The change of the pH was done manually injecting the new solution into the samples compartment. Although this took only about 15 s, slight differences of applied pressure and speed may cause a change of swelling properties at the surface which may propagate in time.

pH Responsive Dielectric and Ionconductive Properties

To evaluate the dielectric and conductivity properties of the sensor tattoo, electrochemical impedance spectra were taken. As representative of a series of measurements, the Bode plots of uncoated and hydrogel coated tattoos immersed in artificial sweat @ pH 6 and @ pH 4 are plotted. In the Bode plots of the impedance (see figure 4.a), the absolute value of the impedance *Zmod* increased with increasing frequency in all the investigated samples.

In the frequency region from 10 Hz to 1000 Hz, the *Zmod* of a coated tattoo immersed in pH 4 has a plateau at (7.1 ± 0.3) Ω, with the error being the deviation within the plateau. The plateau rises to (15.7 ± 0.7) Ω when the sample is exposed to pH 6, resulting in a pH responsive change of *Zmod* of 215 % within the pH range. Above 1000 Hz, *Zmod* increases and the pH responsiveness is lost. The *Zmod* of the uncoated tattoo increases from 10 Hz to 700 Hz and reaches there a plateau at (42.8 ± 0.4) Ω and (36.0 ± 0.6) Ω in pH milieu of pH 4 and pH 6, respectively. PEDOT:PSS itself is also pH responsive with a dissociation constant pKα of 2.9. Although the pKα value is way below the used region, the evaluated pH response of *Zmod* was 20 %. Above 10 kHz the *Zmod* increases again for both curves and the pH responsiveness diminishes.

The Bode plot of the phase, which is the phase shift of the applied potential to the measured current sweep, of the four representative measurements are plotted in figure 4.b. At the frequency of 10 Hz the phase of an uncoated tattoo immersed in solution of pH 6 is 38 °, which decreases reaching at 4000 Hz a local minimum of 5 ° and further increases again. When applying a solution of pH 4 the shape of the phase does not change but the curve is slightly shifted by 2.5° to lower phases. A tattoo coated with a hydrogel in pH 6 has at 10 Hz a phase of 20 ° which decreases till 300 Hz to 2 ° and further increases again. The same sample in pH 4 has a phase of 0 ° at 10 Hz rises continuously with frequency. The different shapes of the phase versus frequency of a tattoo coated with a hydrogel in either pH 4 or pH 6 are clearly visible and verify the pH

dependent dielectric properties of the coated sensor tattoo. At 120 Hz the two curves intersect with each other. At this frequency the phase shows no pH dependency.

A series of EIS measurements with varying the artificial sweat pH value were collected. The *Zmod* and the phase at frequencies of 10 Hz and 1000 Hz for an uncoated tattoo were plotted in figure 4.c. The top row of the plot displays the set pH value. As the small difference of the phase curves of the uncoated tattoo already revealed, the pH dependency is barely visible and neglectable small. The *Zmod* is slightly pH dependent which converges after 2 times cycling between pH 6 and pH 4 to a *Zmod* of (40 ± 1) Ω and (44.5 ± 0.5) Ω at pH 6 and pH 4, respectively. Nearly the same plot but with a coated sample instead is depicted in figure 4.d. A slight difference can be observed in the set pH values as also incremental steps between pH 4 and pH 6 were set during one loop. The phase exhibits a reversible pH response at both frequencies. At 10 Hz the phase switches between (20 ± 1) ° and (0.3 ± 0.3) ° in pH 6 and pH 4, respectively. In contrast, the phase at 1000 Hz is as well pH responsive but flipped up to down with a phase of (3.6 ± 0.8) ° and (18 ± 1) ° in pH 6 and pH 4, respectively. The *Zmod* of the coated tattoo exhibits as well a pH responsive and reversible behavior at both frequencies. Varying between (7.2 ± 0.4) ° and (14 ± 2) ° for pH 4 and pH 6 at 10 Hz, respectively. And at 1000 Hz from (8.2 ± 0.5) ° to (17 ± 3) ° again for pH 4 and pH 6, respectively. Although the *Zmod* responsiveness towards pH (see figure 4.e) is with more than 200 % of change rather high, the small response in the range of pH 4 to pH 5 as well as the large error of this parameter reduces its credibility as a trustworthy connection to the pH value. While on the contrary the error of the phase is rather small (< 1°) with an excellent pH responsiveness. The phase in respect to the pH value is plotted in figure 4.f. With increasing pH, the phase increases at 10 Hz and decreases at 1000 Hz.

Comparing the pH responsive swelling of the hydrogel with the pH responsive phase shift of the tattoo coated with the hydrogel permits the conclusion, that the dielectric properties is correlated with the swelling.

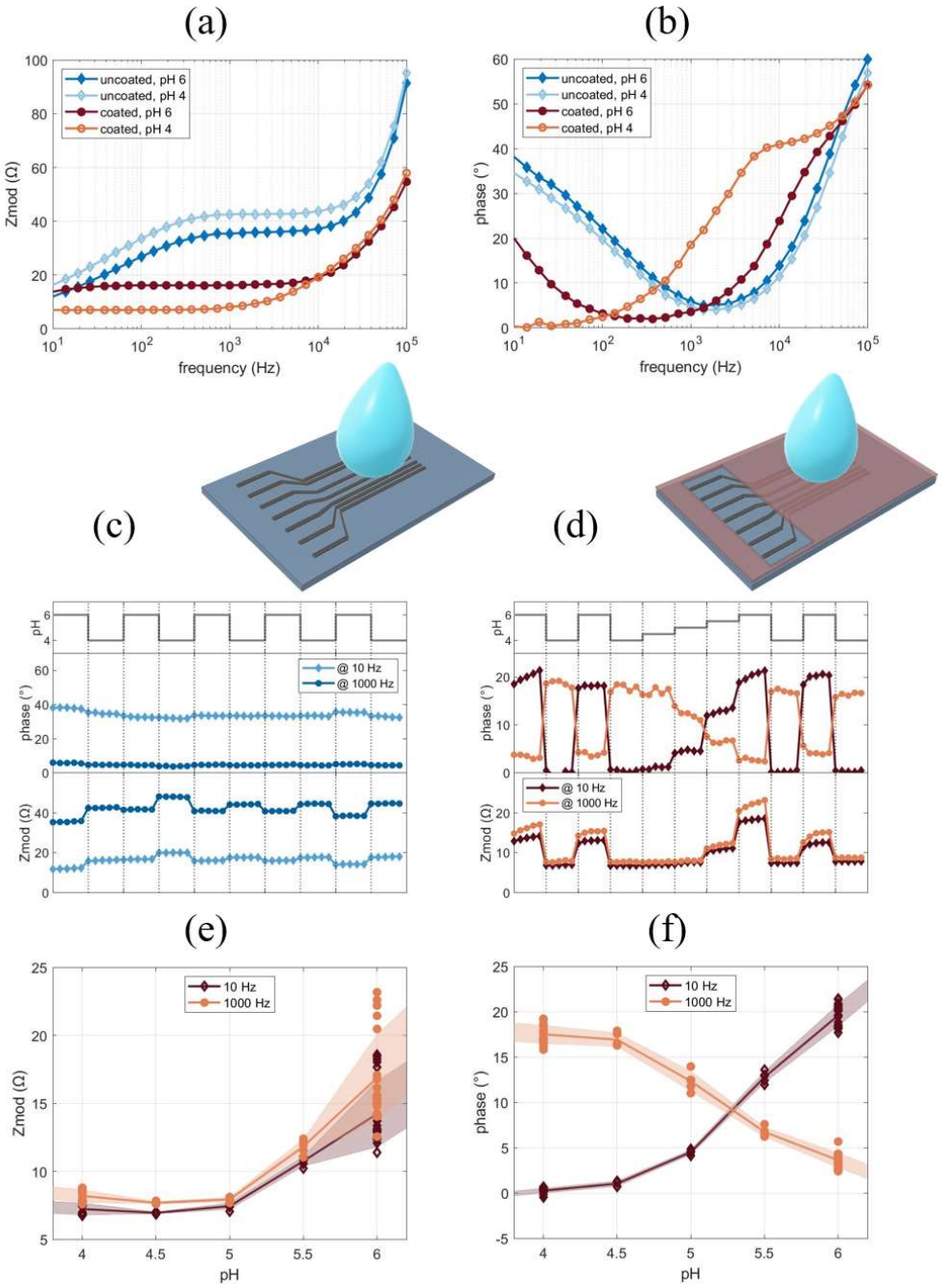

Figure 4: (a) Bode plot of the impedance of the coated and uncoated tattoo immersed in artificial sweat of pH 4 and pH 6. (b) Bode plot of the phase with the same measurement. (c) Schematic of the uncoated tattoo. Zmod and phase shift at 10 Hz and 1000 Hz evaluated at different pH with an uncoated tattoo. (d) Schematic of a tattoo coated with a hydrogel. Zmod and phase shift at 10 Hz and 1000 Hz evaluated at different pH with a coated tattoo. (e) Zmod versus pH at 10 Hz and 1000 Hz for a coated tattoo. (f) Phase shift versus pH at 10 Hz and 1000 Hz for a coated tattoo.

IV.3.6 pH Sensor Tattoo in Action

To go beyond proof of concept and demonstrate the sensors capability as a wearable device, easy and cheap read out hardware and software are mandatory. A microcontroller (Arduino) was used as signal generator and read out terminal for the current response. In figure 5.a**,** an oscilloscope visualized the signals of the uncoated tattoo in artificial sweat of pH 6 and pH 4 and a tattoo coated with a hydrogel at pH 6 and pH 4. Within one of these plots the applied voltage sweep, the current response (converted to a voltage signal) and further amplified current signal can be seen. While the uncoated sample seems to have no response towards the pH value, the coated tattoos reply is linkable to the set pH. At pH 6 the current response rises after the positive edge and converges then to a constant value. At the falling edge the signal decays exponentially back to 0 V. In contrary, at pH 4 the current response increases till a local maximum and decreases again converging to a constant value. At the falling edge the current response decays below zero, passes a negative peak and converges to zero again. After this signal got further amplified, which was needed to get a measurable signal for the Arduino, the peak got pronounced and the signals below 0 V got lost (because it was a rail-to-rail amplifier which can only operate above 0 V), which can only be ascribed to the non-linear behavior of the chosen amplifier.

The echo measured by the Arduino, which is the time between the positive voltage edge to the current response, versus the pH value is depicted in figure 5.a. In the first row the set pH value switching between 6 and 4 is plotted. While the echo of the uncoated tattoo has no pH dependency, the echo of the coated tattoo responds well to the artificial sweat pH.

In retrospective, the hardware and software could have been easily improved (Arduino due – faster, different amplifier + upconverter – to also be able to measure the negative response or simply tracking datapoints of the analog signal and evaluate the shape), which would enhance the gained responses quality, but already this simple attempt led to a measurable response which emphasizes the idea of a sensor tattoo that can easily be read out by non-sophisticated electronics.

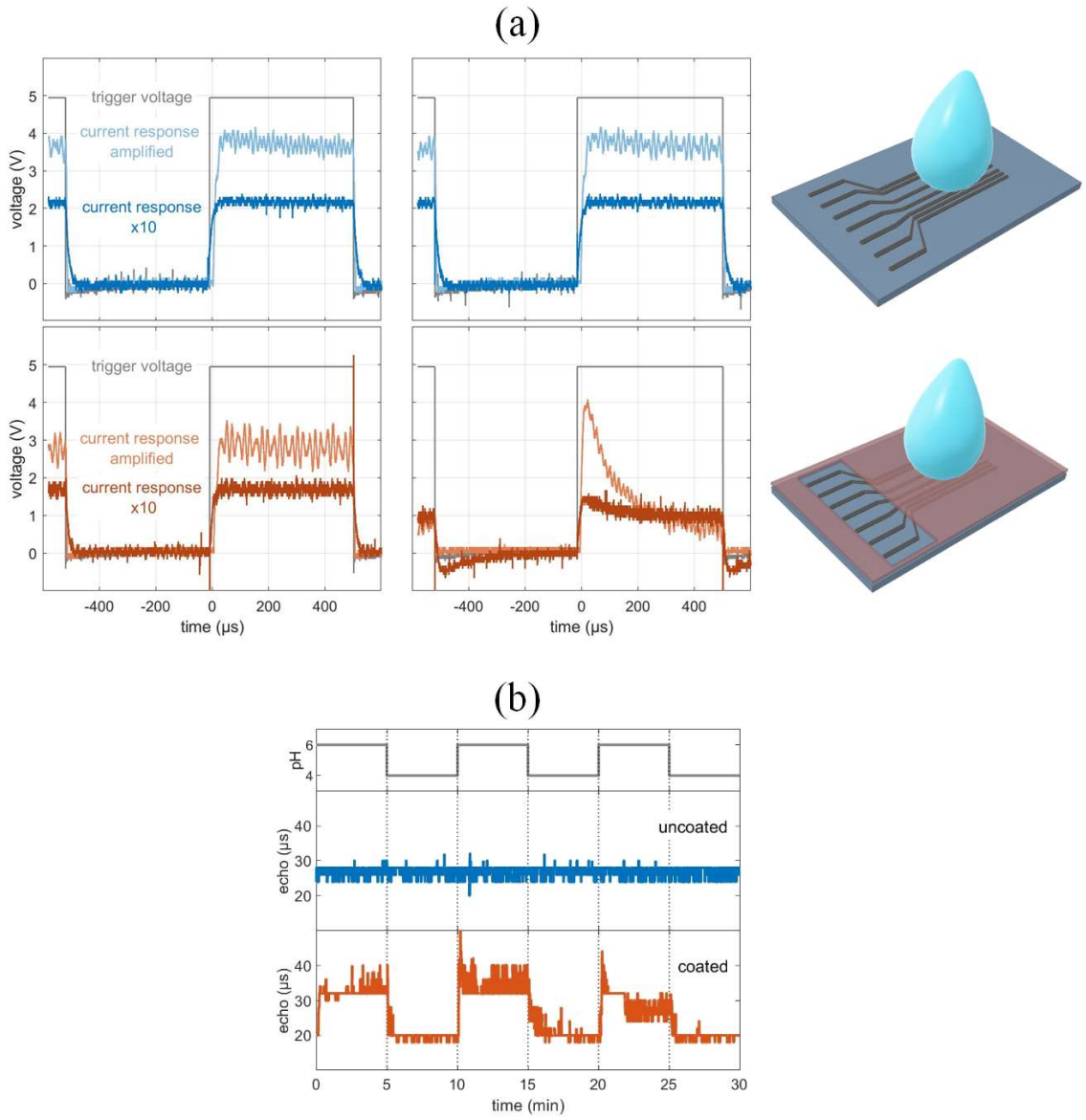

Figure 5: (a) Oscilloscope measurement of the trigger voltage, the current response and the amplified current response of an uncoated and coated tattoo in artificial sweat of pH 4 and pH6. (b) Echo time, which is the time between the positive edge of the trigger and the current response in artificial sweat of pH 4 and pH 6.

IV.3.7 Conclusions

A pH skin sensor tattoo was successfully fabricated by screen printing of PEDOT:PSS electrodes and further depositing a pH responsive hydrogel p(MAA-DEGDVE) via iCVD directly on a temporary tattoo substrate. During the fabrication the applicability of the tattoo did not get compromised and the ability to conformally adhere to the complex topology of rough surfaces was retained. The measured electrode width (0.40 ± 0.02) mm fit excellent the designed value of 0.4 mm and the height of the electrode of (1230 ± 44) mm implies full retention of the ultra-thin features of the tattoo. The possibility to apply the sensor tattoo not only facing into the substrate but also in direction out of the substrate can lead to various application possibilities. The synthesis of the hydrogel layer by iCVD on the tattoo was proved. The deposited hydrogel has equal height (~200 nm) on the reference wafer, the tattoo surface and the electrode surface. Together the results bear out excellent controllability of the morphology during manufacturing process.

The pH responsive swelling of the hydrogel layer was evaluated with a thickness increase of 37.0 % and 24.6 % in artificial sweat of pH 6 and pH 4, respectively, in respect to the dried state. The Bode plot of the impedance of the sensor tattoo coated with the hydrogel immersed in artificial sweat exhibits a pH responsive shift of the plateau at the frequency range from 10 Hz to 1500 Hz from (7.1 ± 0.3) Ω to (15.7 ± 0.7) Ω at pH 4 to pH 6, respectively, which is about 215 % increase. The uncoated tattoo in this plot is generally shifted to higher values and has also a pH responsive shift from (42.8 ± 0.4) Ω and (36.0 ± 0.6) Ω at pH 4 to pH 6, respectively. The Bode plot of the phase (the phase shift versus the applied frequencies) evidences distinct features of the sensor tattoo coated with the hydrogel at pH 4 and pH 6, while the uncoated sensor tattoo indicates no response towards the pH. The absolute value of the impedance and the phase shift at the frequency of 10 and 1000 Hz of the sensor tattoo sub-sequentially immersed in artificial sweat of different pH values were extracted. The selected value demonstrates for the sensor tattoo coated with hydrogel excellent reversible pH responsiveness while only little or no responsiveness of an uncoated sensor tattoo can be seen. The phase shift was identified as the best property to link to the pH.

In a self-made microcontroller setup an Arduino was used as trigger and read out terminal to demonstrate the sensors capability as a wearable device that can be operated without sophisticated lab equipment.

IV.3.8 Experimental Section/Methods

Device Fabrication and Mixture of Artificial Sweat

Screen Printing of Electrodes

The temporary transfer tattoo paper used in this study is commercially available (The Magic Touch Ltd., UK) and composed of a decal transfer paper and a glue sheet. The decal transfer paper consists of a paper carrier sheet, a starch-dextrin water soluble layer and an ethylcellulose layer (thickness ~ 500 nm). The glue sheet is made of a silicone paper carrier, an acrylic glue layer (thickness ~ 700 nm), and a plastic liner. When applying a tattoo onto a target surface (e.g. skin), first the paper carrier needs to be removed from the glue sheet which needs to be further connected to the decal paper with the acrylic glue facing the ethylcellulose layer. Then the plastic liner needs to be removed and the second side of the acrylic glue is pressed on the desired surface. When wetting the decal paper, the starch-dextrin layer dissolves and the paper carrier can be removed and the ethylcellulose layer sticks to the target surface due to the acrylic glue.

In this project, the decal transfer paper was used as substrate for screen printing PEDOT:PSS electrodes. To produce the pattern for the screen printing a UV-curing emulsion (Ultra Coat 535, CPS – Chemical Products and Services, I&W Handels GmbH, Austria) was applied on the mesh (Saatilene, I&W Handels GmbH, Austria, mesh counts of 77T). The electrode design was printed on a print paper which acted as a mask during the UV illumination (time: 200s). Afterward the screen was washed with water. The PEDOT:PSS ink (Clevios S V4 Stab, Heraeus, Germany) was redispersed before applying it on the decal transfer paper with a screen lift-off of 0 mm with one single move.

Hydrogel Coating via initiated Chemical Vapor Deposition

The pH responsive hydrogel coating was synthesized via initiated Chemical Vapor Deposition (iCVD) in a custom built iCVD chamber, described elsewhere.[60] The monomer species were methacrylic acid (MAA, 99%, Merck, Darmstadt, Germany), di(ethylene glycol) divinyl ether (DEGDVE, , 99%, Merck, Darmstadt, Germany) and the ethylene-glycol-dimethacrylate (EGDMA, 98%, Sigma Aldrich, Germany), and the initiator was tert-butyl peroxide (TBPO, 98%, Sigma Aldrich, Germany). The substrates, namely a silicon wafer and the tattoo with the screen printed PEDOT:PSS electrodes, were kept at a temperature of 30 °C by a chiller/heater system (Thermo Scientific Accel 500 LC). All edges of the tattoo paper were taped by Kapton adhesive tape (Tesa 51808 Kapton) on the chamber bottom to prevent coating of the backside. Kapton adhesive tape was used also to mask the part of the tattoo electrodes that needed to be contacted afterwards, for preventing their coating during the iCVD process. The temperature of the MAA, DEGDVE and EGDMA monomer jars were set to 70 °C, 70 °C and 85

°C, respectively, mixed in a heated line and were further fed into the reactor chamber. The MAA, DEGDVE, EGDMA and TBPO (unheated, separated line) flowrates were 4.4 sccm, 0.4 sccm, 0.2 sccm and 1 sccm, respectively, set by needle valves. The working pressure was set to 400 mTorr. Thermal decomposition of the initiator TBPO was induced via a hot filament (270 ± 10) °C of nickel-chromium wires (Goodfellow, UK). The deposition was started with only the EGDMA and the TBPO line opened. After 2 minutes the MAA and DEGDVE lines were additionally opened. Again after 2 minutes the EGDMA line was closed. With this procedure a strong adhesive bond from the polymer layer to the substrate can be expected which should prevent delamination. The polymer thickness on the silicon wafer was in situ monitored by laser interferometry ((He–Ne Laser with λ = 633 nm, Thorlabs, USA). After a layer thickness of 200 nm the deposition was terminated at 68 minutes deposition time.

Platform for Mounting the Ultra-thin Tattoo via Printed Circuit Board

To connect to the electrodes and stabilize the tattoo when the paper carrier is removed, a printed circuit board (PCB) was designed (figure 6). The PCB has on one side a form that can be plugged into a 7 pole SATA cable (typically used to connect to hard drives) to easily connect the wires of the cable further to any kind of measuring device. In the middle the PCB has a routed hole because the tattoo sensor surface is facing in direction of the PCB when it is connected. The hole acts like a compartment that make the sensor accessible and can hold solutions within. Between the tattoo sensor and the PCB the glue sheet of the tattoo was placed to improve the adhesion. The glue sheet was cut out via a laser cutter (ULS2.30, Universal Laser System equipped with a 30 W CO_2 laser source at 10.6 µm wavelength) removing the areas were the tattoo should not be covered, namely the sensor part in the middle and the part where the electrodes of the tattoo and of the PCB should connect.

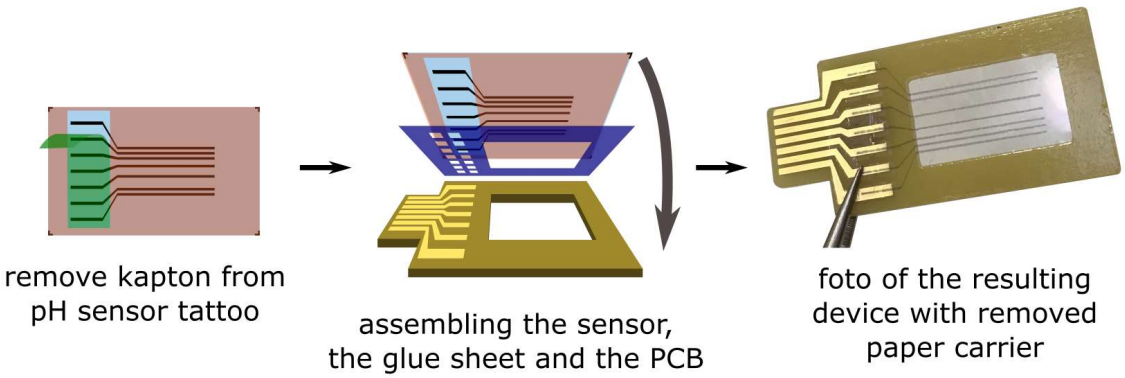

Figure 6: Assembling of the tattoo the glue sheet and the PCB.

Artificial Sweat

Artificial sweat was prepared based on the ISO 3160-0 recipe which is typically used for testing degradation processes of wearable body sensors. Milli-Q water was mixed with NaCl (Merck, Art.6404), NH_4Cl (Merck), acetic acid (Fluka >99.8%, 45731) and lactic acid (Sigma Aldrich, W 261106, 85%). The concentrations were: NaCl 20 g/l, NH_4Cl 17.5 g/l, acetic acid 5 g/l and lactic acid 15 g/l. A solution of NaOH (150 g/l) in Milli-Q water was used to set the pH value. In contrast to the recipe, the pH value was not set to 4.7 but solutions at pH 4, 4.5, 5, 5.5 and 6 were prepared. This pH values fits well the desired range of typical sweat, does not corrode any lab equipment and provides a stable buffer solution.

Device Characterization Methods

Applicability – Scanning Electron Microscopy

Scanning electron microscopy (SEM) imaging was used to observe the applicability of the sensor tattoo. For this purpose, one sample was produced via floating technique. A small part of the sensor tattoo was cut out with scissors and floated on the surface of demineralized water facing the carrier paper into the water. The starch-dextrin layer dissolved and the paper carrier sheet sank while the ethylcellulose layer with the electrodes and the hydrogel layer remained floating on the water surface. With a silicon wafer the sample was lifted from underneath out of the water. A silver layer of 20 nm was physically vapor deposited with a thermal evaporator operating at a pressure of $1 \cdot 10^{-3}$mbar and at a deposition rate of (0.65 ± 0.1) As^{-1}. The fingertip silicone replica was produced by first creating a negative of a fingertip made of clay (Fimo) which was further hardened by 110 °C for 30 min: then this negative was coated with polydimethylsiloxane (PDMS) (Dow Corning Silicone Elastomer Kit 1:10 mixing ratio curing agent to prepolymer), which was further cured at 85 °C for 2 hours. After peeling the PDMS fingertip replica out of the negative, a cut-out piece of the sensor tattoo was placed on it facing the hydrogel toward the replica surface, wetted with demineralized water and the paper carrier sheet was removed. Scanning electron microscope (Jeol JSM-6490LV, Labco GmbH, Pressbaum, Austria) images were recorded at 10 keV and 20 keV acceleration voltage.

Morphology – Atomic Force Microscopy and Profilometry

Atomic Force Microscopy (AFM) was utilized to get insight about the morphology properties of all surfaces present in the tattoo sensor. An AFM operating in tapping mode was used. The scanned area was set to 50x50 μm^2, the time per line to 1.2 s, the points per line to 512, the setpoint to 60 %, the P-gain to 3500, the D-gain to 1000 and the vibration amplitude to 180 mV. AFM imaging was carried out on the surface of a tattoo transferred onto a silicon wafer via the floating technique described previously. The data were afterwards leveled and the statistical

data were evaluated via the software Gwyddion. The roughness R_{rms} was calculated as the root mean square error in respect to the average height function of a chosen area.

The thickness of the individual layers of the sensor tattoo were measured with an AlphaStep D-500 Profilometer from KLA-Tencor. The sensor tattoo was transferred onto a silicon wafer. Line scans were taken starting on the silicon wafer and crossing the step onto different surfaces of the sensor tattoo, namely the EC layer, the EC coated with the hydrogel p(MAA-DEGDVE), the screen printed electrodes (PEDOT:PSS) on EC and the EC/PEDOT:PSS/hydrogel trilayer. Profilometry scanning parameters were set to: speed 0.05 mm s^{-1}, scan length 0.5 mm, stylus force 0.2 mg. Data were afterwards leveled via the native software of the instrument. The statistical evaluation of the height and the roughness were calculated taking the line scan after the border of the step and calculating the average and the root-mean-square deviation of the height, respectively. Additional cross section scans of the electrodes were performed with scanning properties as followed: scan speed 0.1 mm/s, scan length 1mm, stylus force 0.2 mg. The width was measured between the spots were the declining electrode exceeded the height of 0 nm. Three electrodes were measured to get the statistical error.

Chemical Composition – Infrared Spectroscopy

The chemical composition within the hydrogel was measured with Fourier Transform infrared spectroscopy with a Michelson interferometer (Bruker IFS 66v/S) in transmission mode. The measurement chamber was kept at a vacuum of about 5 mbar to prevent absorption from air. Measurements of spectra were taken from a bare silicon wafer, a wafer coated with the hydrogel p(MAA-DEGDVE), an EC layer transferred from a temporary tattoo paper, a transferred EC/hydrogel tattoo and the same sample but after immersing it for 15 minutes in pH 4 and for 15 minutes in pH 6 to verify the chemical retention after the acid environment. The spectrum of the wafer coated with the hydrogel was divided by the silicon wafer to obtain the hydrogel layers absorption only. All spectra were afterwards baseline corrected. The scan properties were chosen as followed, resolution 4 cm^{-1}, scan-time 1000 scans, range (4000 - 500) cm^{-1}, aperture 8 mm.

pH Responsive Swelling - Ellipsometry

The film thickness of the hydrogel upon swelling in artificial sweat at different pH values was measured with spectroscopic ellipsometry (J. A. Woollam ESM-3000, Lincoln, NE, USA). A tight sealed liquid cell (J. A. Woollam, Lincoln, NE, USA) was used to expose the sample to the different solutions while in-situ spectra were taken each 4 seconds at an angle of 75 ° in the spectral region from 370 nm to 1000 nm. Each 10 minutes the artificial sweat within the cell (cell volume about 4 ml) was exchanged by injecting 10 ml of artificial sweat at different pH values

into the inlet of the cell. At the outlet the drained solution was tested with a pH indicator paper to verify the complete change of the pH to the desired new value. The spectrum of the hydrogel in dry state (measured in air) was fitted with a three-layer model consisting of a silicon substrate, a native silicon dioxide (2 nm) and a Cauchy layer, representing the hydrogel. While measuring in artificial sweat, the Cauchy layer was replaced by an effective material approximation model, which averages the defined optical properties of two different materials weighted by the materials ratio within the layer. One material optical property were the obtained parameters of the hydrogel in dried state, and the other material was water. The thickness of this layer and the ratio of the two materials were then the only fitting parameters. This is a typical procedure for transparent swollen hydrogels.

pH Responsive Dielectric Properties – Electrochemical Impedance Spectroscopy

To take Electrochemical Impedance Spectroscopy (EIS) measurements, the tattoo sensor was mounted on the designed PCB and the paper carrier sheet was removed. The PCB was connected into a SATA 7 plug-in where on the other side the cables were unshielded and further connected to the working, working sense, reference and counter electrode of an Gamry Instrument (Reference 600). Artificial sweat solutions of different pH were subsequently inserted into the PCBs compartment area. Galvanostatic EIS measurements were performed in the frequency range of 10 Hz to 100 kHz, with a resolution of 7 points per decade, with an AC current of 10^{-5}A and no offset DC current. With a second sensor tattoo the experiment was repeated. The resulting shapes and values of the bode plots as well as the pH responsive behavior could be successfully reproduced.

Arduino as Trigger and Read-out Terminal

To proof that the sensor can be operated also with cheap and non-sophisticated equipment, in a first attempt a microcontroller (Arduino Uno) was used as a terminal platform. An output pin of the Arduino generated a pulsed signal with 50 % duty cycle with a frequency of 1 kHz between 0 V and 5 V. As PEDOT:PSS starts to chemically oxidize or reduce above 100 mV, the voltage signal was down transformed via a voltage bridge to 7 mV which was pinned to the first electrode of the sensor tattoo. The second electrode was connected with a micro-current device, which is a self-made electronic device that is capable of transferring nA current signals to a voltage signal between -3 V and 3 V, which was further connected to common ground. The output voltage signal of the micro-current device needed to be further increased with was done by a rail-to-rail amplifier operated in non-inverting amplification mode. After that the signal was pinned back to a digital input of the Arduino. In this configuration the applied voltage sweep can

be compared with the resulting current response. Because the experimental results of the electrochemical impedance spectra identified the phase as the most reliable parameter to be able to link to a pH, the echo, which is the time between the applied positive voltage signal edge till the current response reaches a threshold. To track the signal sweep of the applied voltage, the voltage signal after the micro-current device, which should be directly linked to the current response and the further amplified voltage signal directly before the Arduino input, an oscilloscope was utilized.

Acknowledgements

The project has received funding from the Women in Science fellowship by L'Oréal and the UNESCO.

IV.3.9 References

1. Ling, Y. et al. Disruptive, Soft, Wearable Sensors. Adv. Mater. *32*, 1–13 (2020).

2. Kenry, Yeo, J. C. & Lim, C. T. Emerging flexible and wearable physical sensing platforms for healthcare and biomedical applications. Microsystems Nanoeng. *2*, (2016).

3. Trung, T. Q. & Lee, N. E. Flexible and Stretchable Physical Sensor Integrated Platforms for Wearable Human-Activity Monitoringand Personal Healthcare. Adv. Mater. *28*, 4338–4372 (2016).

4. Someya, T. & Amagai, M. Toward a new generation of smart skins. Nat. Biotechnol. *37*, 382–388 (2019).

5. Gao, Y., Yu, L., Yeo, J. C. & Lim, C. T. Flexible Hybrid Sensors for Health Monitoring: Materials and Mechanisms to Render Wearability. Adv. Mater. *32*, 1–31 (2020).

6. Han, S. et al. Battery-free, wireless sensors for full-body pressure and temperature mapping. Sci. Transl. Med. 10, (2018).

7. Lim, H. R. et al. Advanced Soft Materials, Sensor Integrations, and Applications of Wearable Flexible Hybrid Electronics in Healthcare, Energy, and Environment. Adv. Mater. *32*, 1–43 (2020).

8. Mitsubayashi, K. & Arakawa, T. Cavitas Sensors: Contact Lens Type Sensors & Mouthguard Sensors. Electroanalysis *28*, 1170–1187 (2016).

9. Pankratov, D., González-Arribas, E., Blum, Z. & Shleev, S. Tear Based Bioelectronics. Electroanalysis 28, 1250–1266 (2016).

10. Tricoli, A., Nasiri, N. & De, S. Wearable and Miniaturized Sensor Technologies for Personalized and Preventive Medicine. Adv. Funct. Mater. 27, 1–19 (2017).

11. Heikenfeld, J. Non-invasive Analyte Access and Sensing through Eccrine Sweat: Challenges and Outlook circa 2016. Electroanalysis 28, 1242–1249 (2016).

12. Bariya, M., Nyein, H. Y. Y. & Javey, A. Wearable sweat sensors. Nat. Electron. 1, 160–171 (2018).

13. Choi, J., Ghaffari, R., Baker, L. B. & Rogers, J. A. Skin-interfaced systems for sweat collection and analytics. Sci. Adv. 4, 1–10 (2018).

14. Song, Y. et al. Wireless battery-free wearable sweat sensor powered by human motion. Sci. Adv. 6, 1–11 (2020).

15. Proksch, E. pH in nature, humans and skin. J. Dermatol. 45, 1044–1052 (2018).

16. Lambers, H., Piessens, S., Bloem, A., Pronk, H. & Finkel, P. Natural skin surface pH is on average below 5, which is beneficial for its resident flora. Int. J. Cosmet. Sci. 28, 359–370 (2006).

17. Kim, E. et al. The alkaline pH-adapted skin barrier is disrupted severely by SLS-induced irritation. Int. J. Cosmet. Sci. 31, 263–269 (2009).

18. Anastasova, S. et al. A wearable multisensing patch for continuous sweat monitoring. Biosens. Bioelectron. 93, 139–145 (2017).

19. Nyein, H. Y. Y. et al. A Wearable Microfluidic Sensing Patch for Dynamic Sweat Secretion Analysis. ACS Sensors 3, 944–952 (2018).

20. Dang, W. et al. Stretchable wireless system for sweat pH monitoring. Biosens. Bioelectron. 107, 192–202 (2018).

21. Nakata, S. et al. A wearable pH sensor with high sensitivity based on a flexible charge-coupled device. Nat. Electron. 1, 596–603 (2018).

22. Nyein, H. Y. Y. et al. A Wearable Electrochemical Platform for Noninvasive Simultaneous Monitoring of Ca2+ and pH. ACS Nano 10, 7216–7224 (2016).

23. Tessarolo, M., Gualandi, I. & Fraboni, B. Recent progress in wearable fully textile chemical sensors. Adv. Mater. Technol. 3, 1–7 (2018).

24. He, W. et al. Integrated textile sensor patch for real-time and multiplex sweat analysis. Sci. Adv. 5, 1–9 (2019).

25. Ferrari, L. M. et al. Ultraconformable Temporary Tattoo Electrodes for Electrophysiology. Adv. Sci. 5, 1–11 (2018).

26. Zucca, A. et al. Tattoo Conductive Polymer Nanosheets for Skin-Contact Applications. Adv. Healthc. Mater. 4, 983–990 (2015).

27. Ferrari, L. M., Keller, K., Burtscher, B. & Greco, F. Temporary tattoo as unconventional substrate for conformable and transferable electronics on skin and beyond. Multifunct. Mater. 3, (2020).

28. Bandodkar, A. J., Jia, W. & Wang, J. Tattoo-Based Wearable Electrochemical Devices: A Review. Electroanalysis 27, 562–572 (2015).

29. Bonacchini, G. E. et al. Tattoo-Paper Transfer as a Versatile Platform for All-Printed Organic Edible Electronics. Adv. Mater. 30, 1–8 (2018).

30. Sonner, Z. et al. The microfluidics of the eccrine sweat gland, including biomarker partitioning, transport, and biosensing implications. Biomicrofluidics 9, (2015).

31. Windmiller, J. R. et al. Electrochemical sensing based on printable temporary transfer tattoos. Chem. Commun. 48, 6794–6796 (2012).

32. Bandodkar, A. J. et al. Tattoo-based noninvasive glucose monitoring: A proof-of-concept study. Anal. Chem. 87, 394–398 (2015).

33. Kim, J. et al. Wearable temporary tattoo sensor for real-time trace metal monitoring in human sweat. Electrochem. commun. 51, 41–45 (2015).

34. Bandodkar, A. J. et al. Tattoo-based potentiometric ion-selective sensors for epidermal pH monitoring. Analyst 138, 123–128 (2013).

35. Kim, J. et al. Noninvasive Alcohol Monitoring Using a Wearable Tattoo-Based Iontophoretic-Biosensing System. ACS Sensors 1, 1011–1019 (2016).

36. Guinovart, T., Bandodkar, A. J., Windmiller, J. R., Andrade, F. J. & Wang, J. A potentiometric tattoo sensor for monitoring ammonium in sweat. Analyst 138, 7031–7038 (2013).

37. Rekhi, G. S. & Jambhekar, S. S. Ethylcellulose - a polymer review. Drug Dev. Ind. Pharm. 21, 61–77 (1995).

38. Alf, M. E. et al. Chemical vapor deposition of conformal, functional, and responsive polymer films. Adv. Mater. 22, 1993–2027 (2010).

39. Coclite, A. M. et al. 25th Anniversary Article: CVD polymers: A new paradigm for surface modification and device fabrication. Adv. Mater. 25, 5392–5423 (2013).

40. Tenhaeff, W. E. & Gleason, K. K. Initiated and oxidative chemical vapor deposition of polymeric thin films: ICVD and oCVD. Adv. Funct. Mater. 18, 979–992 (2008).

41. Lau, K. K. S. & Gleason, K. K. Initiated Chemical Vapor Deposition (iCVD) of poly(alkyl acrylates): An experimental study. Macromolecules 39, 3688–3694 (2006).

42. Lau, K. K. S. & Gleason, K. K. Initiated Chemical Vapor Deposition (iCVD) of poly(alkyl acrylates): A kinetic model. Macromolecules 39, 3695–3703 (2006).

43. Park, H. J. et al. Paper-based bioactive scaffolds for stem cell-mediated bone tissue engineering. Biomaterials 35, 9811–9823 (2014).

44. Lee, H. S., Kim, H., Lee, J. H. & Kwak, J. B. Fabrication of a conjugated fluoropolymer film using one-step iCVD process and its mechanical durability. Coatings 9, (2019).

45. Unger, K. & Coclite, A. M. Conformal coating of powder by initiated chemical vapor deposition on vibrating substrate. Pharmaceutics 12, 1–11 (2020).

46. Decandia, G. et al. Initiated chemical vapor deposition of crosslinked organic coatings for controlling gentamicin delivery. Pharmaceutics 12, (2020).

47. Krauter, M., Tazreiter, M., Perrotta, A. & Coclite, A. M. Deposition of Ion-Conductive Membranes from Ionic Liquids via Initiated Chemical Vapor Deposition. Macromolecules *53*, 7962–7969 (2020).

48. Karandikar, P. & Gupta, M. Fabrication of ionic liquid gel beads via sequential deposition. Thin Solid Films *635*, 17–22 (2017).

49. Coclite, A. M. Smart surfaces by initiated chemical vapor deposition. Surf. Innov. 1, 6–14 (2013).

50. Unger, K., Resel, R. & Coclite, A. M. Dynamic Studies on the Response to Humidity of Poly (2-hydroxyethyl methacrylate) Hydrogels Produced by Initiated Chemical Vapor Deposition. Macromol. Chem. Phys. 217, 2372–2379 (2016).

51. Buchberger, A., Peterka, S., Coclite, A. M. & Bergmann, A. Fast optical humidity sensor based on hydrogel thin film expansion for harsh environment. Sensors (Switzerland) 19, 1–11 (2019).

52. Werzer, O., Tumphart, S., Keimel, R., Christian, P. & Coclite, A. M. Drug release from thin films encapsulated by a temperature-responsive hydrogel. Soft Matter 15, 1853–1859 (2019).

53. Muralter, F., Perrotta, A. & Coclite, A. M. Thickness-Dependent Swelling Behavior of Vapor-Deposited Hydrogel Thin Films. Proceedings 2, 757 (2018).

54. Unger, K. et al. Novel Light-Responsive Biocompatible Hydrogels Produced by Initiated Chemical Vapor Deposition. ACS Appl. Mater. Interfaces 9, 17408–17416 (2017).

55. Petruczok, C. D., Armagan, E., Ince, G. O. & Gleason, K. K. Initiated chemical vapor deposition and light-responsive cross-linking of poly(vinyl cinnamate) thin films. Macromol. Rapid Commun. *35*, 1345–1350 (2014).

56. Sayin, S. et al. Electrospun Nanofibers With pH-Responsive Coatings for Control of Release Kinetics. Front. Bioeng. Biotechnol. 7, 1–12 (2019).

57. Tufani, A. & Ozaydin Ince, G. Smart membranes with pH-responsive control of macromolecule permeability. J. Memb. Sci. *537*, 255–262 (2017).

58. Lau, K. K. S. & Gleason, K. K. Initiated chemical vapor deposition (iCVD) of copolymer thin films. Thin Solid Films 516, 678–680 (2008).

59. Zhao, Y., Luo, Y. W., Li, B. G. & Zhu, S. PH responsivity and micelle formation of gradient copolymers of methacrylic acid and methyl methacrylate in aqueous solution. Langmuir 27, 11306–11315 (2011).

60. Ranacher, C. et al. Layered Nanostructures in Proton Conductive Polymers Obtained by Initiated Chemical Vapor Deposition. Macromolecules 48, 6177–6185 (2015).

Chapter V

Conclusions and Outlook

In this thesis, humidity, light and pH responsive hydrogels were polymerized via initiated chemical vapor deposition (iCVD) and investigated.

The first presented work, named "Dynamic Studies on the Response to Humidity of Poly (2-hydroxyethyl methacrylate) Hydrogels Produced by Initiated Chemical Vapor Deposition", focuses on the fundamental understanding of the swelling behavior of smart hydrogels upon exposure to humidity and water and how it can be controlled during the synthesize process of initiated chemical vapor deposition (iCVD). Each smart hydrogel consists of functional groups, that react towards a certain stimulus, and cross-linking agents that prevent dissolution (in tradeoff cause less swelling). The ratio of incorporated cross-linker was successfully tuned in the copolymer of 2-hydroxyethyl methacrylate and the cross-linker ethylene glycol-dimethacrylate p(HEMA-co-EGDMA) by varying the monomer vapor flow rates during the process verified by infrared spectroscopy demonstrating the controllability of copolymer composition during the iCVD process. While no hydrogel dissolved in relative humidity up to 84 ± 2%, only samples of more than 25% incorporated EGDMA were stable in water. Pure pHEMA in humidity swelled up to 30%. The higher the EGDMA ration within the copolymer, the less swelling was observed. The calculation of the Flory interaction parameter χ versus the relative humidity, describing the intermixing of water vapor and the hydrogel, revealed the smart responsive behavior of the hydrogel upon exposure to humidity in a sigmoidal function. While below 75% relative humidity, χ decreases from 2.8 to 1.1 and converges then to 1.

This valuable insight about the iCVD deposited hydrogel p(HEMA-co-EGDMA) was the starting point for the next work, with the title "Novel light-responsive biocompatible hydrogels produced by initiated chemical vapor deposition", where this copolymer was further functionalized with azobenzene moieties to obtain a light responsive hydrogel. For that purpose, during the iCVD process pentafluorophenyl (PFPA) monomers were additionally flown into the chamber to create a top-coat. The latter, upon postdeposition, reacts with amino groups to integrate azobenzene into the hydrogel surface. Upon exposure to UV light hydrogels exhibit higher and faster swelling caused by the photoisomerization of azobenzene from an unpolar trans-isomer to a polar cis-configuration with an increased dipole moment which was demonstrated in water and humid environment. The reversible photoisomerization and swelling via visible green

light was shown during cycled light and humidity exposure. The demonstration of the hydrogel to also be applicable as cell cultivation platform opens up the new field of light-controlled cell growth or cell determination.

An emerging field of applications of smart hydrogels produced via iCVD is drug delivery systems. A responsive coating of pharmaceutics, that dissolve only in a certain environment, is an exceptional structure to release drugs only at the needed spot within the body and therefore minimize the overall dosage. The dry and conformal process of iCVD seems to be a promising technique to coat also drugs but so far, iCVD is rarely used towards pharmaceutical powder because of the compromised gas-solid contact. In the work "Conformal Coating of Powder by Initiated Chemical Vapor Deposition on Vibrating Substrate", an iCVD reactor was adapted with speakers to vibrate the samples to AC/DC's song "Thunderstruck", which demonstrated a conformal coating of certain powders with particles >100 µm and a good flowability.

Again, the decisive possibility of iCVD, to coat delicate substrates, was used during a fabrication of a pH skin sensor tattoo. On a temporary tattoo paper PEDOT:PSS electrodes were screen printed and further deposited with a smart hydrogel of methacrylic acid cross linked with di(ethylene glycol) divinyl ether. The pH responsive behavior was measured by means of swelling and dielectric properties in artificial sweat of different pH levels, via spectroscopic ellipsometry and electrochemical impedance spectroscopy. At a frequency of 1000 Hz the created tattoo sensor shows a distinct phase shift depending on the pH value. This phase shift was so significant, that measurements were possible in a self-made microcontroller setup without the need of sophisticated lab equipment.

The explored spectrum in this thesis ranges from the fundamental understanding of the smart hydrogels' response to a stimulus, to application-oriented responsive hydrogel platforms and ending with an implementation of a smart hydrogel in a novel bio-sensor device.

The prosperous outlook of iCVD synthesized smart hydrogels is based on the unique properties of a dry, conformal and controllable delivery method that is applicable to delicate and structured substrates. Especially the shown work emphasizes the possible applications in the field of stimuli-controlled cell-cultivation, responsive drug encapsulation and bio-sensors.

A Appendix

This section provides further documents and information about the author of this thesis. In the following, a list of scientific contributions, an accepted project proposal and a publication of which the author of this thesis is co-author, will be presented.

AI Scientific Contributions

AI.1 Publications

i. Unger, K. & Coclite, A. M. Conformal coating of powder by initiated chemical vapor deposition on vibrating substrate. Pharmaceutics 12, 1–11 (2020).

ii. Decandia, G. et al. Initiated Chemical Vapor Deposition of Crosslinked Organic Coatings for Controlling Gentamicin Delivery. Pharmaceutics 12, 213 (2020).

iii. Unger, K. et al. Novel Light-Responsive Biocompatible Hydrogels Produced by Initiated Chemical Vapor Deposition. ACS Appl. Mater. Interfaces 9, 17408–17416 (2017).

iv. Unger, K., Resel, R. & Coclite, A. M. Dynamic Studies on the Response to Humidity of Poly (2-hydroxyethyl methacrylate) Hydrogels Produced by Initiated Chemical Vapor Deposition. Macromol. Chem. Phys. 217, 2372–2379 (2016).

v. Unger, K. et al. Distributed Bragg reflectors: Morphology of cellulose acetate and polystyrene multilayers. in International Conference on Transparent Optical Networks (IEEE Computer Society, 2014). doi:10.1109/ICTON.2014.6876716.

vi. Oberdorfer, B. et al. Absolute concentration of free volume-type defects in ultrafine-grained Fe prepared by high-pressure torsion. Scr. Mater. 63, 452–455 (2010).

AI.2 Oral Presentations

i. pH Sensor Tattoo. NAWI Graz Scientific Advisory Board Meeting, 2020, Graz, Austria
ii. Stimuli Responsive Hydrogels via initiated Chemical Vapor Deposition. NAWI Physics Doctoral Seminar, 2020, Graz, Austria
iii. Multi-Stimuli Responsive Polymer Gels via initiated Chemical Vapor Deposition. International Conference on Processing and Manufacturing of Advanced Materials - THERMEC'2016, 2016, Graz, Austria
iv. Initiated Chemical Vapor Deposition of thin film functional polymers. Functional Integrated nanoSystems – nanoFIS, 2014, Graz, Austria
v. Distributed Bragg Reflectors: Morphology of Cellulose Acetate and Polystyrene Multilayers. International Conference on Transparent Optical Networks, 2014, Graz, Austria

AI.3 Poster Presentations

i. pH Sensor Tattoo. Advanced Materials Day, 2020, Graz Austria
ii. Multi-Stimuli Responsive Polymer Gels via initiated Chemical Vapor Deposition. International Conference on Processing and Manufacturing of Advanced Materials - THERMEC'2016, 2016, Graz, Austria
iii. Hydrogels produced with Initiated Chemical Vapor Deposition. Advanced Materials Day, 2015, Graz Austria
iv. Light responsive hydrogels produced with initiated chemical vapor deposition. Advanced Materials World Congress, 2015, Stockholm, Sweden
v. Hydrogels produced with initiated chemical vapor deposition. European Conference on Organized Films, 2014, Genua, Italy
vi. Structural Analysis of Proton Conductive Polymers by initiated Chemical Vapor Deposition, Solvay Workshop, 2014, Brussels, Belgium
vii. Three S: Smart Multi Stimuli-responsive Supports for Controlled Cell Growth, Advanced Materials Day, 2014, Graz, Austria

AII All-polymer tattoo pH sensors - Women In Science Project Proposal

AII.1 Preface

The author of this thesis submitted a project proposal to the Women in Science National fellowship program and got accepted, which will be presented in the following section. The text and illustrations are identical to the submitted version.

AII.2 Abstract

The design of a flexible pH sweat sensor that is bio-compatible, has skin-alike elasticity and is sustainable in acidic environments is a challenging task. Current trends in research tend to an organic compound consisting pH sensor for medical diagnostic applications. But so fare the manufacturing process of such sensors is not feasible nor scalable. In this proposal a novel all-polymer sensor approach will be presented that address all the challenges mentioned above and use a manufacturing process that is direct and scalable. Polymer electrodes will be ink-jet printed on temporary tattoo paper and coated with a bio-compatible pH responsive hydrogel via initiated Chemical Vapor Deposition. Such pH responsive hydrogels absorb different amounts of water depending on the pH. Upon swelling of the gel film the conductivity will increase and the resistance will decrease. The pH can therefore be detected by means of resistance measurements through impedance spectroscopy. Hydrogel-based pH sensors have a remarkable great sensitivity to pH. The use of temporary tattoo paper as substrate material will have two major advantages. One being the fact that tattoo transferred hydrogels will be in intimate contact with the skin leading to more precise and faster detection of the pH of the skin. The other being that the printed polymer electrodes can directly act as read out terminals for the hydrogels response. For the first time tattoo electrodes will be coated with a responsive material via a vapor-based technique. This novel combination enables for a very thin sensor, excellent conformal adhesion to the skin and great pH sensitivity. All through the use of direct and scalable methods, which in combination open the door for a wide range of possible interesting applications.

AII.3 Introduction

Body fluids such as sweat, saliva or tears contain various chemical substances that provide information about the state of health. Sweat is of particular interest as its composition is directly related to that of blood.[1] Sweat is a complex mixture of several ion species, ammonium, glucose

and lactate among others and therefore provides rich source of readily available information about our health.[2] The pH level of eccrine sweat is slightly acid with a pH in the range of 4.5 to 7 forming the so-called acid mantel of the skin.[3] This mantel is a natural barrier for bacteria or virus infections and other contaminants that might penetrate the skin. With the acid skin in combination with the alkaline blood our body is equipped with a great defense against bacteria pathogens. Different exogenous (skin diseases, hormones, ...) or endogenous (alkaline cosmetics, drugs, ...) factors have influences on the pH level of the skin.[4] A disrupted pH-level leads to a dehydrated, broken and vulnerable skin. Wearable flexible devices for electrophysiological measurements have become of major interest in health care diagnostics because of their non-invasive way of permanent monitoring the patient. pH-sensors were already successfully implemented in badges, wrists or temporary tattoos.[2] The goal of this project is to develop a highly flexible and easily applicable pH skin sensor by using a temporary tattoo as sensor carrier. As sensing media for the first time a pH responsive hydrogel will be used in a tattoo sensor, which will change its electrical properties among pH.

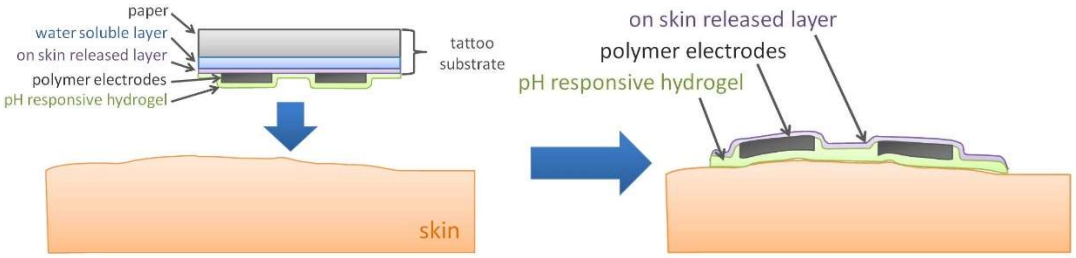

Figure 1: Left: cross-section of the tattoo pH sensor before the application. The tattoo substrate consists of a paper, a water-soluble layer and a layer that will be released onto the skin. The polymer electrodes will be coated with a pH responsive hydrogel. Right: after wetting, the sub-micrometer thick layer, the electrodes and the hydrogel is released conformal and adhesive onto the skin.

A temporary tattoo is based on screen-printing of functional inks on a sacrificial paper. When the tattoo is applied on the target skin, water is used to dissolve the sacrificial layer and the ink as well as a submicrometer-thick film is released onto the skin surface conformal and adhesive (see figure 1). Which is favorable as, among others, irregular or very low sample production (1 nL/min/mm2) is one challenge when measuring sweat directly on the skin and a well connected sensor minimize the dead volume in between the sensor and the skin.[5] The group of Greco et al., showed that tattoo electrodes have a skin contact impedance comparable to standard pre-gelled and dry body electrodes in short (1 h) and long-term (48 h) studies.[6] With a thickness down to even 1 µm and their flexible nature they show a conformal adhesion to the skin. Even hair can grow through without loose of contact. Therefore tattoo sensors are suitable for

different electrophysiological measurements. A typical tool to electrochemically measure the pH level is a glass-electrode. When two liquids of different pH levels are brought into contact on opposite sides of a thin glass membrane a electrical potential can be measured. However, a glass-electrode can not be miniaturized into a wearable device. Therefore in the last few decades new approaches were developed based on ion-sensitive electrodes and their change of potential, current or impedance depending on pH. State-of-the-art sensor types include potentiometric sensor, ion-sensitive field-effect transistor, chemoresistor, and electrolyte-gated field effect transistors.[3] Such sensors are primarily made of inorganic materials, including metals (e.g., Pd, Bi, Sb, Ag), metal oxides (e.g., TiO2, ZnO, ...), and others. These materials suffer from reduction of the electrodes in alkaline or acidic media. Further such sensor techniques are often not bendable and can not be conformally applied on the skin. Thin polymer films with different material properties (conducting, semi-conducting, isolating) were already synthesized which sustain alkaline or acidic conditions[7] and are highly flexible and therefore show a great potential to overcome the mentioned above problems. Nevertheless either the electrodes or the sensing part of the sensor remained an inorganic materials or rigid components so far. Typical organic pH sensing media are polypyrrole, polyaniline, and polythiophene[8] or pH responsive hydrogels. Because of bio-compatibility and sustainability in alkaline or acid media polyanilin was already used in pH skin sensors successfully by the group of Wang.[9] Nevertheless the electrochemical deposition technique for polypyrrole, polyaniline, and polythiophene requires toxic solutions[10] therefore can not be deposited directly on a tattoo sheet as the paper would either swell or dissolve. A direct deposition technique is favorable in terms of feasible and scalable manufacturing process. pH responsive hydrogels are polymer networks that reversible change the absorbed water depending on the pH level. Such hydrogels comprise weak acidic or weak basic functional groups which can be ionized depending on the pH and the ionic strength of the solution media. The swelling versus the pH shows a first or second order phase transition with a material characteristic apparent dissociation constant (pKa). At pH above pKa the acid units depronate and repel each other resulting in swelling of the network structure which is therefore conductive. While at pH below pKa the acid units can form strong hydrogen bonds with each other and the polymer chain collapses and is a resistor. At the phase transition hydrogel-based pH sensors show an extraordinary sensitivity in the order of up to 10^{-5} pH units.[7] Their working range of sensors spans are up to three pH units. A typical read-out strategy for hydrogel-based pH sensors is impedance measurements.[11] At frequencies from 100 Hz to 100 kHz the period is much greater than the dielectric relaxation time of the considered materials.[12] Therefore the electrode impedance is primarily resistive. With a swelling of gel film the conductivity will increase which

is accompanied by a decrease of the resistance. Impedance measurements are suitable for bio-analysis of human body.[13]

Poly-methacrylic acid (pMAA) is a widely used bio-compatible pH responsive polymer (e.g. stimuli drug release platform.[14] It has an apparent dissociation constant of pKa ≈ 4.8 which suits the pH range of sweat (4.5 to 7) perfectly. A technique to synthesize pMAA films is initiated Chemical Vapor Deposition (iCVD).[15] iCVD is a dry and scalable technique that can directly polymerize thin and conformal coatings with high retention of functional groups on all kind of substrates.[16,17] iCVD was already used to deposit different stimuli-responsive coatings (against: humidity,[18] light,[19] temperature,[20] ...).

The vision of this project is to design an all-polymer, highly exible, and sustainable tattoo hydrogel-based pH skin sensor. A temporary tattoo will be ink-jet printed with polymer electrodes and further deposited with pMAA with iCVD. A pH tattoo skin sensor single made of polymers with a feasable direct process technique is likely to overcome the problems of skin alike mechanical properties, sustainability and scalable manufacturing nowadays pH skin sensors need to face.

AII.4 Research methodology and approach

Objective 1: Synthesis of ph responsive and stable pMAA hydrogel film.

In a first investigation, the hydrogels will be deposited on silicon wafers to study their response and morphology. iCVD will be used as a deposition method. In this technique free-radicals are formed by thermal decomposition of a initiator molecule. The initiator and monomer units enter the iCVD reactor as vapors. The labile bonds present in the initiator (e.g., the O-O bond in tert-butyl peroxide) decomposed by interacting with a relatively hot filament (150 °C - 300 °C)(see figure 2). The functional groups in the monomer decompose typically at temperatures higher than 500 °C, therefore fully retain its structure.[21,22] Hydrogels, such as pMAA typically need a cross-linker (e.g. ethylene glycol dimethylacrylate) to save it from dissolving. A good iCVD deposition recipe needs to be found to obtain stable but responsive polymer films. Parameters like the ow rate (0.01 sccm to 0.2 sccm) of cross-linker, the chamber pressure (200mTorr to 500mTorr) or the substrate temperature (20 °C to 50 °C) will be varied to gain di_erent polymer-network variations of pMAA. The iCVD-reactor will be a custom build chamber which has already been used in several projects for deposition of stimuli responsive polymers[18,20,23] (see figure 2). The samples will be further characterized in terms of chemical composition and functional group retention with Fourier transform infrared spectroscopy (Bruker IFS 66v/S). A software, developed within our research group (already published [24]), will be used to analyze the

spectra and extract the cross-linker fraction of the polymer. Swelling experiments will be performed with spectroscopic ellipsometry (J.A.Woollam ESF-300, shown in figure 3). A liquid cell will be used to hold the liquids in a tight seal above the thin hydrogel films. The pMAA swelling response will be measured in different pH levels and salt solutions which contain alkali metal and alkaline earth metal ions in the biological signiffcant range of sweat (which is: Na^+ with 10-100mM, Cl^- with 10-100mM, K^+ with 1-18.5mM, Ca^{2+} with 0.41-12.4mM and Na^{44+} with 0.1-1mM [3]), similar as it was already performed in other studies.[25–27] Additionally the swelling in artificial sweat will be tested. Artificial sweat is a developed solution that mimics true human eccrine sweat with different pH levels (2-9) and which is used in research especially in the field of body sensors.[28] The first project milestone will be reached, when stable and responsive polymer films were deposited and characterized.

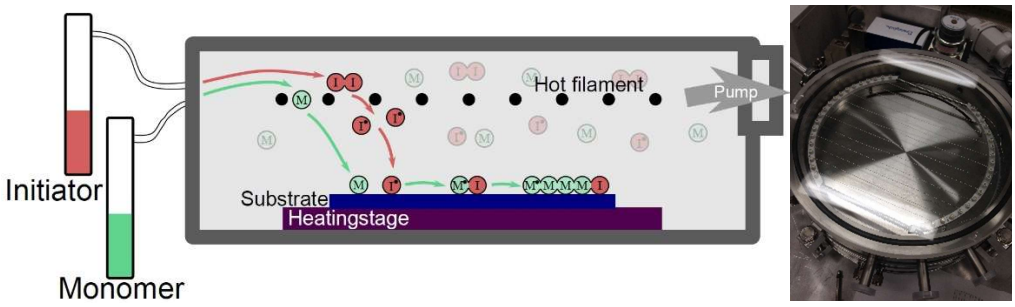

Figure 2: Left: schematic of an iCVD process. The initiator and monomer enter the chamber as vapors. Only the initiator decomposes and starts the free radical polymerization at the substrate surface. Right: foto of an iCVD reactor seen from above.

Figure 3: Ellipsometer (J.A. Woollam ESF-300) with liquid cell.

Objective 2: Implementation of the hydrogel on temporary tattoo paper containing the electrodes and device testing.

Commercially available temporary transfer tattoo paper kit (Tattoo 2.1, by The Magic Touch Ltd., UK) will be used as a substrate.[6] The tattoo paper consists of three layers, a paper, a starch- dextrin coating (water-soluble layer), and a ethylcellulose layer. When the tattoo is applied on the skin and wet the starch-dextrin dissolves and the submicrometer-thick ethylcellulose film is released onto the skin surface. Ink-jet printing will be used to deposit conductive polymer electrodes made of poly(3,4-ethylenedioxythiophene):polystyrene sulfonate (PEDOT:PSS) on the tattoo. The ink-jet printer of this project is a Fujifilm Dimatix DMP 2850 (figure 5) and is capable to print materials like conducting polymers, graphene, metal nanoparticles, organic semiconductors or dielectrics on glas, paper, plastics or metal sheets with a resolution down to 20 µm. PEDOT:PSS is a conductive and bio-compatible polymer which is extensively used as it is readily available as a waterborne dispersion for ink-jet printing.[28,29] A particular care will be devoted to optimizing a suitable electrode design for sensing purposes. Hydrogel-based pH sensors with 2 electrodes for electronic impedance measurements were already produced.[12] An electrode array, as depicted in figure 4 on the left side, has the benefit of high accuracy due to the array geometry. Additional a 4-point electrode setup will be tested where a current is applied at the outer electrodes and the voltage is measured between the inner electrodes. Voltage measurements are high-impedance measurements and therefor the spreading resistance effects (contact-resistance between hydrogel and the electrodes) are not dominant. As iCVD forms conformal and adhesive films the contact resistance directly between the hydrogel and the electrodes after the deposition can be assumed as negligible. However during cycles of swelling hydrogels tend to slightly delaminate maybe resulting in a contact resistance which would influence the impedance signal of a 2-point electrode setup.[30] Generally spoken a 2-point setup can be used when measuring high resistive media and a 4-point setup should be used when testing a low resistive media where the contact resistivity is of the same order as the resistivity of the media. The pH responsive hydrogel swelling is not only depending on the pH but as well on the amount of sweat present on the skin. To address this problem a second, not pH responsive measurement (bare tattoo electrodes) as reference is mandatory.

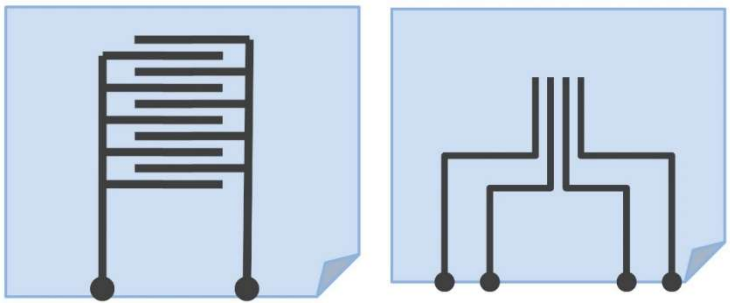

Figure 4: Schematic of a 2-point and 4-point measuring electrodes setup.

pMAA films will be deposited on the tattoo electrodes with the optimized deposition conditions. After the deposition the hydrogel coated tattoo will be tested in terms of retention of shape and applicability. The adhesion of the hydrogel and the electrodes before and after the hydrogel swelling will be determined with atomic force microscopy (Nanosurf Easyscan 2). In the frequency range of 100 Hz to 100 kHz electronic impedance measurements (Gamry Reference 600) will be performed by use of the same solution as already used in the swelling experiments. This enables to link the swelling and the impedance response of pMAA. Further electronic impedance measurements in larger time scales (24 h) in artificial sweat will be performed to characterize the sustainability of the sensor. The sensors durability versus strain will be tested with a custom build motorized stretch device. Finally the sensor will be applied on a skin-phantom, calibrated and tested versus other skin pH meter. Suitable phantoms could be, e.g. agarose gel slab swollen with artificial sweat (controlled composition, various pH) and electrolytes to mimic the typical nominal impedance of skin. Such phantom are a suitable test-bench before to go on human subjects in a later step. The second and last milestone is reached when a flexible and sustainable tattoo pH skin sensor is accomplished.

Figure 5: Left: Ink-jet printer (Fujifilm Dimatix DMP 2850). Right: printed tattoo electrodes (©Lunghammer - TU Graz).

AII.5 Innovative nature of the project and research questions

For the first time:

- a vapor based technique will be used to deposit a smart material on a tattoo sheet. This novel combination of tattoo-electrodes and iCVD-smart-polymers could open the door for a multitude of possible interesting applications.
  Research objective: How will the morphology and the adhesion of an iCVD coated film on tattoo electrodes look like?
- an all-polymer tattoo pH sensor will be produced. Neither the electrodes nor the sensing part will contain metal or metal-oxides and fully will be made of polymers. The deposition techniques are feasible and scalable.
  Research objectives: Will the polymer-based sensor be comparable to standard-sensors in terms of sensitivity? How is the sustainability of the polymer layers in acid and alkaline media present in sweat? How is the durability of the sensor versus cycled strain comparable to skin-movements?
- a hydrogel-based pH skin sensor will be elaborated. Although hydrogels are not ion-selective, they show excellent sustainability and mechanical properties for bio-senors.
  Research objective: How will the hydrogel react on cycled wetting and drying? How fast is the hydrogel response-time?
- pMAA response measurements against different salt solutions will be performed. pMAA is often used in drug delivery systems. The pMAA acts as a host for small-drug molecules which get released at a certain pH level because of dissolution of pMAA. However, the response against ions needs to be elaborated as body fluids always contain ions.
  Research objective: How much is the inuence of ions in concentrations similar to sweat on the swelling and electrical response of pMAA? Will the swelling and the electrical response be linked?

AII.6 Persons involved

During her PhD the applicant, Katrin Unger, has gained substantial experience in the field of stimuli responsive polymers and iCVD. She has worked successfully with plenty of different monomers, substrates and stimuli resulting in three first author papers. Her PhD adviser Anna Maria Coclite is an expert in the field of smart polymers[18,19,31] and chemical vapor deposition techniques[16] and current ERC grant winner. She will be additionally supported by Francesco Greco, who is highly experienced in tattoo electronics.[6,28]

AII.7 Work plans

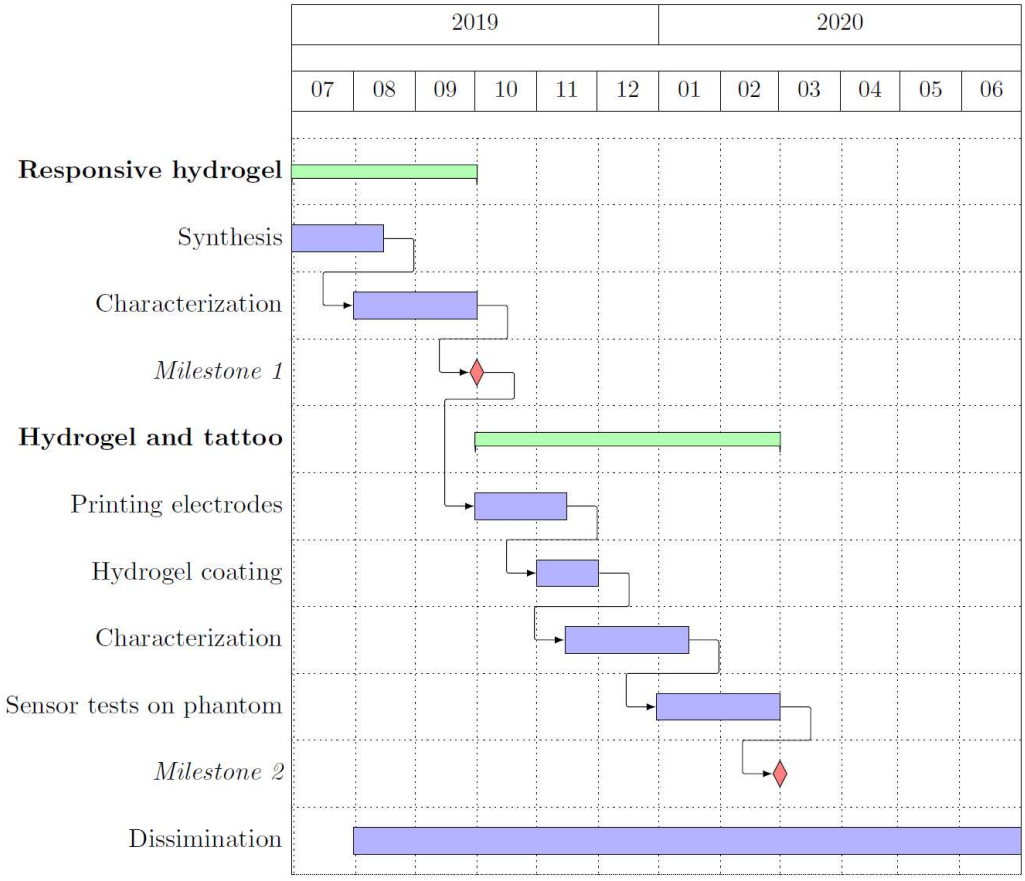

AII.8 References

1. Sonner, Z. *et al.* The microfluidics of the eccrine sweat gland, including biomarker partitioning, transport, and biosensing implications. *Biomicrofluidics* **9**, (2015).

2. Heikenfeld, J. Non-invasive Analyte Access and Sensing through Eccrine Sweat: Challenges and Outlook circa 2016. *Electroanalysis* **28**, 1242–1249 (2016).

3. Bariya, M., Nyein, H. Y. Y. & Javey, A. Wearable sweat sensors. *Nat. Electron.* **1**, 160–171 (2018).

4. Ali, S. M. & Yosipovitch, G. Skin pH: From basic science to basic skin care. *Acta Derm. Venereol.* **93**, 261–267 (2013).

5. Bandodkar, A. J., Jia, W. & Wang, J. Tattoo-Based Wearable Electrochemical Devices: A Review. *Electroanalysis* **27**, 562–572 (2015).

6. Ferrari, L. M. *et al.* Ultraconformable Temporary Tattoo Electrodes for Electrophysiology. *Adv. Sci.* **5**, 1–11 (2018).

7. Richter, A. *et al.* Review on Hydrogel-based pH Sensors and Microsensors. *Sensors* **8**, 561–581 (2008).

8. Yuqing, M., Jianrong, C. & Keming, F. New technology for the detection of pH. *J. Biochem. Biophys. Methods* **63**, 1–9 (2005).

9. Bandodkar, A. J. *et al.* Tattoo-based potentiometric ion-selective sensors for epidermal pH monitoring. *Analyst* **138**, 123–128 (2013).

10. Cosnier, S. Biosensors based on electropolymerized films: New trends. *Anal. Bioanal. Chem.* **377**, 507–520 (2003).

11. Mir, M. *et al.* Aqua-gel pH sensor: intelligent engineering and evaluation of pH sensor based on multi-factorial testing regimes. *Sens. Rev.* **39**, 178–189 (2019).

12. Sheppard, N. F., Tucker, R. C. & Salehi-Had, S. Design of a conductimetric pH microsensor based on reversibly swelling hydrogels. *Sensors Actuators B. Chem.* **10**, 73–77 (1993).

13. Lisdat, F. & Schäfer, D. The use of electrochemical impedance spectroscopy for biosensing. *Anal. Bioanal. Chem.* **391**, 1555–1567 (2008).

14. Qiu, Y. & Park, K. Environment-sensitive hydrogels for drug delivery. *Advanced Drug Delivery Reviews* vol. 53 321–339 (2001).

15. Lau, K. K. S. & Gleason, K. K. Particle surface design using an all-dry encapsulation method. *Adv. Mater.* **18**, 1972–1977 (2006).

16. Coclite, A. M. *et al.* 25th Anniversary Article: CVD polymers: A new paradigm for surface modification and device fabrication. *Adv. Mater.* **25**, 5392–5423 (2013).

17. Gupta, M. & Gleason, K. K. Large-scale initiated chemical vapor deposition of poly(glycidyl methacrylate) thin films. *Thin Solid Films* **515**, 1579–1584 (2006).

18. Muralter, F., Perrotta, A. & Coclite, A. M. Thickness-Dependent Swelling Behavior of Vapor-Deposited Smart Polymer Thin Films. *Macromolecules* **51**, 9692–9699 (2018).

19. Unger, K. *et al.* Novel Light-Responsive Biocompatible Hydrogels Produced by Initiated Chemical Vapor Deposition. *ACS Appl. Mater. Interfaces* **9**, 17408–17416 (2017).

20. Werzer, O., Tumphart, S., Keimel, R., Christian, P. & Coclite, A. M. Drug release from thin films encapsulated by a temperature-responsive hydrogel. *Soft Matter* **15**, 1853–1859 (2019).

21. Lau, K. K. S. & Gleason, K. K. Initiated Chemical Vapor Deposition (iCVD) of poly(alkyl acrylates): A kinetic model. *Macromolecules* **39**, 3695–3703 (2006).

22. Reeja-Jayan, B. *et al.* A Route Towards Sustainability Through Engineered Polymeric Interfaces. *Adv. Mater. Interfaces* **1**, 1–30 (2014).

23. Unger, K., Resel, R. & Coclite, A. M. Dynamic Studies on the Response to Humidity of Poly (2-hydroxyethyl methacrylate) Hydrogels Produced by Initiated Chemical Vapor Deposition. *Macromol. Chem. Phys.* **217**, 2372–2379 (2016).

24. Tazreiter, M., Christian, P., Schennach, R., Grießer, T. & Coclite, A. M. Simple method for the quantitative analysis of thin copolymer films on substrates by infrared spectroscopy using direct calibration. *Anal. Methods* **9**, 5266–5273 (2017).

25. Zhao, B. & Moore, J. S. Fast pH- and ionic strength-responsive hydrogels in microchannels. *Langmuir* **17**, 4758–4763 (2001).

26. Khare, A. R. & Peppas, N. A. Swelling/deswelling of anionic copolymer gels. *Biomaterials* **16**, 559–567 (1995).

27. Horkay, F., Tasaki, I. & Basser, P. J. Osmotic swelling of polyacrylate hydrogels in physiological salt solutions. *Biomacromolecules* **1**, 84–90 (2000).

28. Zucca, A. *et al.* Tattoo Conductive Polymer Nanosheets for Skin-Contact Applications. *Adv. Healthc. Mater.* **4**, 983–990 (2015).

29. Eom, S. H. *et al.* Polymer solar cells based on inkjet-printed PEDOT:PSS layer. *Org. Electron.* **10**, 536–542 (2009).

30. Hwang, J.-H., Kirkpatrick, K. S., Mason, T. O. & Garboczi, E. J. Experimental limitations in impedance spectroscopy: Part IV. Electrode contact effects. *Solid State Ionics* **98**, 93–104 (1997).

31. Pilz, J. *et al.* Tuning of material properties of ZnO thin films grown by plasma-enhanced atomic layer deposition at room temperature. *J. Vac. Sci. Technol. A Vacuum, Surfaces, Film.* **36**, 01A109 (2018).

AIII Initiated Chemical Vapor Deposition of Crosslinked Organic Coatings for Controlling Gentamicin Delivery

Initiated Chemical Vapor Deposition of Crosslinked Organic Coatings for Controlling Gentamicin Delivery

by Gianfranco Decandia [1], Fabio Palumbo [2,*], Annalisa Treglia [1], Vincenza Armenise [1], Pietro Favia [1,2], Federico Baruzzi [3], Katrin Unger [4], Alberto Perrotta [4] and Anna Maria Coclite [4]

[1] Department of Chemistry, University of Bari Aldo Moro, Via Orabona 4, 70126 Bari, Italy

[2] Institute of Nanotechnology, National Research Council of Italy, c/o Department of Chemistry, University of Bari Aldo Moro, Via Orabona 4, 70126 Bari, Italy

[3] Institute of Sciences of Food Production, National Research Council of Italy, Via G. Amendola 122/O, 70126 Bari, Italy

[4] Institute of Solid State Physics, NAWI Graz, Graz University of Technology, Petersgasse 16, 8010 Graz, Austria

* Author to whom correspondence should be addressed.

Pharmaceutics **2020**, *12*(3), 213; https://doi.org/10.3390/pharmaceutics12030213

Received: 8 January 2020 / Revised: 22 February 2020 / Accepted: 25 February 2020 / Published: 1 March 2020

(This article belongs to the Special Issue Coating Design: From Nanoparticle to Solid Dosage)

Reference: Decandia, Gianfranco; Palumbo, Fabio; Treglia, Annalisa; Armenise, Vincenza; Favia, Pietro; Baruzzi, Federico; Unger, Katrin; Perrotta, Alberto; Coclite, Anna M. 2020. "Initiated Chemical Vapor Deposition of Crosslinked Organic Coatings for Controlling Gentamicin Delivery" Pharmaceutics 12, no. 3: 213.

AIII.1 Preface

This report was conducted at the University of Bari in collaboration with the Graz University of Technology. The thesis' author introduced the first author of this paper, Gianfranco Decandia, to initiated chemical vapor deposition, and the characterization methods of the polymer films. The presented contribution is reproduced identical in text and illustration with permission from the publisher.

AIII.2 Abstract

A coating consisting of a copolymer of methacrylic acid and ethylene glycol dimethacrylate was deposited over a gentamicin film by initiated chemical vapor deposition with the aim of controlling the drug release. Gentamicin release in water was monitored by means of conductance measurements and of UV-vis Fluorescence Spectroscopy. The influence of the polymer chemical composition, specifically of its crosslinking density, has been investigated as a tool to control the swelling behavior of the initiated chemical vapor deposition (iCVD) coating in water, and therefore its ability to release the drug. Agar diffusion test and microbroth dilution assays against Staphylococcus aureus and Pseudomonas aeruginosa on cellulose coated substrates confirmed that the antibacterial activity of the drug released by the coating was retained, though the release of gentamicin was not complete.

Keywords: initiated chemical vapour deposition; drug delivery; poly(methyl methacrylate) (PMMA) copolymer; antibacterial test

AIII.3 Introduction

Gentamicin is a broad-spectrum aminoglycoside antibiotic produced from *Micromonospora purpurea* and active against a wide range of gram-positive and gram-negative bacteria [1]. It is a mixture of four major congeners designated as C_1, C_2, C_{1a} and C_{2a}, differing in their degree of methylation on the purpurosamine ring [2]. Gentamicin binds irreversibly to the bacterial 30S ribosomal subunit, causing misreading of t-RNA, leaving the bacterium unable to synthesize proteins vital to its growth [3]. The effectiveness of its antibacterial activity is however undermined by its high water solubility, which hinders the penetration to cells and in turn to the treatment of intracellular bacterial infections. Therefore, several studies are nowadays devoted to the development of controlled delivery systems that would target the bioactive agents to the site of infection and maintain a high local concentration without producing adverse systemic effects due to prolonged exposure to the antibiotic.

Drug delivery systems are engineered technologies for the controlled release or targeted delivery of therapeutic agents from a variety of polymeric and inorganic vehicles. Several synthetic approaches based on immobilization or *in situ* release of bactericidal substances such as antibiotics and metal derivatives have been extensively explored to produce antibacterial layers [4–7]. *In situ* delivery of antimicrobials can be achieved embedding polymeric matrices with the active compounds; matrices thus act as barriers limiting their diffusion in the surrounding medium. The release kinetic can be controlled by properly choosing the characteristics of the

polymeric interlayer: normally a hydrophilic behavior of the coating can speed the release rate up, letting water penetrate easily in the polymeric network of the film and favoring the active additive leakage [8].

A fine level of control on drug release kinetics can be acquired when hydrogel coatings are employed (for example, from poly(ethylene glycol) di-acrylate and its co-polymers): hydrogels, in fact, can swell when in contact with an aqueous environment because of massive water absorption. This makes polymeric network looser and creates larger paths for the active compound diffusion [9–11]. In addition, it is also possible to synthesize stimuli-responsive hydrogels, which are able to release drug upon a specific stimulus, such as changes in pH or temperature [12–16]. Poly(methacrylic acid) (PMAA) nanogels exhibit a sharp volume phase change upon increasing pH: in acidic conditions, the carboxylic groups are not ionized, and the PMAA nanogels are in a collapsed state, whereas at higher pH values, the coulombic repulsions between the deprotonated carboxylic groups induce the swelling of the nanogels [12]. These systems are helpful to protect sensitive drugs from the acidic environment of the stomach or in cases where a specific release in the gastrointestinal tract is required.

Stimuli-responsive hydrogels can be successfully deposited by initiated Chemical Vapor Deposition (iCVD): a low-energy, one step, film forming process that can be advantageously used to embed a bio-active molecule in a polymer encapsulant layer. This technique allows for solvent-free processing under mild conditions, thus minimizing a potential impact on the integrity of the active compound, and retention of the monomer structure in the encapsulating coating [17,18].

Some examples of drug delivery systems based on iCVD are present in literature. Ibuprofen [19] and campothecin [20] were encapsulated within a crosslinked PMAA thin film deposited by means of iCVD. In both cases, the drug release was pH dependent: at low pH the cross-linked film acted as diffusion barrier, while at neutral pH the film allowed the free diffusion of the drug out of the encapsulant. The crosslinker density in the polymer coating allows to tune the release kinetics of several orders of magnitude, from hours to days [21]. In another study, McInnes *et al* [22] reported the deposition by iCVD of a temperature-responsive polymeric coating of poly(N-isopropylacrylamide-co-diethylene glycol divinyl ether) (pNIPAM-co-DEGDVE) onto porous silicon loaded with an anticancer drug. Thanks to the thermoresponsive nature of such layer, the drug release was temperature dependent. Werzer et al. expanded such study exploring the combined effect of pH and temperature on different drugs delivered from pNIPAM-co-DEGDVE encapsulants [23]. This study highlighted that pH and temperature influenced both drug delivery rate and its interaction with the barrier coating.

In this work, a thin film of gentamicin has been encapsulated by means of iCVD with a methacrylic acid (MAA) based film with a variable crosslinking degree, modulated by the addition

of ethylene glycol dimethacrylate (EGDMA). Previous works were mostly based on model drugs, of which relatively uniform thin films are easily accessible from simple solution processes such as spin coating or drop casting from organic solvents that easily wetted the glass substrates. Thin films of water-soluble drugs, like gentamicin, are not obtained easily on glass. In this regard, the present work advances the state of art by demonstrating the encapsulation and controlled release of a water-soluble antibiotic.

AIII.4 Materials and Methods

Materials

Methacrylic acid (99%, Aldrich, Germany), ethylene glycol dimethacrylate (98%, Aldrich, Germany) and tert-butyl peroxide (TPBO, 98%, Aldrich, Germany) were used in the iCVD process as, respectively, monomer, crosslinker and initiator without further purification. The drug layer was obtained from solutions of Gentamicin Sulphate (powder, from Apollo Scientific) in distilled water.

Square pieces of silicon (2.5x2.5 cm^2) were used as substrates for Fourier Transform Infrared (FTIR), and ellipsometry analyses. Rectangular pieces of silicon (2.5x5 cm^2) were used for swelling experiments. Conventional glass slides (cut into 2.5x2.5 cm^2 squares) were used as substrates for conductimetry release tests.

Deposition of the Drug Layer

The drug thin film was obtained by drop casting or spin coating on silicon and glass substrates treated with an O_2 plasma (Femto, version 1, Diener Electronic) for 2 minutes, to generate a more hydrophilic surface and to improve the adhesion of the layer.

Drop casted layers were prepared by placing 20-500 µL of gentamicin solution (10 mg/mL) onto carefully leveled substrates. Samples were then stored in ambient for 24h under a fume hood to let the solvent evaporate.

Spin coated layers were prepared using a standard spin coating device (Ingenieurbüro Reinmuth, Germany): 300 µL of gentamicin solution were dropped onto the substrates and spinned between 1000-2000 rpm. The spin time was set to 50 seconds, to complete e solvent evaporation.

Initiated Chemical Vapor Deposition Reactor Setup

iCVD layers were deposited using a custom-built setup, as described in ref. 21. Substrates were placed in a cylindrical vacuum chamber, on a stage thermoregulated at 30 °C by a water recirculating chiller.

The MAA and EGDMA monomers were heated to 70 °C and 75 °C, respectively, and fed into the reactor through a heated mixing line. The vapor flow rate was controlled by needle valves. The initiator, TBPO, was kept at room temperature and fed into the reactor through a mass flow controller. The flow-rate of MAA (3 - 5 sccm) and EGDMA (0.07 - 0.2 sccm) was varied, to obtain polymers with different degree of crosslinking, while the flow rate of TBPO was fixed at 0.8 sccm. The deposition was carried out at a constant working pressure of 500 mTorr, and at a filament temperature of 300°C. The polymer layers were grown up to a thickness of 200 nm, monitored in situ by laser interferometry.

Samples Characterization

The thickness of the drug layer was measured by means of a Dektak IIA profilometer. FT-IR was carried out to determine the chemical composition of the iCVD coatings. FT-IR spectra (4 cm^{-1} resolution, in the range 800-4000 cm^{-1}) were obtained in transmission mode with a Bruker IFS 66 v/s spectrometer. Data were processed with OriginPro and a software developed by M. Tazreiter *et al.* [24], allowed for determination crosslinker film content.

Ellipsometry (M-2000V, J.A. Woollam Co.Inc.) was performed primarily to measure the thickness of the iCVD coating, collecting data at three incidence angles (65 °, 70 ° and 75 °) in the wavelength range from 370 to 1000 nm. Experimental data were fitted with CompleateEASE® software. The iCVD polymer was modeled with a Cauchy function since it is transparent in the measured wavelength range. To evaluate the swelling behavior of the coating, the samples were placed in a liquid cell (Woollam, USA), filled with distilled water and ellipsometer measurements were collected at a single incidence angle of 75 °. The effective medium approximation (EMA) was used to model the composite consisting of polymer and water. The model mixes the optical constants of water with those of the dry Cauchy layer (i.e. polymer) according to their relative fraction (the fitting parameter).

Gentamicin Release Tests

To evaluate gentamicin release through the iCVD coatings, Electrochemical Impedance Spectroscopy (Gamry Instrument, Reference 600) has been used in "single frequency" mode. Since the antibiotic is a sulphate salt, its presence can increase the conductivity when dissolved in pure

water: by monitoring the conductivity variation of the release solution, the gentamicin concentration has been calculated using a calibration curve.

The analysis was carried out in a four-probe configuration, at AC voltage of 15 mV and at a frequency of 1 kHz. The release test was carried out placing a four electrodes probe kit into 200 mL of distilled water, and, after two minutes from the start of the measurement, the sample was inserted. The release solution was kept at 37 °C and under stirring. Current and voltage were measured every 20 seconds for 2 hours giving the solution impedance as output. The measurements were repeated three times on different samples deposited in the same conditions.

The calibration curve was carried out starting from pure distilled water and adding 150 µL of gentamicin solution (500 µg/mL) up to cover the desired concentration range. The impedance was measured after every addition.

Antimicrobial Activity Valuation.

The antimicrobial activity of the gentamicin released by the coatings was evaluated against Staphylococcus aureus DSM799 and Pseudomonas aeruginosa DSM939 (Leibniz Institute, DSMZ-German Collection of Microorganisms and Cell Cultures GmbH, Braunschweig, Germany).

Immediately after overnight incubation [25], about 105 microbial cells of target strains, handled and standardized as previously reported [26], were plated onto Plate Count Agar (Biolife Italiana srl, Milan, Italy) before disk diffusion assays. Antimicrobial disk susceptibility assays were carried out as defined by CLSI with slight modification. Positive control filter paper disks (6 mm) charged with 10 µg gentamicin, defined as the breakpoint amount able to distinguish sensitive or resistant strains (http://www.eucast.org/clinical_breakpoints/), as well as sterile filter paper blank disks (6 mm) were purchased from KAIROSafesrl (Trieste, Italy). Standard disks and coated with the encapsulated gentamicin were placed over the inoculated agar surface; after 2 h at 4 °C, plates were incubated at 37 °C for 24 h. Three replicates for each disk were placed onto three di erent agar plates. Antimicrobial activity was evaluated measuring the area of inhibition zones instead of their diameter. A six-point standard curve for both S. aureus DSM799 and P. aeruginosa DSM939 of active gentamicin loaded on blank disk was drawn in the range 20.62–0.64 µg/disk. In order to compare halos produced over different agar plates, jpg format pictures were imported into Adobe Photoshop CS2 image analysis software (Adobe Systems Incorporated, San Jose, CA, USA); the number of pixel of each halo (excluding the number of pixel relative to the disk) was converted to square millimeter after normalization with the average number of pixel of all disks measuring ~30 mm^2 [27]. The amount of active gentamicin released from coated disks was then normalized using commercial disks loaded with 10 µg gentamicin. Halo measurements

were independently performed at least three times; the amounts of estimated gentamicin released into the agar matrix producing inhibition halos were analyzed using an unpaired two sample equal variance t-test (Microsoft Excel®2010, after installation of Data Analysis add-in). Difference between the control and treated samples was considered significant at $p < 0.01$. On the basis of results from disk diffusion assays a further evaluation of gentamicin antimicrobial activity was carried out. Two coated disks were stirred at 37 °C for 2 h in 15 mL of saline solution in order to obtain a 30 μg/mL gentamicin solution. Bacterial cultures, with an average of OD600nm of 0.325 ± 0.05, measured immediately after overnight incubation and corresponding to about 8 log cfu/mL, were diluted 100 times in 180 μL of Oxoid™ Iso-Sensitest Broth (Thermo Fisher Scientific, Milan, Italy) and then 20 μL gentamicin extracted solutions were added, following a two-fold dilution scheme. Bacterial growth was monitored by measuring optical density every 10 min with the Varioskan Flash spectrofluorimeter (ThermoFischer Scientific, Waltham, MA, USA) at a wavelength of 600 nm as previously reported for the evaluation of the effect of antimicrobial activity on microbial growth kinetics [28]. After determination of minimal inhibitory concentration (MIC), the gentamicin concentration at which any increase in OD reading was observed during 24 h of incubation, 20 mL of Iso-Sensitest Broth were inoculated with 200 μL of broth from well of incubated microplate. The minimal bactericidal concentration (MBC) was defined as the lowest concentration at which no growth was observed after incubation (37 °C for 24 h). The assay was replicated independently two times.

To confirm the antibacterial test results, release solutions were analyzed with fluorescence spectrophotometry upon derivatization with o-phtaldehyde (OPA). OPA (40 mg) was dissolved in 1 mL methanol and mixed with 5mLof sodium tetraborate solution (0.1 M). Then, 50 μL of 2-mercaptoethanol were added and mixed for 1 min. 250 μL of such OPA solution were vigorously mixed with the release aliquot for 1 min and transferred in a cuvette. The analysis was carried out with a fluorescence spectrophotometer (Varian Cary Eclipse; excitation 335 nm, emission 440 nm). Calibration was carried out with gentamicin standard solutions in the range 1–50 μg/mL.

AIII.5 Results and Discussion

Characterization of the iCVD Coatings on Bare Substrates

MAA-EGDMA copolymers were deposited by iCVD varying the fraction of the crosslinker, EGDMA. The chemical analysis of the different copolymers measured by FT-IR is shown in Figure 1 in the range 1000–2000 cm-1 and in Supplementary Materials Figure S1 in SI on a larger wavenumber range. The copolymers are characterized by the O–H stretching band

relative to the acid group of MAA at 3250 cm-1, the carbonyl stretching band, due to carboxylic acid and ester moieties, in the range 1700–1800 cm-1, and the C–O band at 1150 cm-1 attributable to both monomers structure. In Figure 1, it can be appreciated that the carboxylic C=O absorption is composed of two contributions, one at 1703 cm-1 and the other at 1730 cm-1, whose relative intensity changes with the composition of the coating. The former is due to the acid carboxylic groups, while the latter component can be attributed to ester moieties. Starting from the spectra of the MAA and EGDMA homopolymers a best fitting procedure of the FTIR spectra has been carried out to get the composition of the deposited copolymers as a percentage of each monomer, and in turn the crosslinker volume fraction, as it can be observed in Figure S2 in Supplementary. The copolymer spectrum was fitted with a linear combination of the corresponding homopolymer absorbance spectra, following the routine explained in ref. [24] The evaluated composition in terms of crosslinker percentage is reported in Figure 1. Since the coatings should work as drug-release systems in an aqueous environment, the swelling in water was tested depending on the crosslinking. The swelling behavior is very important since it is correlated to the drug diffusion through the iCVD polymer and then to the release kinetics [29]. In Figure 2 it can be observed that the thickness of different iCVD coatings increases due to the swelling in water, as measured by means of ellipsometry: the coating with the lowest fraction of EGDMA (29%) swells the most, with around 45% of water uptake (in terms of thickness increase), while the one with 85% of EGDMA shows negligible swelling. Polymers containing less than 29% of EGDMA dissolved in water. The amount of crosslinker leads to changes in the mesh size (i.e., the distance between two consecutive crosslinks) of the polymers and this in turn affects the diffusivity of the water in/out of the layer [21]. In particular, a higher amount of crosslinker leads to a smaller mesh and less swelling, as it can be seen in Figure 2. The small thickness loss for the 29% EGDMA sample, observed after 1 min immersion, can be related to a mass loss. It is common for iCVD hydrogels, characterized by important swelling, to lose some weakly bond oligomers present on the surface at the immersion in water. The sample with 60% EGDMA shows a bump in the thickness increase curve that could be considered within the experimental error.

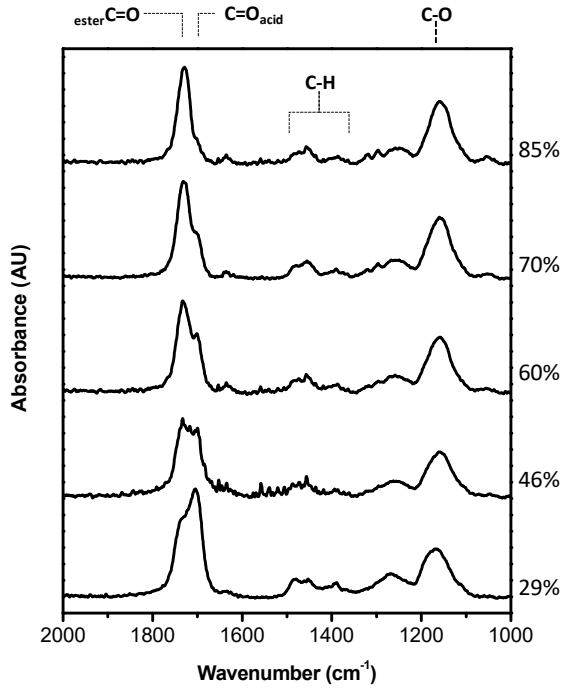

Figure 1. Fourier Transform Infrared (FT-IR) spectra of different copolymers with different methacrylic acid (MAA)/ ethylene glycol dimethacrylate (EGDMA) composition. Percentages on the right are EGDMA film volume fractions.

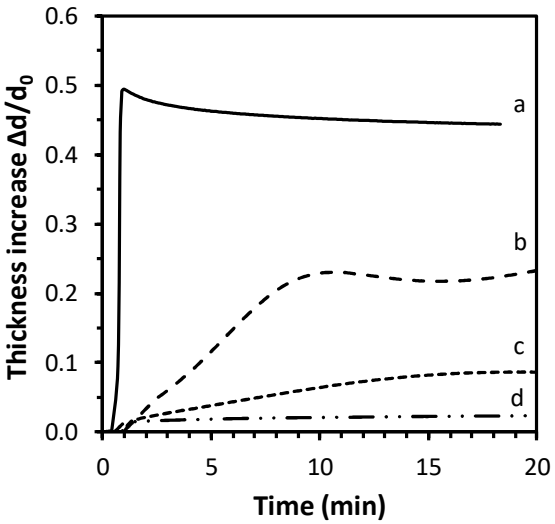

Figure 2. Swelling behavior, in terms of thickness increase, $\Delta d/d_0$, of different iCVD coatings with 29% (a), 60% (b), 70% (c) and 85% (d) EGDMA. The error bar in the measurements is ±1%.

Gentamicin Release Tests

Drug delivery systems were prepared by depositing the iCVD MAA-EGDMA copolymers on top of a thin film of gentamicin. The first step was the optimization of the deposition of a homogeneous gentamicin thin film. As it can be observed in the supporting information file (table S1 in SI), drop casted gentamicin resulted very non homogeneous in thickness: the difference in thickness between the center and the border was very important. The thickness of the spin coated coatings was more homogeneous (standard deviation in thickness around 5%) and controllable by changing the speed rotation rate and spin solution concentration.

Gentamicin release was evaluated by measuring the conductance of the released solution. Before investigating the drug release, the variation of conductance due to drug-free iCVD polymer in solution has been evaluated. Figure 3 shows a comparison between the conductance of a drug containing layer (300 μg gentamicin solution 10 mg/mL, drop casted) with a iCVD polymer (200 nm thick, 46% EGDMA) on top and the same iCVD polymer without gentamicin. The sample containing gentamicin, once dipped in pure water, lead to a variation of conductance of almost 100 μS in 72 min, differently from the gentamycin free iCVD polymer that gave negligible conductance variation. This result indicated that the iCVD coating does not influence the detection of the drug.

Once the calibration was accomplished, as reported in figure S3, the gentamicin release was investigated. In Figure 4 the results for the sample obtained from drug spin coating (1500 rpm, 100 mg/mL gentamicin) and iCVD film deposition with different percentage of crosslinker, together with an uncovered gentamicin spin coated layer, are reported.

It can be observed that the addition of the iCVD layer effectively limits the drug release. In particular, the higher the crosslinker content, the slower the gentamicin release rate is. Higher release rates can be related also to the larger swelling of the samples with lower crosslinking degree.

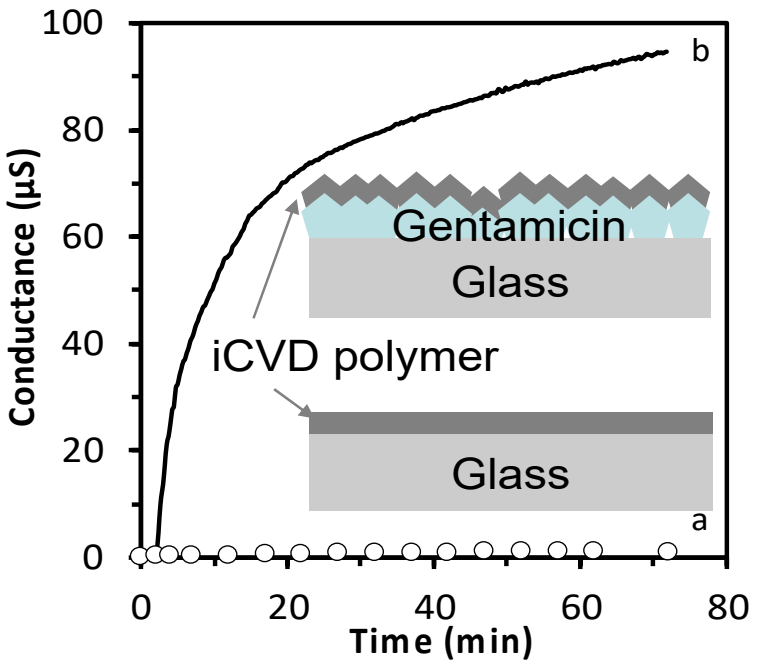

Figure 3. Conductance variation due to the release test from (a) iCVD coating alone (white dots) and (b) drug layer with iCVD coating on top (continuous line). Drug layer obtained by drop casting (drop volume = 300 µl, [Gent] = 10 mg/ml), iCVD coating thickness ~ 200 nm with a EGDMA volume fraction of 46%, immersed in distilled water.

More details on the release mechanism can be understood by the mathematical models applicable to the release data. Previously, good fits were obtained by applying the diffusion model based on reservoir systems, in which the drug is encapsulated by an outer membrane and gradually released [21,23]. In such model, the rate limiting step is the diffusive transport of the drug through the membrane, and therefore the release can be described by an analytic expression derived by the Fick's law, which works under the conditions that the drug is released in a volume of solution at least three times higher than the volume required for a saturated solution (i.e., sink condition), that there is a negligible (or rapid initial) polymer swelling and that the drug permeability does not change in time. This model describes the time-dependence of the fractional release Mt/M∞ as:

$$\frac{M_t}{M_\infty} = M_{max}\left(1 - e^{-k_{er}(t-t_0)}\right) \qquad (1)$$

where k_{er} is an effective release constant, Mmax estimates the maximum amount of drug release from the system under investigation and t_0 is a lag time, accounting for a dissolution onset

different from the start of the experiment. t_0 was added as fitting parameter to take into account that since this release study concerns very crosslinked films, the hypothesis of a negligible or rapid initial swelling may not hold. The fitting results can be observed in Figure 4b for the 80% EGDMA and Table 1. The R^2 values are close to unity for most of the systems, indicating a good agreement of the model with the experimental data. The release constant, k_{er}, decreases from the uncoated sample to the coated ones and among those, the one with the 85% EGDMA shows the lowest release constant. The values for the release constants obtained in this study are in agreement with the release constants obtained by previous studies based on similar crosslinked hydrogels [21].

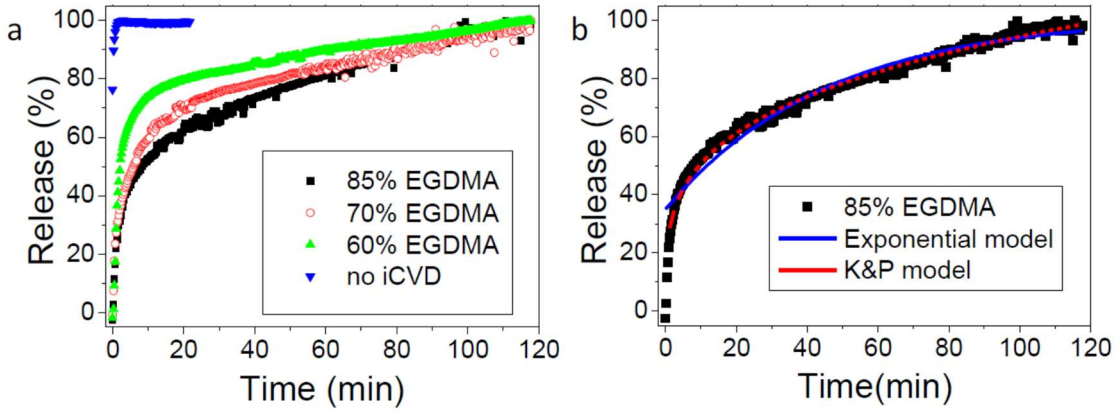

Figure 4. Percentage of released gentamicin from spin coated samples ([Gent] = 100 mg/mL, v = 1500 rpm) without iCVD coating and coated with a 200 nm iCVD layer with different EGDMA volume fractions: 60%, 70% and 85%. Average values obtained measuring the conductivity of three replicates, a maximum standard deviation of 12% was estimated for each data point. Total content of gentamicin is 45 ± 5 μ g/cm2. (b) Gentamicin release data for the 85% EGDMA polymer coating fitted with the exponential model of Equation (1) and with the Korsmeyer and Peppas model.

Table 1: Fitting results of the release data. The first four parameters refer to the model of Equation (1). The last two to the Korsmeyer and Peppas model.

Sample	R2	Mmax	k_{er} (min^{-1})	t_0 (min)	R2 (K & P model)	N (K & P model)
no iCVD	0.99	99.5	2.86	0.1	-	-
EGDMA 60%	0.81	99.3	0.06	11.9	0.91	0.14
EGDMA 70%	0.92	90.0	0.04	11.4	0.97	0.21
EGDMA 80%	0.92	93.7	0.02	11.8	0.99	0.27

Another simple model that is usually applicable to such thin film systems for drug release is the Korsmeyer and Peppas model, even though it mostly describes matrix systems, where the drug is embedded in the polymer and not coated by it, like in reservoir systems. Nevertheless, the Korsmeyer and Peppas model could also fit our experimental data with R2 values closer to unity than the exponential model. The coefficient in the Korsmeyer and Peppas model can give hints on the different types of transport mechanisms. [29] Coeffcients below 0.5, like those obtained with our fittings (Table 1), are characteristics of Fickian transport. The Korsmeyer and Peppas model was not applicable to the experimental release data from the bare drug, i.e., without iCVD coating.

For completeness, when gentamicin was deposited by drop casting the barrier effect of the iCVD coating was not effective, likely because of the non-homogeneity of the active layer, as shown in Figure S4 in Supplementary. Optical microscope images have shown, in fact, defects on the iCVD coatings deposited onto drop casted gentamicin: these may have negatively influenced the barrier characteristics of the iCVD polymer. The defects are present before immersion in water and they are attributable to the fact that the underlaying layer of gentamicin is so rough that it is difficult to obtain a continuous, low-defective iCVD layer on top, in the chosen deposition conditions.

Antibacterial Activity of the Samples

In order to compare the antimicrobial activity of gentamicin loaded cellulose disks coated with different iCVD polymer, a regression curve of gentamicin antimicrobial activity was drawn for *S. aureus* DSM799 and *P. aeruginosa* DSM939. On the basis of these results it was possible to estimate the amount of active gentamicin released by the disks as reported in Table 2.

Table 2: Amount of active gentamicin released from gentamicin loaded disks against the pathogens.

Bacteria	**EGDMA Volume Fraction**		
	60%	70%	85%
S.aureus DSM700	12.0 ± 0.5 µg	7.1 ± 0.4 µg	8.0 ± 0.8 µg
P.aeruginosa DSM 939	13.1 ± 0.3 µg	7.9 ± 0.2 µg	8.9 ± 0.7 µg

For both pathogenes, the estimated amount of active gentamicin release from 60% EGDMA coated disks, calculated by using the regression curve of antimicrobial activity (area of inhibition halos) produced by a gentamicin solution, resulted to be a significantly different ($p < 0.01$) from 70% and 85% EGDMA coated disks, according to independent t-test evaluation.

An example of inhibition halo produced by gentamicin loaded cellulose disks coated with different iCVD polymer against S. aureus DSM 799 is presented in Figure 5.

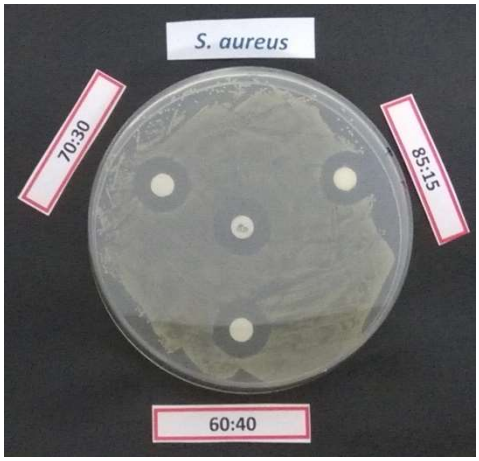

Figure 5. Inhibition halos produced by gentamicin against S. aureus DSM799 released by cellulose disks coated with different iCVD polymer of different crosslinker content (as reported in the labels). The positive disk control (10 μg gentamicin/disk) is in the center.

After 24 h incubation, it can be observed that the samples released less than 30 μg active gentamicin, the amount originally loaded. In addition, these results confirmed that the gentamicin release through the less crosslinked coating (60% EDGMA) is more important, as demonstrated by the higher activity by microbroth dilution method.

In order to understand if the reduced activity found in disk samples could be due to limitation in the release or in partial inactivation of gentamicin, samples were kept in physiologic solution as described in "material and methods" section and surnatant were tested for antibacterial activity.

On the basis of 24 h growth kinetic it was possible to define MIC and, after a following incubation in fresh microbiological medium, the MBC values, in the hypothesis that gentamicin for each disk was completely released and totally active (maximum 20 μg/mL in broth). The estimated amount gentamicin producing MIC and MBC from the disk coated with 60% EDGMA iCVD polymer, compared to that obtained by gentamicin stock solution is shown in Table 3.

Table 3: Minimal inhibitory concentration (MIC) and minimal bactericidal concentration (MBC) values, in μg/mL, of active gentamicin released from disks producing MIC in comparison with that produced by free gentamicin in water. iCVD layer prepared with an EGDMA volume fraction of 60%.

Extracted Solution	**S. aureus DSM799**		**P aeruginosa DSM939**	
	MIC	MBC	MIC	MBC
Gentamicin released from iCVD coated disks	5	10	5	10
Gentamicin control solution	2.5	5	2.5	5

Apparently, the measured activity was about half the one expected for the dropped gentamicin amount. To better rationalize this result, the amount of gentamicin in the extracted solutions was determined by fluorescence spectroscopy upon OPA derivatization. This analysis led to an amount of gentamicin released from the iCVD coated samples equal to 18 ± 1 μg, instead of expected 30 μg which means that the MIC and MBC values were overestimated. Considering the actual released gentamicin concentration, i.e., 60% of the estimated one, it is possible to correct the MIC value, obtaining 3 μg/mL. This result indicates that the gentamicin is not completely released from the cellulose disc, but the part released is more or less as active as the standard gentamicin, although the microdilution method is unable to define the real MIC value of coated cellulose disk, as a single value between 2.5 μg/mL and 5 μg/mL. The reason for the reduced release could be related to a strong coupling of the iCVD coating to the cellulose membrane resulting in a more difficult release of the coated drug. This topic deserves further studies to optimize substrate and coating coupling.

AIII.6 Conclusion

Different drug release behaviors were achieved by depositing an iCVD polymer onto a gentamicin layer, deposited by different techniques. The release kinetic strongly depends on the chemical composition of the iCVD polymers: in particular, it has been shown that gentamicin release slowed down when the EGDMA volume fraction of the coatings was increased. An increase of the volume fraction of the EGDMA from the 70% to the 85% reduces the drug released after twenty minutes of twenty percentage points. This is due to the increased crosslinking as a consequence of the presence of EGDMA, that alter the swelling characteristics of the barrier coating. In addition, it has been demonstrated that the way the gentamicin is deposited affects the homogeneity of the drug layer and in turn of the iCVD polymer and the antibiotic release as well. Samples obtained by spin coating and drop casting coated with an iCVD layer containing 85% of EGDMA released in water respectively the 70% and the 90% of the loaded gentamicin after 40 min. As far as antimicrobial activity is concerned, it can be concluded that released gentamicin retain most of the antibacterial activity, demonstrating that such process does not induce alteration in the antibiotic molecule. However, for reasons that necessitate more investigations, but likely associated to the coupling of the barrier coating with the three-dimensional support, about 40% of coated gentamicin is not released from the cellulose disks used to determine the gentamicin activity.

Acknowledgements

The activity reported in this paper has been partly funded by Regione Puglia "Apulian Industrial Plasma Laboratory, LIPP" and the Italian Ministry for Education (MIUR) under grant PONa3_00369 SISTEMA.

AIII.7 References

1. Weinstein, M.J.; Wagman, G.H.; Oden, E.M.; Marquez, J.A. Biological activity of the antibiotic components of the gentamicin complex. *J. Bacteriol.* **1967**, *94*, 789–790.

2. Cooper, D.J.; Yudis, M.D.; Guthrie, R.D.; Prior, A.M. The gentamicin antibiotics. Part I. Structure and absolute stereochemistry of methyl garosaminide. *J. Chem. Soc. C Org.* **1971**, 960.

3. Hahn, F.E.; Sarre, S.G. Mechanism of action of gentamicin. *J. Infect. Dis.* **1969**, *119*, 364–369.

4. Aviv, M.; Berdicevsky, I.; Zilberman, M. Gentamicin-loaded bioresorbable films for prevention of bacterial infections associated with orthopedic implants. *J. Biomed. Mater. Res. Part A* **2007**, *83A*, 10–19.

5. Lucke, M.; Schmidmaier, G.; Sadoni, S.; Wildemann, B.; Schiller, R.; Haas, N.P.; Raschke, M. Gentamicin coating of metallic implants reduces implant-related osteomyelitis in rats. *Bone* **2003**, *32*, 521–531.

6. Mohorčič, M.; Jerman, I.; Zorko, M.; Butinar, L.; Orel, B.; Jerala, R.; Friedrich, J. Surface with antimicrobial activity obtained through silane coating with covalently bound polymyxin B. *J. Mater. Sci. Mater. Med.* **2010**, *21*, 2775–2782.

7. Radin, S.; Ducheyne, P. Controlled release of vancomycin from thin sol-gel films on titanium alloy fracture plate material. *Biomaterials* **2007**, *28*, 1721–1729.

8. Procaccini, R.A.; Studdert, C.A.; Pellice, S.A. Silver doped silica-methyl hybrid coatings. Structural evolution and antibacterial properties. *Surf. Coatings Technol.* **2014**, *244*, 92–97.

9. Cometa, S.; Iatta, R.; Ricci, M.A.; Ferretti, C.; De Giglio, E. Analytical characterization and antimicrobial properties of novel copper nanoparticle–loaded electrosynthesized hydrogel coatings. *J. Bioact. Compat. Polym.* **2013**, *28*, 508–522.

10. Lin, C.C.; Metters, A.T. Hydrogels in controlled release formulations: Network design and mathematical modeling. *Adv. Drug Deliv. Rev.* **2006**, *58*, 1379–1408.

11. De Giglio, E.; Cafagna, D.; Cometa, S.; Allegretta, A.; Pedico, A.; Giannossa, L.C.; Sabbatini, L.; Mattioli-Belmonte, M.; Iatta, R. An innovative, easily fabricated, silver nanoparticle-based titanium implant coating: Development and analytical characterization. *Anal. Bioanal. Chem.* **2013**, *405*, 805–816.

12. Argentiere, S.; Blasi, L.; Morello, G.; Gigli, G. A novel pH-responsive nanogel for the controlled uptake and release of hydrophobic and cationic solutes. *J. Phys. Chem. C* **2011**, *115*, 16347–16353.

13. Dai, S.; Ravi, P.; Tam, K.C. pH-Responsive polymers: synthesis, properties and applications. *Soft Matter* **2008**, *4*, 435.

14. Gupta, P.; Vermani, K.; Garg, S. Hydrogels: From controlled release to pH-responsive drug delivery. *Drug Discov. Today* **2002**, *7*, 569–579.

15. Yin, Z.C.; Wang, Y.L.; Wang, K. A pH-responsive composite hydrogel beads based on agar and alginate for oral drug delivery. *J. Drug Deliv. Sci. Technol.* **2018**, *43*, 12–18.

16. Bartil, T.; Bounekhel, M.; Cedric, C.; Jeerome, R. Swelling behavior and release properties of pH-sensitive hydrogels based on methacrylic derivatives. *Acta Pharm.* **2007**, *57*, 301–314.

17. Perrotta, A.; Werzer, O.; Coclite, A.M. Strategies for Drug Encapsulation and Controlled Delivery Based on Vapor-Phase Deposited Thin Films. *Adv. Eng. Mater.* **2018**, *20*, 1700639.

18. Christian, P.; Ehmann, H.M.A.; Coclite, A.M.; Werzer, O. Polymer Encapsulation of an Amorphous Pharmaceutical by initiated Chemical Vapor Deposition for Enhanced Stability. *ACS Appl. Mater. Interfaces* **2016**, *8*, 21177–21184.

19. Lau, K.K.S.; Gleason, K.K. Particle functionalization and encapsulation by initiated chemical vapor deposition (iCVD). *Surf. Coatings Technol.* **2007**, *201*, 9189–9194.

20. McInnes, S.J.P.; Szili, E.J.; Al-Bataineh, S.A.; Xu, J.; Alf, M.E.; Gleason, K.K.; Short, R.D.; Voelcker, N.H. Combination of iCVD and porous silicon for the development of a controlled drug delivery system. *ACS Appl. Mater. Interfaces* **2012**, *4*, 3566–3574.

21. Christian, P.; Tumphart, S.; Ehmann, H.M.A.; Riegler, H.; Coclite, A.M.; Werzer, O. Controlling Indomethacin Release through Vapor-Phase Deposited Hydrogel Films by Adjusting the Cross-linker Density. *Sci. Rep.* **2018**, *8*, 1–12.

22. McInnes, S.J.P.; Szili, E.J.; Al-Bataineh, S.A.; Vasani, R.B.; Xu, J.; Alf, M.E.; Gleason, K.K.; Short, R.D.; Voelcker, N.H. Fabrication and Characterization of a Porous Silicon Drug Delivery System with an Initiated Chemical Vapor Deposition Temperature-Responsive Coating. *Langmuir* **2016**, *32*, 301–308.

23. Werzer, O.; Tumphart, S.; Keimel, R.; Christian, P.; Coclite, A.M. Drug release from thin films encapsulated by a temperature-responsive hydrogel. *Soft Matter* **2019**, *15*, 1853–1859.

24. Tazreiter, M.; Christian, P.; Schennach, R.; Grießer, T.; Coclite, A.M. Simple method for the quantitative analysis of thin copolymer films on substrates by infrared spectroscopy using direct calibration. *Anal. Methods* **2017**, *9*, 5266–5273.

25. de Candia, S.; Morea, M.; Baruzzi, F. Eradication of high viable loads of Listeria monocytogenes contaminating food-contact surfaces. *Front. Microbiol.* **2015**, *6*, 1–12.

26. Bonifacio, M.A.; Cometa, S.; Dicarlo, M.; Baruzzi, F.; de Candia, S.; Gloria, A.; Giangregorio, M.M.; Mattioli-Belmonte, M.; De Giglio, E. Gallium-modified chitosan/poly(acrylic acid) bilayer coatings for improved titanium implant performances. *Carbohydr. Polym.* **2017**, *166*, 348–357.

27. Pinto, L.; Cefola, M.; Bonifacio, M.A.; Cometa, S.; Bocchino, C.; Pace, B.; De Giglio, E.; Palumbo, M.; Sada, A.; Logrieco, A.F.; et al. Data on the antimicrobial effect of essential oils against Penicillium spp. in in vitro conditions and on oranges. *Food Chem.* Submitted.

28. De Candia, S.; Quintieri, L.; Caputo, L.; Baruzzi, F. Antimicrobial Activity of Processed Spices Used in Traditional Southern Italian Sausage Processing. *J. Food Process. Preserv.* **2017**, *41*, e13022.

29. Carbinatto, F.M.; de Castro, A.D.; Evangelista, R.C.; Cury, B.S.F. Insights into the swelling process and drug release mechanisms from cross-linked pectin/high amylose starch matrices. *Asian J. Pharm. Sci.* **2014**, *9*, 27–34.